UILU-ENG 89-3606

Report No. 152

MICROSTRUCTURAL STUDIES OF VAPOR-DEPOSITED NICKEL/CERAMIC COMPOSITES

by

Mihir Mahendra Shah and J. M. Rigsbee
Department of Materials Science and Engineering

A Report of the

MATERIALS ENGINEERING—MECHANICAL BEHAVIOR

College of Engineering, University of Illinois at Urbana-Champaign

December 1989

ABSTRACT

This research program examines fundamental aspects of metal/ceramic interactions through the analysis of model composites produced by plasma-assisted physical vapor deposition (ion plating) and consisting of thin (< 1μm) metallic films on ceramic substrates. The two major aspects of this research are: 1) the investigation of the effects of ion bombardment on the nucleation behavior and growth morphologies of the films, as well as the development of any film/substrate orientation relationships; and 2) the study of the interactions between metals and ceramics in a thin-film geometry, with emphasis on interface compound formation, comparing ion-assisted and high temperature processing.

The primary microanalytical technique employed was cross-section transmission electron microscopy, with scanning electron microscopy and Auger electron spectroscopy utilized as well. In addition, a tensile adhesion test and microhardness indentations were used to evaluate mechanical strength.

An optimal processing window was defined for DC ion plating in the nickel/cordierite system in order to obtain maximum film/substrate adhesion. For the case of RF ion plating of nickel films on basal orientation sapphire substrates, ion bombardment during deposition was shown to have significant effects on the nucleation and growth behavior of the films. Bombardment enhanced adatom mobility was sufficient to result in a crystallographic orientation relationship between the film and the substrate, with close packed planes and directions being parallel. Ion bombardment was not sufficient, however, to produce any interfacial reaction phases in the as-deposited condition. A nickel aluminate spinel did form at the interface upon heat treatment (1000 °C, 2 hrs.) and was always crystallographically related to the substrate, independent of the as-deposited crystallography. Metallic films were more resistant to disbonding than oxide films, with a strong interface being achieved via ion-assisted deposition.

DEDICATION

To my parents, Usha and Mahendra Shah; whose encouragement, support and understanding helped make this dream a reality.

ACKNOWLEDGEMENTS

The author wishes to thank Professor J. M. Rigsbee for the opportunity to be a part of this research effort, as well as for his encouragement and insights. The time and effort invested by the members of the committee; H. L. Fraser, J. Homeny, and W. M. Kriven is also much appreciated. Thanks go to the current and former members of the ion plating research group, without whom this research would not have been possible. Special thanks are due my office mate, J. H. Givens, whose assistance with ion plating was invaluable. The United States Army Corps of Engineers Construction Engineering Research Laboratory is acknowledged for use of their ion plating facility, under the direction of Mr. V. F. Hock. The Center for Microanalysis of Materials of the Materials Research Laboratory and the Center for Electron Microscopy are acknowledged for the use of their analytical intrumentation, with personal thanks going the M. Mochel and N. Finnegan for the STEM/EDS and Auger analyses respectively. Thanks also go to S. R. Peddada for the many discussions examining the behavior of metal/ceramic interfaces and the growth of thin films. The financial support of the IBM Corporation, through its Materials and Processing Science Program, is gratefully acknowledged. Lastly, the friendship and camaraderie of the many graduate students, faculty and staff in materials science who shared in the ups and downs of a PhD program shall not soon be forgotten.

TABLE OF CONTENTS

I. INTRODUCTION 1

II. BACKGROUND 3
A. Thin film technology 3
A.1. Overview 3
A.2. Ion plating 8
A.3. Morphology models 15
A.4. Adhesion 19
B. Metal/ceramic interfaces 21
B.1. Overview 15
B.2. Microstructure 21
B.3. Mechanical properties 26

III. EXPERIMENTAL PROCEDURE 32
A. Deposition 32
B. Materials 34
C. Microanalysis 34
D. Mechanical properties 41

IV. RESULTS 42
A. Nickel/cordierite 42
B. Nickel/alumina 46
C. Nickel/sapphire 51
C.1. As-deposited 51
C.2. Heat treated 74

V. DISCUSSION 105
A. Adhesion 105
A.1. Tensile test 105
A.2. Indentation test 105

B. Morphology 107
B.1. Zone models 107
B.2. RF metallic nickel 108
B.3. Heat treated morphology 109
C. Interface characteristics 110
C.1. Orientation relationships 110
C.2. Phase analysis 111
C.3. Microstructure 113
C.4. Chemistry 113

VI. CONCLUSIONS 115

REFERENCES 116

VITA 122

I. INTRODUCTION

This research program is a fundamental study of metal/ceramic interactions; as related to plasma-assisted physical vapor deposition of thin metallic films on ceramic substrates. A model laminate composite structure is produced via deposition of a thin metallic film on a ceramic substrate, allowing the examination of the nucleation and growth behavior of the film, as well as the interactions between the film and the substrate; both as a function of the plasma-enhanced deposition conditions and as a result of post-deposition annealing treatments. The two major aspects of this research are: 1) the investigation of the effects of ion bombardment on the nucleation behavior and growth morphologies of the films, as well as the development of any film/substrate orientation relationships; and 2) the study of the interactions between metals and ceramics in a thin-film geometry, with emphasis on interface compound formation, comparing ion-assisted and high temperature processing.

All composites examined in this study were fabricated by deposition of thin ($< 1\ \mu m$) metallic or oxide layers on ceramic substrates via ion plating, a plasma-assisted physical vapor deposition technique. The initial phase of the study involved growth of nickel films on cordierite ($2MgO$ - $2Al_2O_3$ - $5SiO_2$) substrates, a possible replacement material for alumina in microelectronics packaging, by DC ion plating. Although an optimal processing window was defined for the nickel/cordierite system, substrate inhomogeneity and phase instability precluded detailed characterization of the composite interface. In order to extract the desired fundamental information, the second phase of the project was established using nickel/alumina as a model system. In this phase, both conventional (argon plasma) and reactive (oxygen plasma) RF ion plating techniques were employed to produce films on single crystal aluminum oxide (sapphire) substrates.

A range of microanalytical instrumentation was utilized for microstructural and microchemical analysis of the composites; including scanning and transmission electron microscopy, energy dispersive spectroscopy and Auger electron spectroscopy. In addition, mechanical

properties, primarily film/substrate adhesion, were determined using a tensile adhesion test and a microhardness indenter. The central focus of the analytical portion was cross-section transmission electron microscopy (XTEM), which yields direct information concerning the structure, crystallography and chemistry of the film, substrate and interface.

Metal/ceramic thin-film composites have their primary application in microelectronics packaging technology, where metallization of a substrate for subsequent joining, brazing and interconnect operations is required. Obtaining an increased understanding of the interactions between metals and ceramics is essential to the development of superior multilayer ceramic substrates and ceramic-reinforced metal-matrix composites.

In summary, this research uses ion plating as a means to produce metal/ceramic thin-film composites in order to evaluate the effects of ion bombardment and post-deposition annealing on film growth and interfacial characteristics.

Specifically:

1) Film morphology is compared with existing structure zone models as a function of ion bombardment conditions.
2) Film/substrate adhesion is evaluated as a function of ion bombardment conditions, with fracture mechanics models applied to qualitatively describe interface properties.
3) Ion bombardment enhanced adatom mobility is investigated; with the crystallographic orientation relationships it produces being compared to those developed during other processing techniques.
4) Interface phase formation upon annealing is monitored; with the reaction criteria and the resulting crystallography correlated with those in the literature.
5) The extent of microstructural damage and interfacial mixing (chemical) as a result of ion-assisted deposition is determined.

II. BACKGROUND

A. Thin film technology

A.1. Overview

Although thin film technology is often regarded as a recent development, it does possess a fairly extensive history. In order to fully appreciate the current state of the art in thin films it is instructive to follow the evolution of the technology, both from an experimental and a theoretical perspective. As early as 1963 thin films were made the topic of a seminar of the American Society for Metals [1]. Included was a series of papers describing preparation and characterization methods; structural, mechanical and electrical properties; and applications of thin films. The initial chapter by K. Behrndt on the preparation of thin films provides the reader with a detailed discussion, complete with 232 references, of the major types of deposition processes from their inception to their current status, with emphasis on the principles involved. It is highly recommended as a window into the early days of modern thin film technology. For a more up to date review of the field the reader is referred to one of the many handbooks available, such as Maissel and Glang [2] and Bunshah et. al. [3].

Thin film growth from the vapor state may be categorized into two major classifications: chemical and physical, with the latter being further subdivided into evaporation and sputtering. Chemical vapor deposition involves the transport of a volatile compound of the coating material in the gas phase over a substrate at which a decomposition reaction occurs, resulting in film growth. Note that the substrate is generally maintained at an elevated temperature in order to promote the reaction. The first report of chemical vapor deposition is due to de Lodyguine [4] who, in 1893, coated carbon lamp filaments with tungsten by heating them in a mixture of H_2 and WCl_6.

Physical vapor deposition is of greater significance to this investigation and thus its two types will be outlined in greater detail. Vacuum evaporation is based on taking a material in a condensed phase

(solid or liquid) through its transition into the vapor state, allowing the vapor flux to migrate through a vacuum toward a substrate and condense, forming a solid film. Transformation to the vapor state is governed by classical thermodynamics and the Claussius-Clapeyron equation {Eq. 1} relating the equilibrium vapor pressures of the two phases [5].

$$\frac{dP}{dT} = \frac{H_g - H_s}{T(V_g - V_s)} \qquad \{1\}$$

This equation may be modified and rearranged for the case of a solid in equilibrium with its vapor to give the vapor pressure {Eq. 2}, making use of tabulated data [2].

$$\log p^* \text{ (Torr)} = AT^{-1} + B + C \log T + DT + ET^{-2} \qquad \{2\}$$

Combining these expressions with the kinetic theory of gasses, the Hertz-Knudsen equation for evaporation rate can be derived. It is given in the form most applicable to vapor deposition in equation {3} [6].

$$W = 3.5 \times 10^{22} \alpha\, p^* (MT)^{-1/2} \qquad \{3\}$$

W = evaporation rate in atoms/cm^2-sec
α = evaporation coefficient ranging from zero to unity
p^* = equilibrium vapor pressure in Torr
T = temperature in Kelvin
M = molecular weight in grams

The atoms emerge with an average energy of 3/2 kT and a spatial distribution which follows a cosine law. Depending on the background pressure in the vacuum chamber, however, the cosine distribution of the atoms breaks down before they condense on the substrate. Vacuum evaporation was first conducted by Nahrwold [7], who in 1887 used joule heating of platinum wires to deposit films. Development of evaporation was limited, however, by vacuum technology and the lack of suitable

evaporation sources. During the last 25 years, fortunately, many of these difficulties have been overcome and vacuum evaporation has become a widely used technique for many industrial and research applications. The full extent of its technical sophistication can be seen in the area of molecular beam epitaxy where Knudsen cell evaporation sources used under ultra-high vacuum (UHV) conditions can produce heterostructures with 10 nm layers [8].

Rather than imparting thermal energy to the solid in order to produce a vapor flux as in the case of evaporation, sputtering uses the transfer of momentum from an incident ion to a target atom, causing it to be ejected from the surface. The processes involved in sputtering may be visualized for simplicity as a series of binary, hard-sphere elastic collisions, with the energy transfer being a function of the masses and energies of the atoms involved. Schematics of the sputtering events and energy transfer are given in figure (1). In most deposition applications, the ions used to cause sputtering are produced in a glow discharge and will have energies in the range of 10 to 1000 eV. At these energies, most of the sputtering will result from low energy knock-ons. Note that the ejection of a sputtered atom must be the result of a sequence of collisions occurring within a cascade. Sputter deposition generally takes place in the linear cascade region in which recoil cascades are generated by the incident ion, but only a small fraction of the atoms in the cascade volume are in motion [2]. Unlike evaporated species which only possess thermal energy (< 1 eV), sputtered atoms have energies on the order of 25 eV. The effectiveness of the sputtering process is expressed by the sputter yield of an ion/target combination. This yield is defined as the number of target atoms ejected per incident ion. Although the sputter yield of a material is often determined experimentally, a complete theoretical analysis of sputtering has been formulated by Sigmund [9]. The details of the model are beyond the scope of this discussion, however, the final result for sputter yield is given in equation {4}.

$$S = \frac{\alpha\, S_n(E)}{16\, \pi^3\, a^2\, U_o} \qquad \{4\}$$

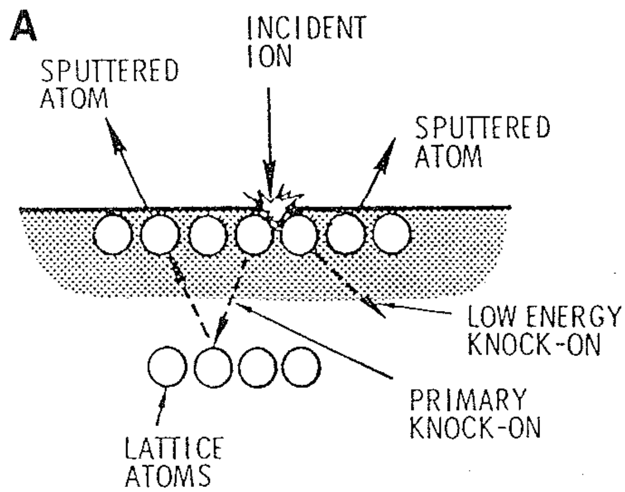

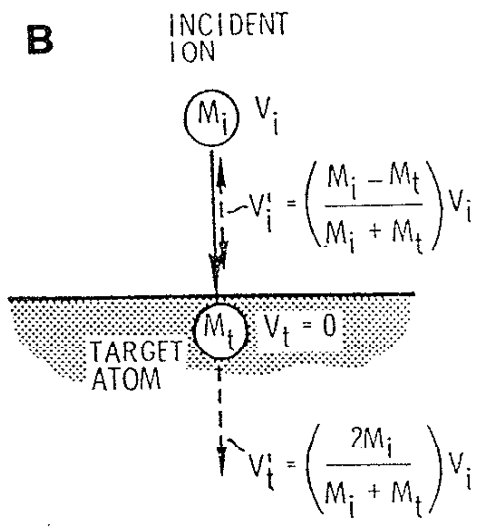

Figure 1: A) Events occurring during sputtering [6]
B) Energy transfer in a collision [6]

S = sputter yield
α = function of the atomic masses
$S_n(E)$ = nuclear stopping cross section of the ions
a = 0.219 Å = screening radius for the Born-Mayer attraction between two atoms
U_o = surface binding energy

The major implications of this expression are that the sputter yield is proportional to the incident ion energy, inversely proportional to the binding energy, and relatively independent of temperature. It also has a much narrower range of values (approximately a factor of 10) as compared to evaporation rates, which may vary over several orders of magnitude for different materials and are exponentially dependent on temperature. Although sputter yield does vary with incident ion species; since the momentum transfer between atoms is most efficient when their masses are equal, argon is most often used as the bombarding species. It has a good mass match with many target materials, is inert, and is relatively inexpensive.

Historically, sputtering was first used as a deposition method by Grove in 1852 [10]. One of its primary attributes has been the ability to deposit almost any material while maintaining constant composition between the target and the film. Refractory materials may also be sputtered more easily than evaporated since they need not be melted and vaporized, avoiding problems of fabricating a suitable source container. The advent of magnetrons [11], in which a magnetic field is used to confine electrons in the glow discharge adjacent to the target, thus greatly increasing the ionization efficiency in the plasma, has further extended the range of sputtering applications. Magnetron sputtering units provide high deposition rates over large areas and are able to be operate at much lower working gas pressures than conventional diode units.

A.2. Ion plating

Ion plating is a plasma-assisted physical vapor deposition technique which combines aspects of both vacuum evaporation and sputtering. The distinguishing characteristic of the process is the presence of a glow discharge at the substrate, causing it to be bombarded by energetic species; both from the working gas and the evaporant flux. It is this high energy particle flux impinging on the substrate surface and/or depositing film, sufficient to cause modifications to the interface region or film properties as compared to non-bombarded deposition, which Mattox used to define ion plating when introducing it into the literature in 1963 [12].

In order to describe the ion plating process, the components of a typical deposition system will be discussed, including a detailed treatment of glow discharge characteristics, followed by a presentation of the atomistic events which occur during the various stages of the deposition procedure. Finally, a summary of the advantages and limitations of ion plating will be given, along with some successful applications of the technique. Specific references will be provided where appropriate, however, much of the discussion is taken from review papers by Teer [13], Mattox [14], and Walley [15], as well as the recent text by Ahmed [16]. This text is highly recommended as a well presented and thorough guide to ion plating, from both a scientific as well as a technological point of view.

A typical ion plating system consists of a vacuum chamber, capable of attaining base pressures of 10^{-6} Torr or better, containing a source for film atoms; a high voltage cathode which also serves as the substrate holder; and a gas flow system to introduce working gas atoms into the system to support the glow discharge. The film atom source may be a resistively heated wire or boat, a sputtering target, or an electron beam evaporator (the most common method). Since a pressure of approximately 10 mTorr of working gas is required to support the glow discharge, systems containing electron beam evaporators must be differentially pumped, with a baffle plate isolating the gun filament from the deposition chamber and maintaining it in a high vacuum environment [17]. High voltage supplied to the cathode/substrate holder may be either direct current (DC) or radio frequency alternating current (RF) depending on the

electrical characteristics of the substrate and the glow discharge intensity desired. RF is much more effective with insulating substrates and produces a more intense discharge, but introduces a great deal of complexity to the system as a result of the shielding required. In addition to these basic requirements, ion plating systems may be equipped with substrate heaters/coolers, residual gas analyzers, deposition rate monitors, discharge enhancement systems, or plasma diagnostics.

Although ion plating is generally termed a plasma-assisted deposition technique, glow discharge assisted would be more specific. The glow discharge present in ion plating only approximates an ideal plasma, which has a well-defined potential and density, with its constituent particles in equilibrium motion [18]. A DC glow discharge is ignited by applying a potential between a cathode (the substrate holder) and an anode (the vacuum chamber, maintained at ground) in a vacuum containing approximately 10 mTorr of working gas. The typical discharge contains a number of distinct regions, shown schematically in figure (2). Note that under ion plating conditions, the positive column is extinguished due to the proximity of the anode and cathode. A glow discharge is created and sustained by electrons, extracted from the cathode, being accelerated across the dark space into the negative glow where they produce electron-ion pairs. Discharge intensity can be enhanced by increasing the number of ions produced in the negative glow. This may be accomplished by injection of electrons from a filament into the glow [19] or by confining the existing electrons in the discharge via an auxiliary anode [20]. Once ions are created in the negative glow, they move via random diffusion through this electrically neutral region. When an ion does reach the boundary between the negative glow and the cathode dark space it is accelerated across the potential difference towards the cathode, gaining energy from the electric field. Energy is also imparted to neutral atoms and clusters in the dark space through collisions with the accelerating ions, resulting in a flux of energetic ions and neutrals bombarding the substrate.

In order to fully understand the nature of the processes occurring during ion plating, one must first be able to characterize the type and energy of the bombarding species. The two types of particles important to

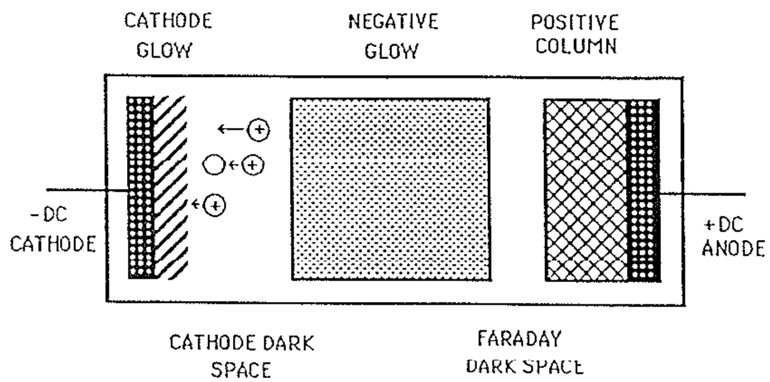

Figure 2: Regions in a DC glow discharge

the deposition process are ions and energetic neutrals. A number of researchers have estimated the ion/neutral ratio in a typical ion plating discharge [13, 21] with results ranging from approximately 0.05% to 2.0%. Consequently, it can be seen that film and substrate modifications in ion plating occur as a result of a small number of energetic ions and a much larger number of energetic neutrals, which originate from collisions in the dark space. The theory of Davis and Vanderslice [22] is used as the basic model to determine particle energies, but is slightly modified by Teer [23] to provide simpler expressions as outlined in the following paragraph.

The assumptions are that all ions originate in the negative glow, the electric field varies linearly from the cathode to the negative glow, symmetric charge transfer collisions determine the energy spectrum, and that the collision cross-section is not a function of energy. By considering the number of ions leaving the negative glow (N_o), the number of collisions in an element of distance dx, and the probability that an ion created at a given point "x" will reach the cathode without further collisions, Teer [23] derives the expression for the number of ions reaching the cathode with a given energy {Eq. 5}.

$$dN = \frac{N_o L}{2l\sqrt{V_c V}} \exp\left[-\frac{(L - L\sqrt{V/V_c})}{l}\right] dV \qquad \{5\}$$

L= dark space length
l = mean free path for charge transfer collisions
V_c = cathode voltage
N_o = number of ions leaving the negative glow

The energy lost by the ions is transferred to the neutrals, approximately 70% of this energy reaching the cathode. The derivation of the average energy of the neutrals [23] gives equation {6}.

$$E = \frac{1}{L} V_c \left[1 - \frac{2l}{L} + \frac{l^2}{L^2}\right] \qquad \{6\}$$

Comparing the expressions for the contribution to the total energy arriving at the cathode for both ions and neutrals {Eq. 7}, it is seen that neutrals carry six times as much energy to the cathode as do ions.

$$E_T(\text{ions}) = \frac{N_o V_c}{10} \qquad \{7a\}$$

$$E_T(\text{neutrals}) = 0.70\left[\frac{9 N_o V_c}{10}\right] \qquad \{7b\}$$

Average energies of the working gas species, reported for typical ion plating conditions with a 3.0 kV bias, are 300 eV for ions and 135 eV for neutrals [16]. In addition to knowing the amount and energies of the discharge gas atoms, we would also like to evaluate the properties of the evaporant flux. The metal atoms will likely undergo events similar to those of the gas atoms, again resulting in deposition of a large number of energetic neutrals. Armour et al. [24], analyzing atoms passing through a pinhole in the cathode, reported the average energy of evaporant ions to be less than one half of the discharge voltage and the evaporant neutrals as less than one third.

RF glow discharges, used in conjunction with insulating substrates, behave similarly to those ignited via a DC bias [6, 18]. For deposition applications RF power supplies are driven at 13.56 MHz, as dictated by the Federal Communications Commission. By reversing anode/cathode roles each half cycle, charge build-up on an insulating substrate is avoided. Although each electrode reverses polarity, the mass of the ions is such that they are relatively unaffected by the changing electric field at the frequencies involved and move only by random diffusion. The electrons, however, can move freely and transfer their charge to the anode very quickly. As a result, each electrode develops a negative bias in the steady state condition. The discharge then appears as a DC discharge with a central negative glow (electrically neutral) region and cathode dark spaces at each electrode. Because both electrodes are biased negatively, particle bombardment will occur at both. Since electrode voltage and area are

related as shown in equation {8}, with "n" computed to be 4 from a theoretical analysis and 1 from experiment, asymmetry can be built into the system to avoid sputtering at both electrodes.

$$\left[\frac{V_1}{V_2} = \frac{A_2}{A_1}\right]^n \qquad \{8\}$$

This is already accounted for in ion plating; since the substrate holder is much smaller than the vacuum chamber itself (the other electrode), it will develop a much larger bias and be the only one subjected to a high energy particle flux.

Now that the energetic particle flux has been characterized, the effects it has on the deposition process may be considered. The types of particles and the events leading to their formation are shown schematically in figure (3). As suggested by Mattox [14], the deposition process will be separated into three stages: prior to deposition, interface formation, and film growth. When the glow discharge is established prior to deposition, sputtering of the substrate by the working gas atoms can remove weakly bound contaminant atoms, induce lattice defects or crystalline disorder, and alter the substrate surface chemistry due to preferential sputtering. Working gas atoms may also be incorporated into the bulk of the substrate. Introduction of film atoms into the particle flux impinging upon the substrate initiates the interface formation segment. Here, particle bombardment causes mixing of film and substrate atoms due to sputtering and redeposition, recoil implantation, and radiation enhanced diffusion. The result is generally a compositionally graded film/substrate interface, characteristic of ion plating, but may also be a new interface compound phase. It is at the end of the interface segment and the beginning of actual film growth that the morphology and crystallography of the film begins to develop. Because the depositing film atoms arrive with greater than thermal energy they posses sufficient mobility, even with the substrate nominally at room temperature, to grow with a preferred orientation. This effect is especially prevalent when single crystal substrates are utilized. Energetic particle bombardment also affects

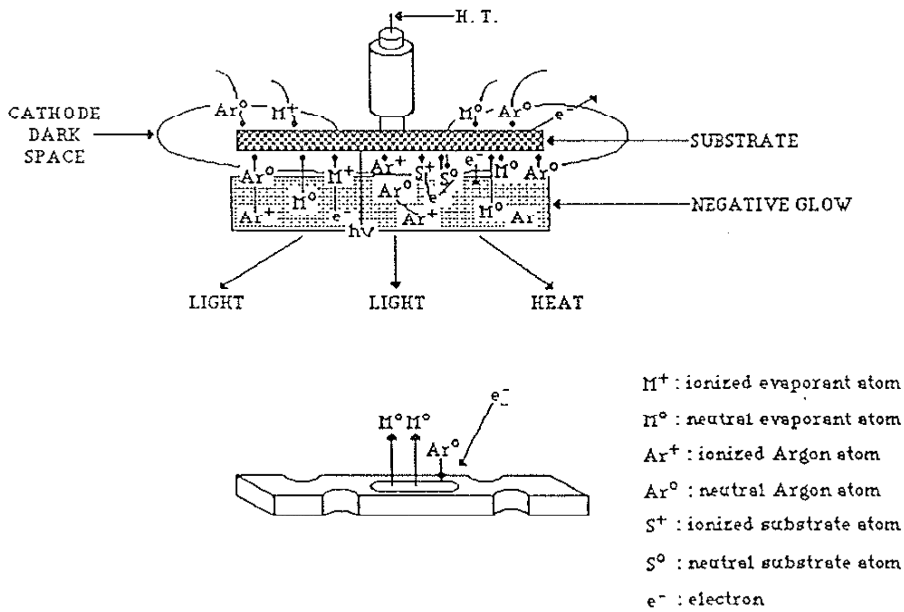

Figure 3: Events occurring during the ion plating process

film morphology, promoting elevated temperature structures in room temperature films. This aspect of thin-film technology will be discussed at length in the following section.

In general, ion plating has many advantages. Glow discharge sputter cleaning provides a clean, active surface for deposition, promoting excellent film/substrate adhesion. Adhesion may be further enhanced by interfacial mixing during initial deposition. Due to the relatively "soft" vacuum in an ion plating environment accounting for a large amount of gas scattering, this process has excellent "throwing power", or the ability to coat complex shapes and hidden surfaces. With the glow discharge able to dissociate molecular bonds, reactive ion plating may be used to deposit oxides or nitrides by evaporating a metallic source material and subsequently combining it with the second component during deposition. Ion plating does have a few limitations, primarily related to process characterization. Because of the complexity involved in analyzing and controlling a glow discharge and its associated variations in energy, it is difficult to identify, from a fundamental standpoint, the events occurring during plating. Ion plating has found a number of successful industrial applications including corrosion protection, decorative coatings and wear resistance [16]. Perhaps the most widely used and thoroughly studied system is that of titanium nitride (TiN) ion plated on steel cutting tools. Drill bits coated with TiN show up to a 400% increase in lifetime vs uncoated bits [25]. The fundamental aspects of TiN reactive ion plating has also received a great deal of attention in the literature, from deposition, microstructure, and property points of view [26, 27].

A.3. Morphology models

One of the major factors affecting the performance of a thin film is its morphology, along with the associated microstructure. Efforts to describe thin-film morphology have been underway since the mid-sixties, with Movchan and Demchishin introducing the first structure zone model (SZM) in 1969 [28]. By analyzing the structure of thick (0.5 to 2.0 mm) films produced by vacuum evaporation, three distinct zones were defined as a function of substrate temperature. When the homologous temperature

(the substrate temperature divided by the melting temperature of the film material, in Kelvin) was below 0.3 (zone 1), the structure consisted of tapered grains with domed tops. Boundaries between grains were not well defined and are largely porous. Dome diameter was also shown to increase with temperature. Zone 2 was characterized by a columnar morphology, with a smooth surface. In contrast to the open boundaries in zone 1, zone 2 exhibited well defined, dense grain boundaries. Above T/T_m of 0.45, the grains became equiaxed (zone 3).

This original SZM was modified by Thornton in 1973 [29] through the addition of a dependence on working gas pressure during magnetron sputtering (Fig. 4). Thornton also made the first distinction between microstructure and morphology, in which morphological features such as a column may be composed of a large number of grains (microstructural features). In the Thornton model, the experimental observations of Movchan and Demchishin were attributed to physical processes. Zone 1 was associated with atomic shadowing during growth; zone 2 with surface diffusion; and zone 3 with bulk diffusion. In addition, a fourth zone present between zones 1 and 2 was identified as being a transition zone and labelled zone T. Zone T being a dense array of fibrous grains. The influence of working gas background pressure was shown to be related to the amount of oblique coating flux arriving at the substrate. With increasing pressure more collisions occur, increasing the oblique flux component, thus enhancing atomic shadowing and promoting a zone 1 morphology. Energetic particle bombardment was reported to counteract atomic shadowing, resulting in a dense coating with a smooth surface [29].

Grovenor, Hentzell and Smith [30] have used higher resolution analyses to examine the morphology of thin films. Zone 1 columns were shown to actually consist of fine (20 nm) equiaxed grains with similar orientations, grouped in bundles. In zone T, surface diffusion became appreciable, allowing adatoms to occupy vacant sites on a growing grain, resulting in local epitaxy between individual film and substrate grains. The final grain structure was thought to be controlled by that of the first grains. This behavior continued through zone 2. Zone 3 was attributed to bulk diffusion and recovery/recrystallization. The controlling factors in

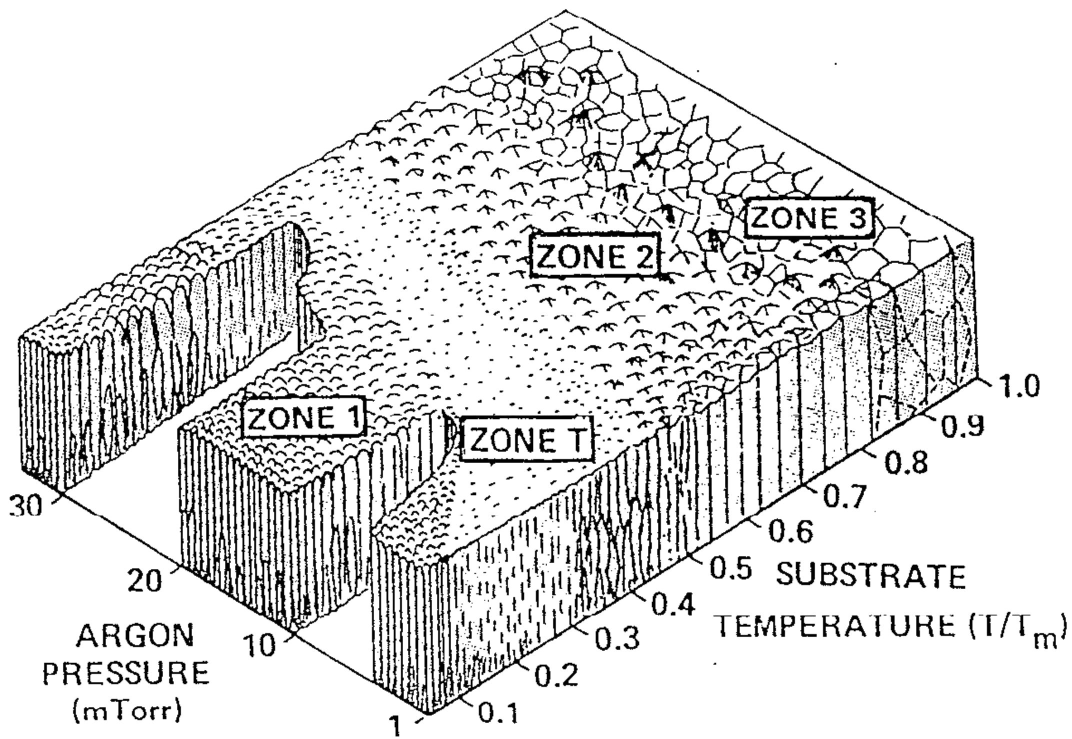

Figure 4: Thornton structure zone model (SZM)

the morphological development were reported to be the percentage of grain boundaries which are mobile.

Messier [31, 32] has proposed a method to quantify film morphology, primarily for low adatom mobility conditions. The model basically predicted random aggregation and clustering, resulting in a fractal configuration; the geometrical shape of the grains remaining constant with film thickness as well as under increasing magnification. In a further effort to quantify morphology, Srolovitz et. al. [33] presented a theory for the development of columnar morphology. Columnar growth was shown to result from a balance between atomic shadowing and surface diffusion, with zone 1 to zone 2 transition temperatures being correctly predicted. Monte Carlo simulations, based on the rearrangement of atoms depositing on a surface due to diffusion and grain boundary curvature, following the evolution of morphology with time/thickness also predicted columnar growth.

Although structure zone models are referred to extensively in the literature, care must be exercised in their application. The universality of SZMs arises from their simplicity; however, this simplicity also limits their accuracy. Variables such as substrate type and microstructure can strongly affect film morphology, yet are not considered in an SZM. Although substrate temperature is the experimentally measured quantity, the true parameter in question is adatom mobility. In addition to being a function of temperature, mobility may also be affected by surface contamination, nucleation site density, and initial adatom energy. Another key parameter omitted is deposition rate, which was up to an extremely high rate of 300 Å/sec in Movchan and Demchishin's experiments and not even mentioned in the other SZMs. One needs not only to consider the adatom mobility, but what that mobility is in relation to the incoming film flux; i.e., how far an atom can move before it is covered up by additional atoms. Structure zone models can be very useful in predicting and describing film morphologies, however, one must be aware of their limitations when applying them to compare various deposition technologies.

A.4. Adhesion

Film/substrate adhesion is an important parameter in thin film technology and numerous methods have been devised to measure it, yet no consensus has been reached as to how to interpret the data. One difficulty arises in the definition of the term "adhesion", and to what phenomena it is referring. Mittal [34], in his thorough review of adhesion, circumvents this problem by defining two types of adhesion: basic and practical. Basic adhesion represents the interfacial bond strength, related to a summation of interatomic forces. It is a fundamental measure of adhesion, and can be correlated to bond strength calculations. Practical adhesion is used to describe the separation of components at an interface. This value may include contributions from film deformation, intrinsic stress relief, and premature failure initiation sites. It is also a function of the test method, failure mode and location. Practical adhesion is what is generally reported in the literature and will be simply termed "adhesion" for the remainder of this discussion.

Adhesion in thin-film technology has recently reviewed by Baglin [35], with emphasis on the effects of ion beams on adhesion. The origins of film/substrate adhesion are discussed in detail, as are the criteria for delamination or adhesive failure. A brief description of the more common experimental techniques for adhesion measurements is presented, along with a number of case histories. A more comprehensive review of experimental methods is given by Chapman and Brown [36]. Although there are a wide variety of adhesion tests, they can be classified into five main groups: tensile, shear, scratch, indentation, and fracture mechanics. Tensile tests are among the easiest to perform, especially for thin-film/substrate geometries, and provide a quantitative value for adhesive strength. These tests are limited, however, by the strength of the epoxy used to attach the test fixture (pin) to the film, misalignment of the stress axis, and uncertainty as to the validity of the actual adhesion value. Shear tests are often used to evaluate adhesives, but have limited applicability to thin film adhesion. Scratch tests are primarily used to examine brittle films. In this test, a stylus is translated across the film surface under increasing loads. Adhesive strength is given as the load at which the film

was removed from the substrate, as determined via microscopy or acoustic emission. Data interpretation with scratch testing is fairly complex, with film deformation possibly contributing significantly to energy dissipation. For many applications, however, it does provide a reasonable approximation to the in-service conditions. Vickers indenters can be used to introduce cracks into a film/substrate couple, with crack length providing a measure of adhesion. This method assumes the cracks propagate along the interface, which is not always the case. The path which the cracks do follow does, however, give a good qualitative indication of adhesion. Fracture mechanics methods have been used to evaluate interfaces produced by elevated temperature processing and are now being extended to thin film geometries. They will not be discussed here, but their use in evaluating metal/ceramic interfaces will be covered in detail in a subsequent section.

An instrument which is in its relative infancy, especially when applied to adhesion testing, yet is gaining popularity is the nano-indenter [37]. The nano-indenter is an ultra sensitive Vickers indenter, with load and displacement controlled in real time with a depth resolution of 0.4 nm. Originally developed for determining modulus and hardness as a function of depth for ion implanted surfaces [38], it is now being applied to interface properties. Because of the high depth and spatial resolution of the system, data may be obtained from very small regions, allowing the user to produce a hardness profile across an interface. Another successful application of the nano-indenter is the measurement of interfacial shear stresses in fiber reinforced composites. By pressing on an individual fiber, the stress required to cause sliding (interfacial disbonding) can be determined. For very thin (~50 nm) films, indents may be made through the film into the substrate, allowing the change in hardness and modulus through the interface to be monitored. As the characteristics and capabilities of the nano-indenter are becoming better understood, the prospects for its use as a means of describing the mechanical properties of interfaces are encouraging.

B. Metal/ceramic interfaces

B.1. Overview

Metal/ceramic composites, both bulk and thin-film, are becoming an increasingly important part of current materials technology in applications ranging from microelectronics to aerospace. The application most relevant to this research is the use of metal films in the microelectronics industry. With the advent of multilayer ceramic packaging technology, the ability to metallize a ceramic substrate has become crucial [39]. These metal films are used as pads to which I/O pins may be brazed, bands for soldering of hermetic enclosures, and contacts to allow circuitry to be externally re-routed. Maintaining mechanical integrity across these metal/ceramic interfaces is a necessity, and can only be ensured by understanding their fundamental characteristics. Metal/alumina interfaces are becoming a major area of research in the composites field due to the prevalence of alumina as a reinforcing material. One example is the case of alumina whisker reinforced aluminum alloy composites [40]. In a similar vein, alumina/mullite interfaces have been tailored, both through optimized processing as well as through the introduction of an interface phase, to provide enhanced composite mechanical properties [41]. The nickel/alumina system is also important in the area of nickel-based superalloys, many of which form alumina scales. Relationships between scale microstructure and adhesion have been demonstrated [42], although on a much more macroscopic level than considered in this program.

Because the interface between a metal and ceramic often determines the performance characteristics of the composite, much research is being conducted in this area, both on actual composites as well as on model systems. Interfaces have been formed via elevated temperature methods such as diffusion bonding or co-sintering, or by vapor deposition techniques. For the case of vapor deposition, ion assisted deposition, ion implantation, elevated substrate temperature, and post-deposition annealing have all been used to modify the metal/ceramic interface.

Once these interfaces have been produced, they are analyzed for their structure, chemistry and mechanical properties. Phase evolution and

crystallographic orientation are examined to yield information regarding metal/ceramic interactions, while adhesion testing and fracture mechanics are used to evaluate the integrity of the bond. Throughout these investigations, experimental results are compared to theoretical models in order to be able to predict metal/ceramic behavior. For example, phase development and crystallographic orientation in diffusion bonded metal/ceramic couples is compared with models describing bonding across an interface [43].

B.2. Microstructure

A large portion of the research into the microstructure of metal/ceramic interfaces is due to the group of M. Ruhle, who is a pioneer in this field. Their program is based upon preparing model interfaces by diffusion bonding of a metal to a single crystal of aluminum oxide (sapphire) and examining them via TEM. Mechanical property analysis is carried out in conjunction with the group of A. G. Evans. A recently published review presented the current state of knowledge in this area; including the various models proposed to describe metal/ceramic interfaces, in addition to a synopsis of their experimental data [43]. The structure of interfaces was discussed using both geometric and atomistic models, with the caveat that although atomistic models which describe the relaxed state of interfaces can be confirmed by high resolution electron microscopy (HREM), much work still remains. Chemistry of interfaces was also discussed both for systems which do not form a reaction layer (Nb/Al_2O_3) and for those which do (Ni/Al_2O_3), with oxygen activity shown to be a key factor in phase development.

A more detailed summary of the microstructure of Nb/Al_2O_3 interfaces is given by Mader and Ruhle [44]. Diffusion bonding conditions were 1200 °C for 2 hr in vacuum, with a macroscopically imposed orientation relationship of:

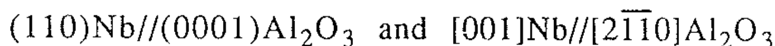

$$(110)Nb//(0001)Al_2O_3 \text{ and } [001]Nb//[2\bar{1}\bar{1}0]Al_2O_3$$

HREM was used to directly image the atomic positions across the interface, confirming the absence of any reaction product. Facets, identified as steps in the alumina surface, were formed at the interface causing significant local strain in the niobium lattice. A large number of small angle grain boundaries were also generated in both the niobium and alumina, resulting in small misorientations across the interface. The distortions present in the niobium allowed its separation into three zones. Within ~5 lattice planes of the interface there is a highly distorted region. Up to ~1μm, dislocations and small angle grain boundaries are present which alter the crystal from the orientations imposed by the bonding conditions to one more energetically favorable. Greater than 1 μm from the interface, a random network of small angle boundaries is present. The Al_2O_3 lattice, however, remains intact even at the interface.

Given the great deal of success achieved in the investigation of the model Nb/Al_2O_3 system, chosen for its good thermal expansion match, the program was extended to include the Ni/Al_2O_3 system. This system is important in two aspects: chemical reactions may occur during bonding and it has technological significance in microelectronics and composite materials. Initial reports described the development of a nickel aluminate spinel ($NiAl_2O_4$) during diffusion bonding and suggested that the presence of oxygen plays a key role in the reaction [45]. More recent microstructural evaluations [46] identified the presence of the spinel in specimens bonded at 1390 °C for 2 hr at 10^{-5} Torr, however, small amounts of residual oxygen in the vacuum may have contributed to the spinel formation. The approximately 1 micrometer thick spinel layer was found to be crystallographically related to the alumina, with close packed planes and directions being parallel. A large number of defects in the spinel were also observed, although no deformation was visible in the nickel. The presence of a critical oxygen concentration (approximately 200 ppm) for spinel formation during diffusion bonding was confirmed by Trumble through comparisons of hydrogen reduced and oxygen charged specimens [47].

Carter and co-workers [48] have developed a method for examining nickel aluminate spinel formation in a thin-film geometry while avoiding

artifacts which may be induced during TEM specimen preparation. By reacting NiO vapor with a pre-thinned alumina TEM disc at 1415 °C for 10.5 hrs, $NiAl_2O_4$ grains were produced on the surfaces and edges of the alumina [49]. Although the NiO is introduced in the vapor state, it is noted that spinel formation is a result of a solid state reaction at the alumina surface. Two different orientation relationships were obtained in these experiments:

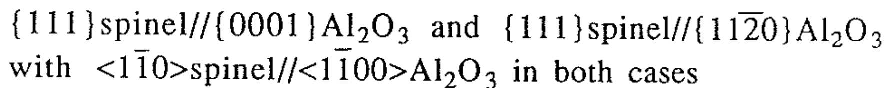

$\{111\}$spinel//$\{0001\}Al_2O_3$ and $\{111\}$spinel//$\{11\bar{2}0\}Al_2O_3$
with $<1\bar{1}0>$spinel//$<1\bar{1}00>Al_2O_3$ in both cases

In order to monitor the development of the nickel aluminate spinel phase, the previous deposition procedure was replaced by a chemical vapor deposition (CVD) process allowing NiO to be deposited at lower temperatures [50]. NiO particles were grown on single crystal, (0001) orientation, pre-thinned TEM samples via decomposition of $NiCl_2$ and H_2O, with a substrate temperature of 860 °C. A number of different orientations and morphologies were obtained for the NiO. A series of heat treatments ranging from 1120 °C to 1200 °C (minimum reaction temperature is given as 1100 °C) for 1 - 2 hours in air were used to produce the desired spinel phase. Again, various orientations were observed, with different orientations being formed at the NiO/$NiAl_2O_4$ interface (FCC/FCC) vs the $NiAl_2O_4/Al_2O_3$ interface (FCC/HCP). Close packed planes and directions were not always aligned. Special orientations may also arise for situations in which the NiO is oriented with the Al_2O_3, i.e., a (111)NiO particle on a (0001)Al_2O_3 surface.

Sparks et. al. determined orientation relationships for vacuum evaporated nickel films on basal orientation sapphire substrates as a function of substrate temperature [51]. For all temperatures reported, the close packed planes and directions were found by x-ray diffraction to be aligned, giving:

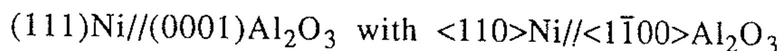

(111)Ni//(0001)Al_2O_3 with $<110>$Ni//$<1\bar{1}00>Al_2O_3$

All of the strain in the film due to the lattice mismatch, 10.3 %, was accommodated via expansion of the nickel lattice in the first few atomic layers at the interface. Note that no investigation of the defect structure at the interface was conducted. Both twin related orientations of (111) growth were determined to exist with equal probability. Morphological examinations in the SEM revealed a tendency toward island growth as the deposition rate is decreased and substrate temperature is increased. Synchrotron radiation experiments measuring the intensity of diffuse scattering from the nickel/alumina interface demonstrated a moderately rough interface, although no direct microstructural observations were given.

As an alternative to elevated temperature deposition, ion bombardment can be used to modify the characteristics of a film/substrate interface. Baglin et. al. [52] used a 500 eV argon ion beam to pre-sputter an alumina substrate prior to evaporation of a copper film. Bonds significantly stronger than those achieved by simple evaporation were produced and remained stable to temperatures of 500 °C. No reaction layer was found, however, XPS results obtained *in-situ* following sub-monolayer copper deposition indicated a ternary bonding environment of Cu, Al and O. Typical epitaxial relationships (close packed planes and directions parallel) were obtained for 500 °C deposition, although no analysis was given for films grown at room temperature. In addition, no films were grown under concurrent ion bombardment during deposition.

Interfacial reactions during co-sintering of copper/glass-ceramic composites were studied by Risbud, Kriven and co-workers [53, 54]. For samples produced at 800 °C, no reaction zone was formed, but copper diffusion extended up to 120 μm. At 1000 °C, a pink reaction zone was found and attributed to metallic copper precipitates.

To briefly summarize the information concerning metal/ceramic interfaces, it is known that a nickel aluminate spinel phase can form in the nickel/alumina system but requires elevated temperature and possibly the presence of oxygen. For vapor deposited films, orientation relationships develop with close packed planes and directions parallel. Lastly,

significant improvements in film adhesion can be attained via medium energy (500 eV) pre-deposition sputtering.

B.3. Mechanical properties

With the increasing number of applications of metal/ceramic systems comes a concern for their reliability. Components are often produced at elevated temperatures and are subject to thermal cycling, resulting in significant thermal stresses. In order to predict the response of metal/ceramic systems, fracture mechanics concepts are being implemented to define stress states, failure criteria, and the pertinent materials parameters involved.

The most extensive investigation into the area of mechanical properties of metal/ceramic interfaces is being conducted by A. G. Evans and his co-workers. Initial experiments were performed by placing Vickers indentations at various points across a niobium/alumina interface [55]. Examination of the indents following an 80 MPa load/unload cycle, with the indented surface in tension, revealed that only cracks near the interface exhibited significant growth. Following the initial mechanical cycle, the specimens were loaded to failure. Failure was determined to initiate from cracks in the alumina which became unstable and grew rapidly. These unstable cracks were then attracted to the interface and propagated in a brittle manner. Note that cracks which terminated at the interface or grew in a stable manner exhibited crack tip blunting and never initiated failure. Because the plasticity of the niobium decreases as crack velocity increases, only rapidly growing cracks could continue to propagate once attracted to the interface by the stress field. Fracture was thus generally not interface limited, but related to crack instability in the ceramic. Strain energy release rate calculations, in addition to the indentation experiments [56], revealed enhanced crack growth near edges, suggesting that bond strength may be controlled by flaws in close proximity to the specimen edges.

Flexural (three and four point bend) testing of alumina/niobium/ alumina composites with notches at one interface on the tensile surface (Fig. 5) was used to examine their fracture behavior [57]. Bond strength

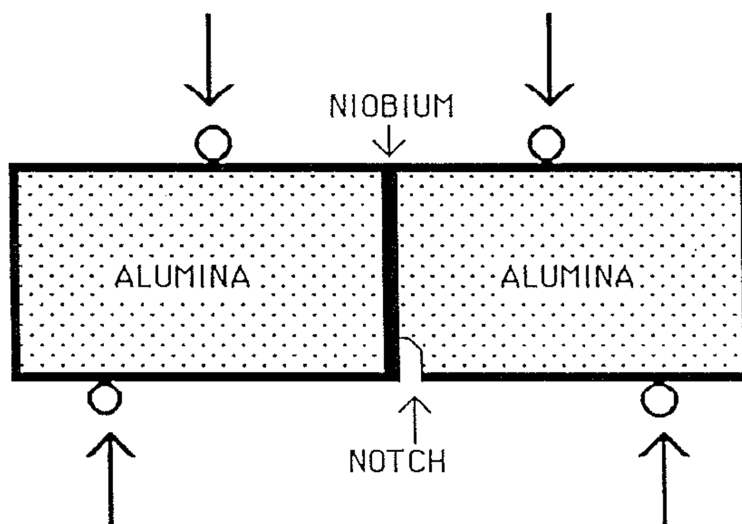

Figure 5: Schematic diagram of four point bend fracture toughness determination geometry

was characterized by the interface fracture energy, an energy balance for the creation of new surfaces. The contribution of the reversible work of adhesion to the interface fracture energy was shown to be small (<10 %); with the major contributions being the plasticity in the metal and irreversible energy dissipation in the ceramic. Crystallographic orientation dependence of the fracture energy was reported to be due to changes in the work of adhesion. Although the work of adhesion was a relatively small contribution, continuum mechanics analyses indicated that the interface fracture energy was directly dependent upon it.

The strength of composites consisting of two alumina blocks bonded at elevated temperatures with a thin (25 - 250 μm) platinum foil was investigated by Dalgleish et. al. [58] using four point bending tests. Indications were that failure (separation) at the interface is sensitive to the platinum layer thickness, while failure in the ceramic is not. Theoretical calculations by Cao et. al. [59] were carried out for samples described above in order to determine the magnitudes of the stresses at or near the interface and interpret trends in the bond strength. No unique trends were observed for the data, demonstrating the importance of determining the dominant fracture characteristics for the system in question. Two interesting results were obtained from this analysis, however. Metals with high thermal expansion coefficients were shown to suppress fracture at specimen edges and metals with low yield strengths could generate bonds sufficiently strong such that failure occurred in the ceramic.

An alternative method to produce a strong metal/ceramic bond is the use of extrinsic toughening mechanisms. Rather than optimizing the intrinsic toughness of the system via microstructural and processing control as in the case of the previous investigations [55-59], Oh et. al. [60] examined the effects of controlled interface geometries which induce crack deflection and bridging, enhancing toughness. Photolithographic techniques were employed to produce pore channels in one substrate, which was subsequently coated with a thin metallic film and diffusion bonded to a second substrate (Fig. 6). By modifying the specific configurations, either crack deflection or crack bridging could be made the

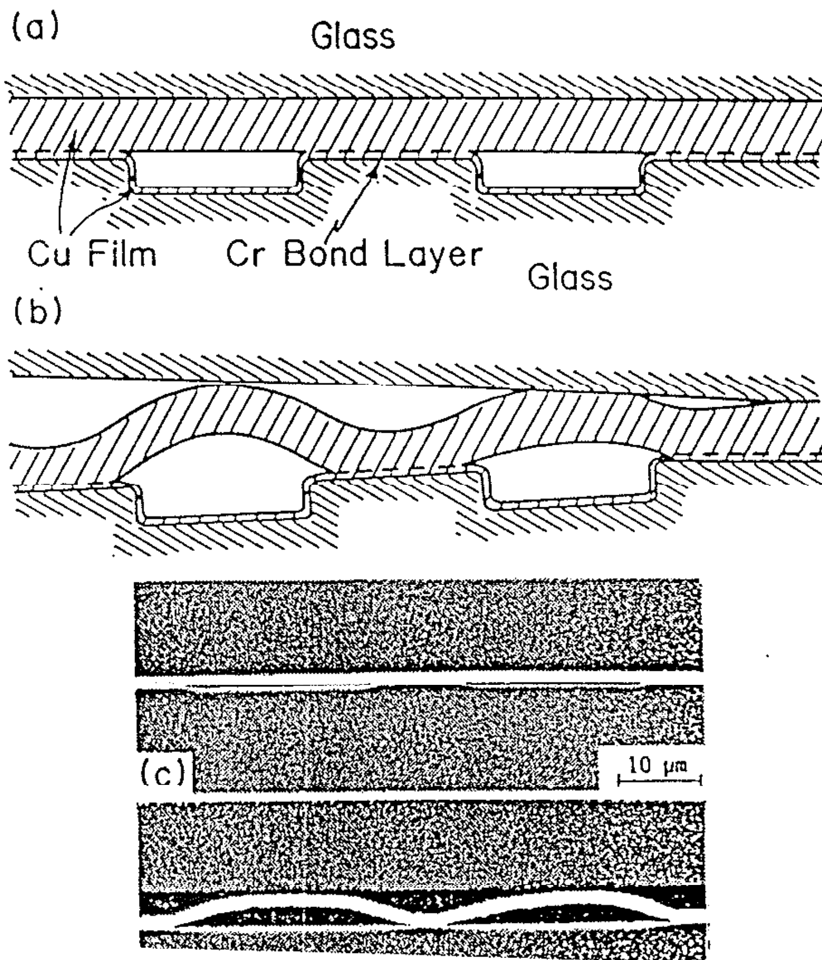

Figure 6: Patterned interface showing controlled microcrack/void geometry [60]

dominant toughening mechanism. Fracture toughness was shown to dramatically increase due to crack bridging by plastic deformation of the bulged segments of the copper film.

Recently, more effort has been put forth into understanding metal/ceramic interface strength for thin-film geometries. Initial investigations into trends in adhesive behavior of thin films as a function of processing were conducted by Chiang et. al. [61]. Vickers hardness indents were placed in the film/substrate system, normal to the film surface. Propagation of lateral cracks, parallel to the interface, was taken as the measure of adhesion. Crack formation was assumed to occur at the interface; if this was not the case, the interface fracture toughness was determined to have a toughness at least as large as the weaker component. In addition, preliminary data demonstrating the quantification of fracture toughness using a model for lateral crack extension was presented.

Evans et. al. have analyzed the decohesion behavior of thin films on both brittle and ductile substrates from an experimental [62, 63], as well as a theoretical [64] point of view. Numerical analysis based upon thin films on substrates, with the film having a larger thermal expansion coefficient - resulting in a residual tension in the film - were conducted using finite element methods. Two major results were derived from the calculations. Cracks were found to seek a path such that K_{II} (the shear component of stress intensity) was equal to zero. For the case of high modulus films, the cracks propagated in the substrate (subsurface to the interface) where decohesion of the film was then determined by the fracture resistance of the substrate. Cracks in low modulus films were attracted to the interface, making the interface strength the important parameter. Also, the presence of a critical film thickness, below which complete film decohesion is inhibited, was identified.

Experimentally, for the case of brittle films on brittle substrates [63], films decohered by initial decohesion along the interface for a distance approximately twice the film thickness, followed by a deviation of the crack into the substrate (4 - 5 film thicknesses below the interface) and propagation parallel to the interface. This crack propagation depth was shown to be consistent with the $K_{II}=0$ criterion. When ductile substrates

were considered [62], maximum film cracking resistance was obtained for systems in which the substrate yield strength was high and the film was very adherent. If substrate yield strength was low, film cracking was enhanced but interfacial failure (crack propagation along the interface) was minimized due to plastic deformation of the substrate blunting the crack tip. The end result was isolated islands of film remaining attached to the substrate. Interfacial failure (decohesion) was promoted by high substrate yield strength and low fracture toughness interface phases. It was also noted that further microstructural correlations are required in this area, as are more detailed investigations into crack initiation.

A completely independent analysis of interface delamination in the SiC/Si and SiC/carbon fiber systems was conducted by Argon et. al. [65]. When a critical thickness was exceeded, the SiC coatings were observed to spontaneously disbond from the substrates due to residual stresses. The analysis of this delamination phenomenon was used to determine the intrinsic toughness of the interface. Note that this method is limited to sharp interfaces whose fracture toughness is less than that of either component, confining crack propagation to the interface.

Although models for the mechanical properties of metal/ceramic interfaces have become quite sophisticated in recent years, some limitations still exist; especially for the case of thin films. The fracture mechanics analyses all treat the film as a continuum when, in reality, the morphological features may play a leading role in mechanical response. Crack initiation is also not considered in many cases. Further understanding of the early stages of disbonding would be extremely beneficial in the preparation of high quality films. At this stage, it is uncertain as to how fracture mechanics concepts may be applied to actual composite interfaces.

III. EXPERIMENTAL PROCEDURE

A. Deposition

All films examined in the current investigation were grown using the ion plating facility of the Construction Engineering Research Laboratory (CERL), operated by the United States Army Corps of Engineers and located in Champaign, Illinois. The ion plating system is a water-cooled, split chamber design, allowing easy access to the interior (Fig. 7). Vacuum seals are made via rubber O-rings. A baffle plate, located at the level of the electron beam hearths, maintains the pressure differential required to support a glow discharge while protecting the gun filaments. The chamber interior is covered with fresh aluminum foil, which is then coated with film material prior to each series of deposition runs in order to prevent cross-contamination and facilitate clean-up. A 0.15 m and a 0.25 m diffusion pump working in parallel, backed by a single rotary pump, evacuate the system to a base pressure of 10^{-6} Torr. Dual electron beam evaporation sources allow deposition of compound and multilayer films, as well as providing redundancy in the case of single element deposition. Working gas is introduced via individual mass flow controllers, with the argon passing through a purification furnace prior to entering the chamber. The system is also equipped with a residual gas analyzer to monitor reaction efficiency during reactive ion plating, as well as monitor vacuum conditions and working gas purity. Glow discharges can be ignited by applying either a DC or an RF bias to the substrate holder, which is water-cooled to stabilize the substrate temperature.

Typical DC operating conditions consisted of a ten minute sputter cleaning cycle with discharge parameters of 2.0 kV and 1 mA; followed by 30 to 60 minutes of nickel evaporation, with or without a discharge. Background pressure was kept at approximately 20 millitorr of argon. For RF films, substrates were sputter cleaned for 10 minutes in a 50/50 mixture of argon and oxygen, compensating for the preferential sputtering of oxygen from the alumina. Deposition was conducted in either a pure argon or 3:1 oxygen:argon working gas environment. Glow discharge

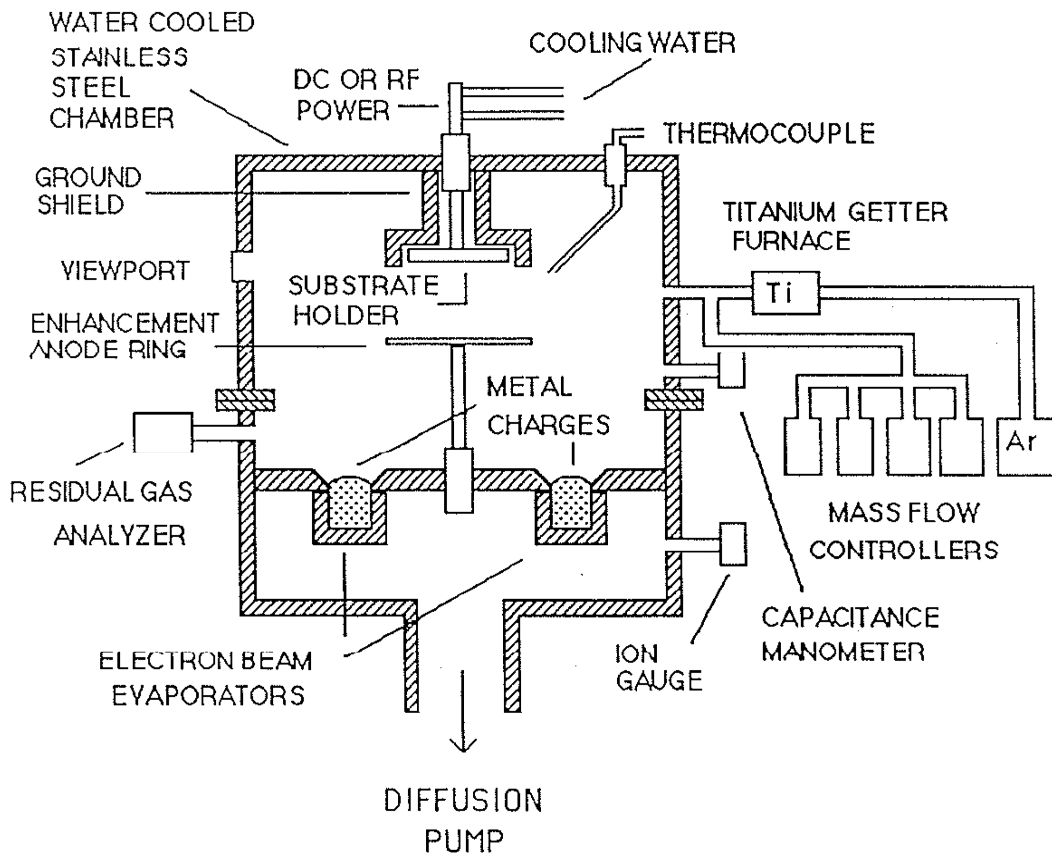

Figure 7: Schematic diagram of the USA-CERL ion plating system

conditions were maintained at a 1.0 kV potential difference with a power density of 2.5 W/cm^2. Post-deposition thermal treatments were carried out using two different methods: either in a vacuum furnace, or by encapsulating the sample in an evacuated quartz tube and placing it in a box furnacc.

B. Materials

Source material for the nickel films was 99.95% pure pellets, consolidated by electron beam melting in the ion plating system. Cordierite substrates were obtained as polycrystalline tiles, crystallized from glass with the nominal composition of $2MgO - 2Al_2O_3 - 5SiO_2$. Surfaces were polished using standard practices to an average background roughness of 25 nm (Fig. 8). Polycrystalline aluminum oxide substrates were used in the as-received condition, having a loosely sintered surface morphology (Fig. 9). Single crystal (0001) orientation (Fig. 10) sapphire substrates with optically smooth surfaces, obtained from Adolph Meller Co. [66], were also used in the as-received condition.

C. Microanalysis

Microanalytical characterization of the film/substrate composites comprised the major portion of this research program. Film morphology was evaluated from fracture sections examined in an ISI-DS 130 dual stage scanning electron microscope (SEM), equipped with a Tracor Northern energy dispersive spectroscopy (EDS) analysis system. SEM, however, could not provide any information concerning the nature of the interface, thus placing the primary emphasis on transmission electron microscopy (TEM) analysis. All composites were examined in cross-section in the TEM (XTEM) allowing direct observation of the structure, crystallography, and chemistry of the film, substrate and interfacial regions. XTEM analyses were conducted using Philips EM 400, EM 420 and EM 430 TEMs with EDAX EDS systems, and a Vacuum Generators HB-5 STEM with a Kevex EDS system. Although XTEM possesses superior resolution and can provide

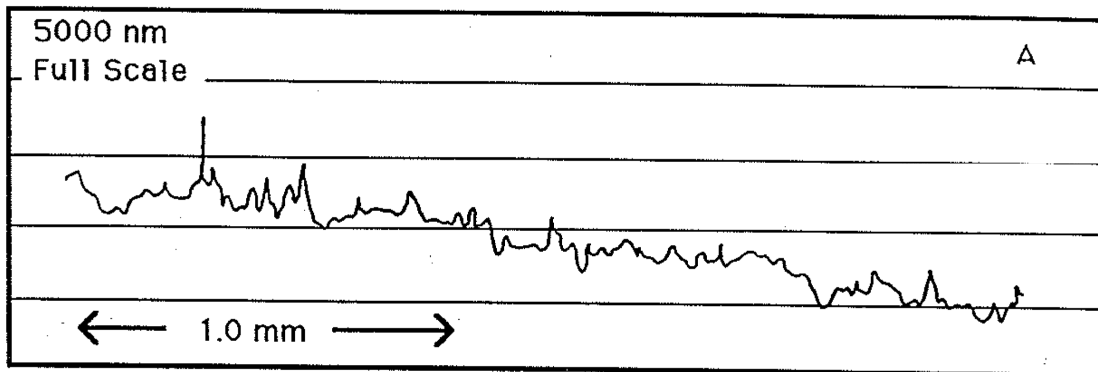

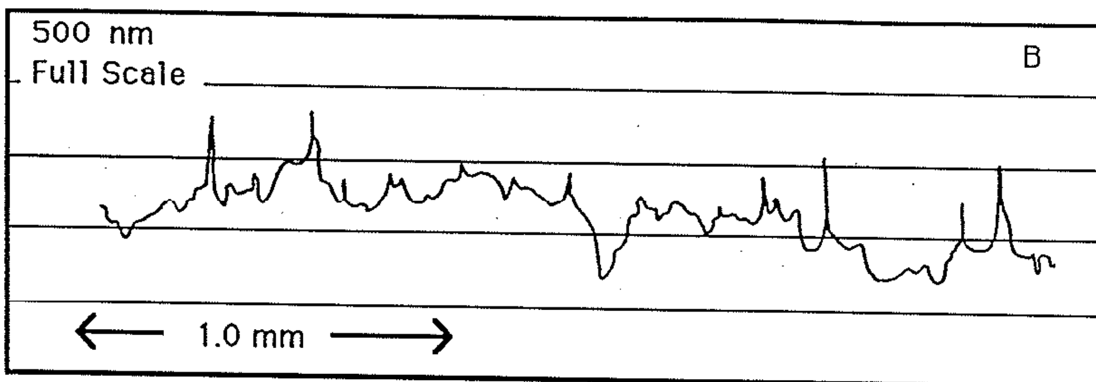

Figure 8: A) Surface profile of as-received cordierite
B) Surface profile of polished cordierite

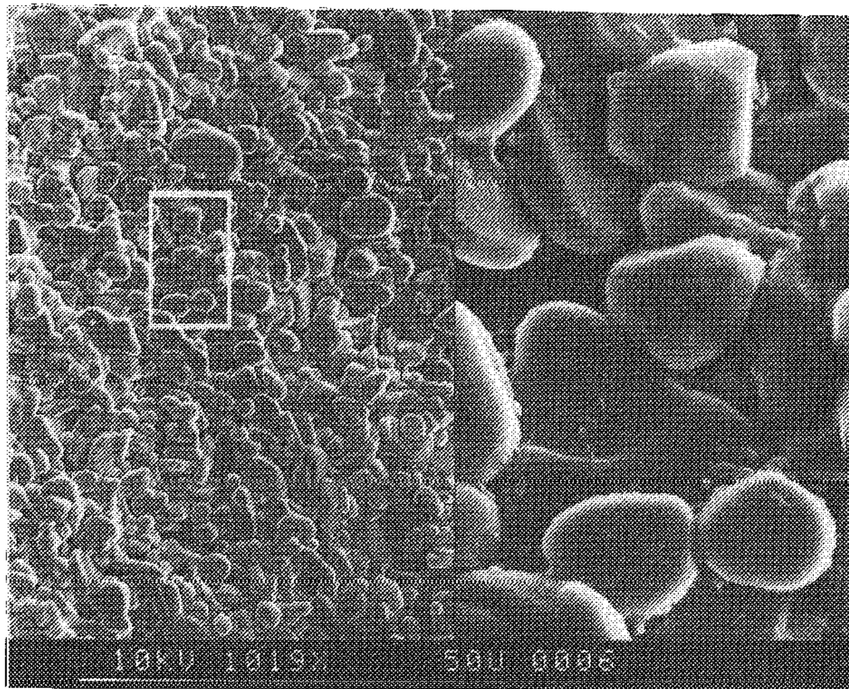

Figure 9: Surface morphology of as-received polycrystalline aluminum oxide substrates

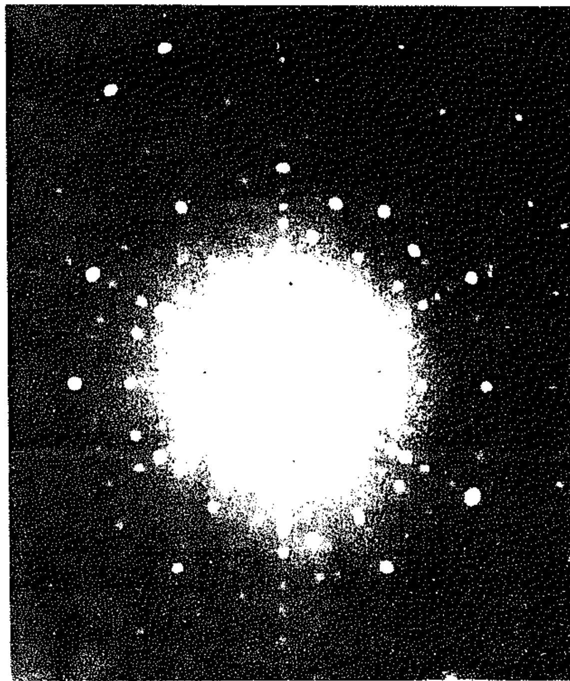

Figure 10: X-ray diffraction Laue pattern of sapphire substrate showing [0001] zone axis (basal orientation)

local crystallographic information, its major obstacle is the difficulty in specimen preparation. In response to this limitation, a variety of novel preparation techniques were devised and refined in-house during the course of this investigation. The basic principle behind these techniques is the sandwiching together of two or more substrates, with the film sides in contact, as introduced by Bravman and Sinclair [67]. Original specimens were encased in an epoxy-filled stainless steel tube and sectioned (Fig. 11). Since the substrates were held in place only by a thin layer of epoxy and the circumferential stress provided by the stainless steel rim, this method was modified to increase specimen stability. In the improved geometry, the sandwich assembly is sectioned, polished on one side, and mounted (polished side down) onto a molybdenum TEM grid with a 1.0 mm diameter hole (Fig. 12). The grid provides complete support without introducing any stresses to the system. Hardman two-component epoxy (double-bubble green) was used for all filling and bonding steps due to its strength and durability under ion and electron bombardment conditions [68]. In both preparation schemes, once the specimens are assembled (sectioned from the tube or mounted on the grid) they are flattened and dimpled using a standard VCR instruments model D400 dimpler. Samples were ion milled to perforation in a Gatan model 600 ion mill, using a liquid nitrogen cooled stage and reduced energy (4 kV) to minimize ion induced damage. Both stationary and limited sector milling, preventing milling parallel to the interface, were tried in order to overcome sputter yield differences between the film and substrate, but did not show any significant benefit and were discontinued. Finally, a thin carbon layer, <10 nm, was deposited onto the sample surfaces to provide electrical conductivity in the TEM. Specimens were imaged using conventional bright field and dark field techniques, although micrographs were taken with the substrate on a zone axis rather than in a two-beam condition in order to ensure the plane of the interface is parallel to the beam direction. Specimens were also inserted into the TEM with the interface perpendicular to the stage axis so that no geometrical artifacts were introduced when tilting to acquire an EDS spectrum. In addition to EDS in the electron microscope, chemical information was obtained using Auger

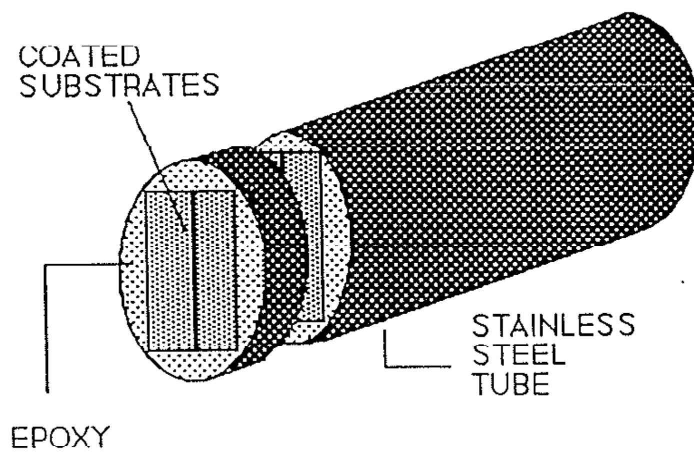

Figure 11: Geometry of original epoxy-filled tube XTEM specimen preparation method

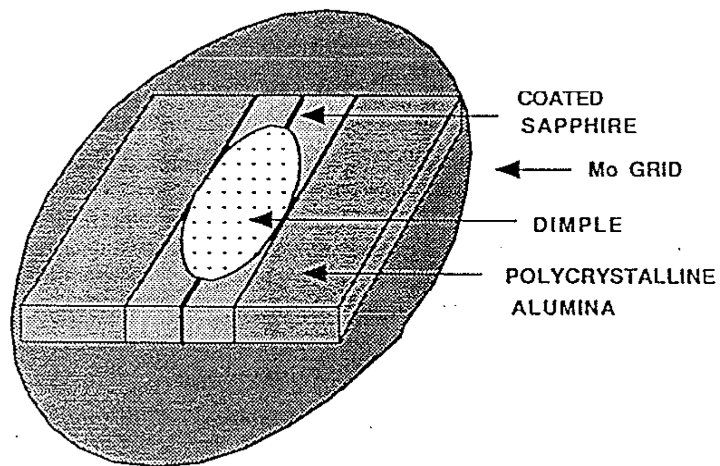

Figure 12: Specimen/molybdenum grid XTEM configuration

electron spectroscopy (AES). The primary function of AES for this investigation was to provide a qualitative comparison of interface widths by recording composition vs depth profiles taken through the composite. AES also provided a means of examining the oxygen content in the case of oxide films, a feature not available with standard EDS.

D. Mechanical properties

Mechanical properties in the nickel/cordierite system were evaluated by measuring film/substrate adhesion using an epoxy-based tensile test. In this commercially available test fixture [69], an epoxy-impregnated aluminum pin is bonded to the film surface and subsequently removed under load conditions approximating pure tension. For the nickel/sapphire system, Vickers microhardness indents were placed through the film into the substrate. Crack propagation and film disbonding around the indent were taken as an indication of film/substrate adhesion. Use of a "nano-indenter" mechanical properties microprobe [37] was also attempted on the nickel/sapphire system. Films were indented, obtaining hardness vs depth profiles, both in plan view and in cross section. The two geometries were thought to provide hardness information in a manner analogous to obtaining chemical information via depth profiling in an Auger and by EDS point analysis in a STEM.

IV. RESULTS

Results in the following section are organized in primarily a chronological fashion, paralleling the evolution of the research program through the various material systems involved. Each system is given its own subsection, with data from each analytical technique (SEM, XTEM) grouped together within the subsections. In the upcoming discussion section (section V), the organization follows along phenomenological guidelines, with further subdivisions for each material system.

A. Nickel/cordierite

Figure (13) contains alpha-step surface profiles of polished cordierite substrates before and after DC sputter cleaning. Although a DC glow discharge was used with an insulating substrate, which generally results in build-up of a surface charge and decreased sputtering, particle bombardment was sufficient to alter the topography of the substrate surface. The larger defects (pits) in the polished surface remain, but the finer protuberances have been smoothed out. A consequence of using the less intense DC (as compared to RF) discharge is the redeposition of contaminants sputtered from other portions of the chamber. Stray particles from the glow will cause sputtering from adjacent fixtures and if this flux is significant in relation to the sputtering rate from the substrate, contamination can result. This was demonstrated by the Auger surface survey taken from a substrate which was only sputter cleaned (Fig. 14). Copper from the surrounding areas of the chamber was found in significant amounts on the uncoated substrate surface. These problems were minimized with an RF discharge which resulted in a higher sputtering rate at the substrate and was also visually observed to be more localized.

Table I shows processing parameters and as-deposited adhesion data for the nickel/cordierite composites. As seen in the table, optimal film/substrate adhesion was obtained for films grown on sputter cleaned substrates without the use of an applied bias during deposition. Although failure load values are presented here, it is instructive to note that these

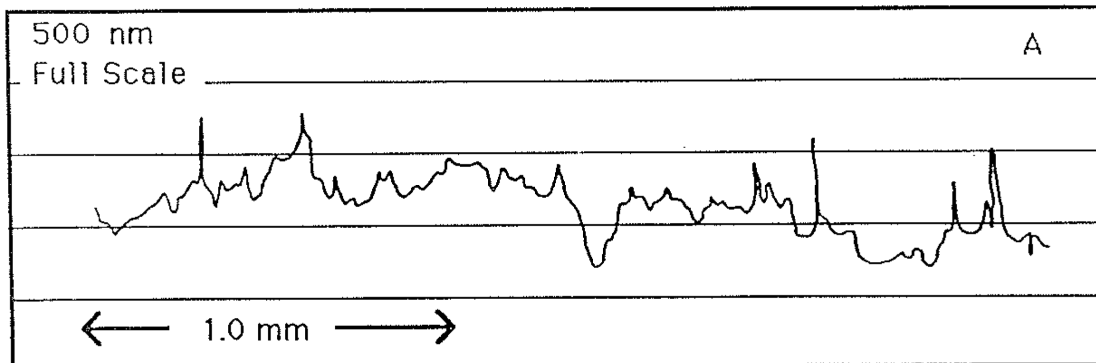

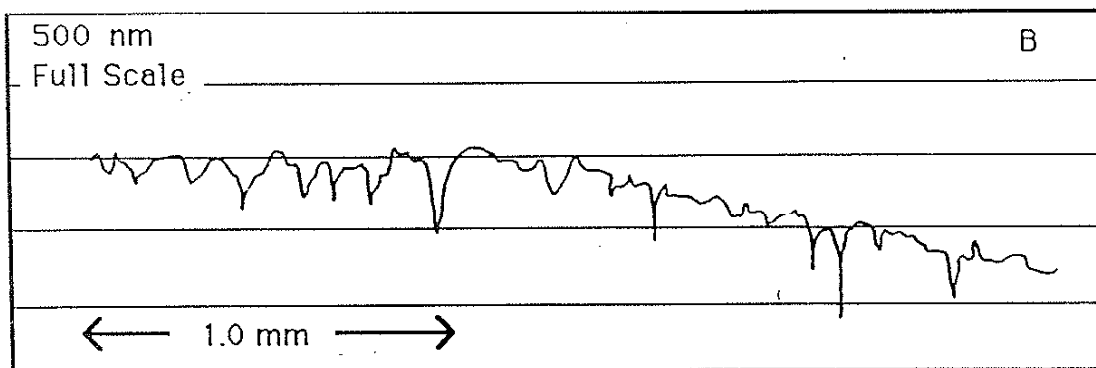

Figure 13: A) Surface profile of polished cordierite
B) Surface profile of polished and sputter cleaned cordierite

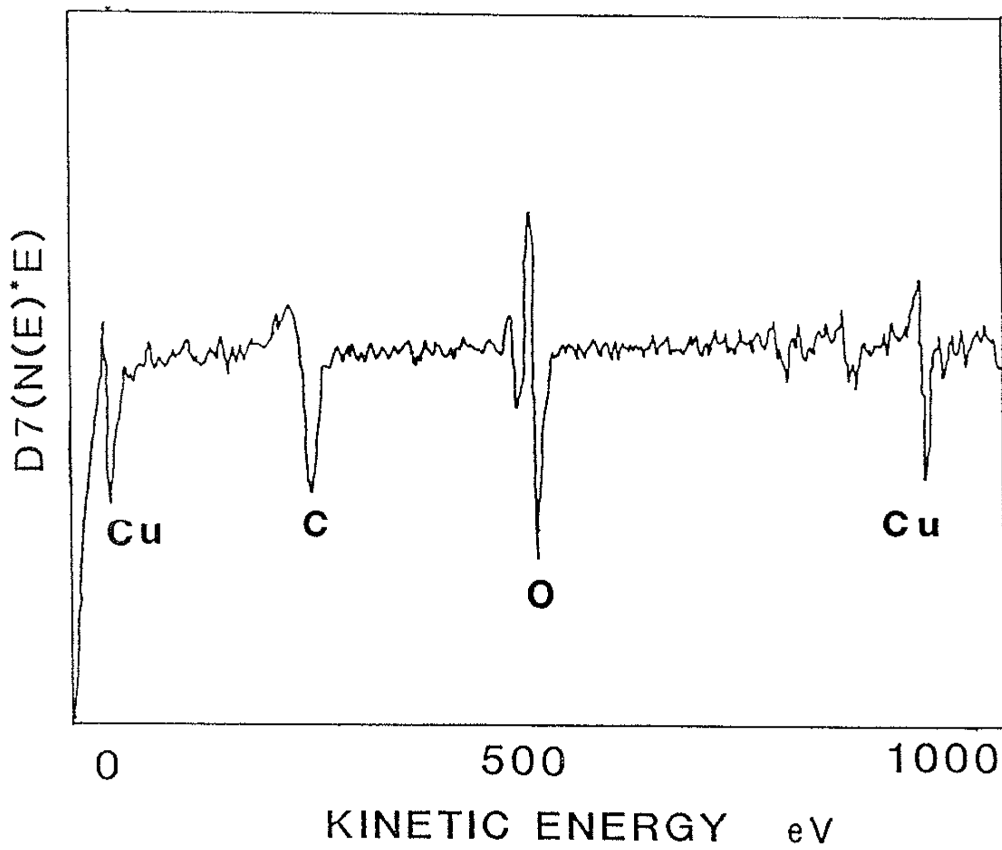

Figure 14: Auger electron spectroscopy survey of a sputter cleaned cordierite surface

Series	Applied Bias (DC)	Sputter Clean	Failure Mode	Failure Load (MPa)
II	0.0 kV	No	Ni/Cord	4.88
	2.0	No	Ni/Cord	27.44
	4.0	No	Mixed	38.02
III	0.0 kV	Yes	No Fails	71.02
	2.0	Yes	Ni/Cord	18.96
	3.0	Yes	Ni/Cord	9.79
IV	0.0 kV	No	Ni/Cord	7.65
	0.0	Yes	Mixed	61.16
	3.0	No	Mixed	53.44
	3.0	Yes	Ni/Cord	28.20

Table I: Specimen parameters and as-deposited adhesion data, Nickel/cordierite

are for comparison only, and that the more relevant indicator is the mode of failure. "Ni/Cord" represents a failure at the interface, while "mixed" indicates failure both at the interface and in the epoxy. Table II contains heat treatment and corresponding failure data for films tested after a thermal cycle (400 °C peak temperature, 45 minutes total time). Although the ion plated (plasma-assisted) films grown on non sputter cleaned substrates maintained a portion of their original strength when cycled in argon, only the evaporated (zero bias) film on the sputter cleaned substrate (the case of maximum as plated adhesion) retained significant mechanical integrity upon cycling in a reducing atmosphere.

A dark field XTEM image, taken with a portion of the polycrystalline nickel diffraction pattern, of a film deposited on an as-polished (non sputter cleaned) cordierite substrate, with a 2.0 kV applied bias, was used to demonstrate the morphology of the film (Fig. 15). The morphology was columnar, with each column consisting of multiple, randomly oriented grains. The presence of an "altered" layer in the substrate, as seen by changes in contrast in the micrograph and attributed to ion bombardment, was also noted. Bright field XTEM of the most adhesive film (0.0 kV, sputter cleaned) again showed a typical columnar morphology, although some porosity was present between columns (Fig. 16). A modified ceramic surface layer, which appeared as a dark band at the film/substrate interface in the bright field micrograph, was shown by EDS (Fig. 17) to contain both film and substrate elements. This layer, identified as being cordierite via bright field/dark field imaging techniques, was thought to provide the excellent mechanical strength of the composite as a result of the formation of a chemically mixed interface region.

B. Nickel/alumina

Because the compositional inhomogeneity and structural instability of the cordierite substrates did not allow detailed interfacial characterization, work was begun using polycrystalline alumina substrates. Evaluation of the mechanical properties of these films via the tensile adhesion test proved unsuitable due to the uncertainty in the contact area

Series	Applied Bias (DC)	Sputter Clean	Atmosphere	Failure Mode	Failure Load (MPa)
II	0.0 kV	No	100 % Argon	Ni/Cord	0.00
	0.0	No	10 H_2 - 90 Ar	Ni/Cord	0.00
	2.0	No	100 % Argon	Ni/Cord	8.89
	2.0	No	10 H_2 - 90 Ar	Ni/Cord	0.69
	4.0	No	100 % Argon	Ni/Cord	8.14
	4.0	No	10 H_2 - 90 Ar	Ni/Cord	0.00
III	0.0 kV	Yes	10 H_2 - 90 Ar	Mixed	41.80

Table II: Specimen parameters and thermally cycled adhesion data, Nickel/cordierite

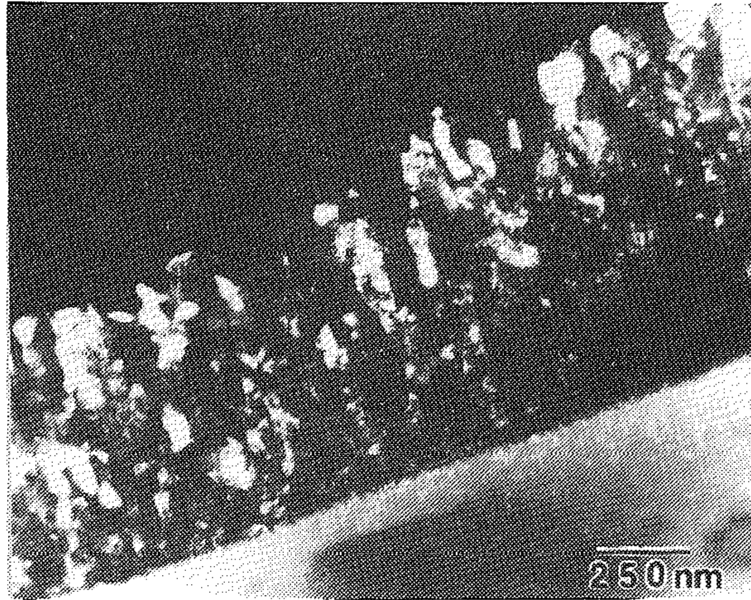

Figure 15: XTEM dark field micrograph, Nickel/cordierite, 2.0 kV, No sputter cleaning

Figure 16: XTEM bright field micrograph, Nickel/cordierite, 0.0 kV, Sputter cleaned

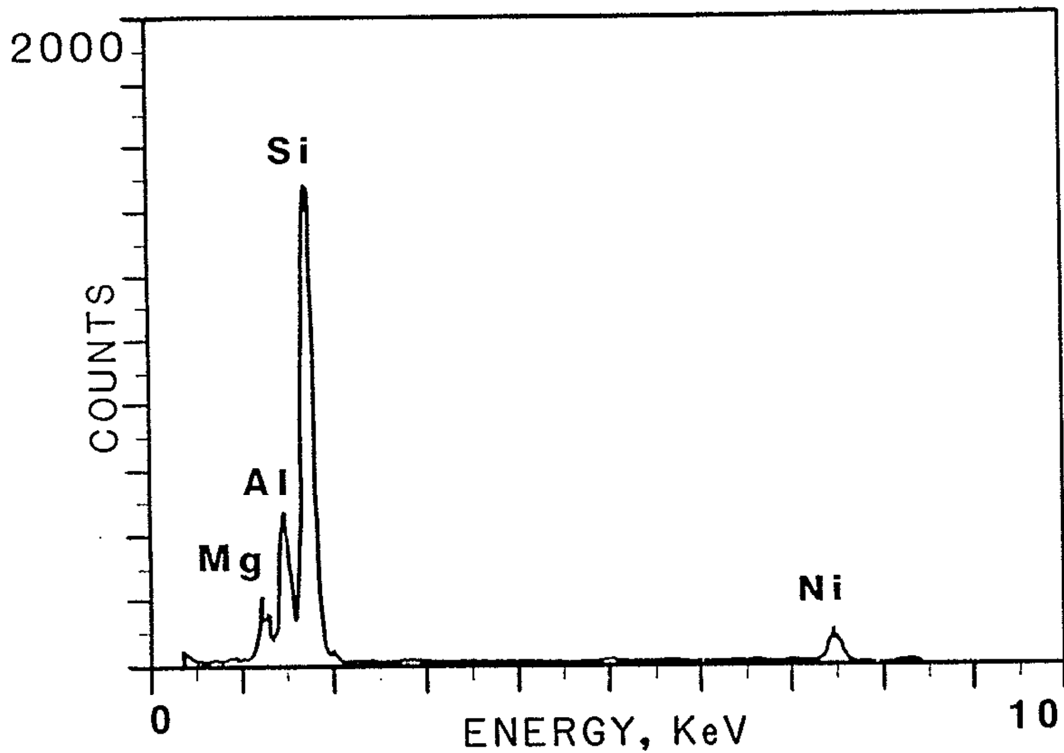

Figure 17: EDS spectrum from interface (dark band), Nickel/cordierite, 0.0 kV, Sputter cleaned

arising from the uneven substrate surface morphology. The adhesion of the surface "nodules" was also in question. XTEM analysis of a nickel/alumina composite (Fig. 18), deposited without an applied bias or sputter cleaning, showed the absence of an interface reaction phase. Film morphology was polycrystalline and columnar, consistent with observations of 0.0 kV films in the nickel/cordierite system. In addition, film growth was shown to conform to the curvature of the surface nodules. Annealing in a vacuum (900 °C, 12 hrs.) caused complete recrystallization of the film, eliminating all traces of the as-deposited morphology, but did not result in a reaction product at the interface as indicated in the XTEM bright field micrograph (Fig. 19). The analysis, however, was impeded by the topography of the substrate and the partial disbonding of the film, most likely due to the recrystallization of the film during the heat treating process, which contributed to the formation of a discontinuous interface.

C. Nickel/sapphire

C.1. As-deposited

In order to eliminate substrate surface irregularities and also introduce the possibility of producing epitaxial films, growth was initiated on optically smooth, single crystal sapphire substrates. Growth conditions for these films are summarized in table III. SEM analysis of the film deposited under conventional high vacuum evaporation conditions (no working gas, no bias, series IA) indicated a reasonably dense columnar morphology. However, as indicated by the curling and subsequent disbonding of the film from the substrate, along with cracking in the film evident in the SEM micrograph, the residual tensile stress in the system was large compared to the interfacial strength (Fig. 20). Metallic nickel films deposited with an RF bias exhibited a rather unique and complex morphology. The SEM micrographs of figure (21), representing specimens grown under similar conditions approximately two years apart, confirmed the reproducibility of this unusual growth behavior. Initial growth was by island formation, with the islands impinging upon one another with time. A scanning electron micrograph of a film deposited for a longer period of

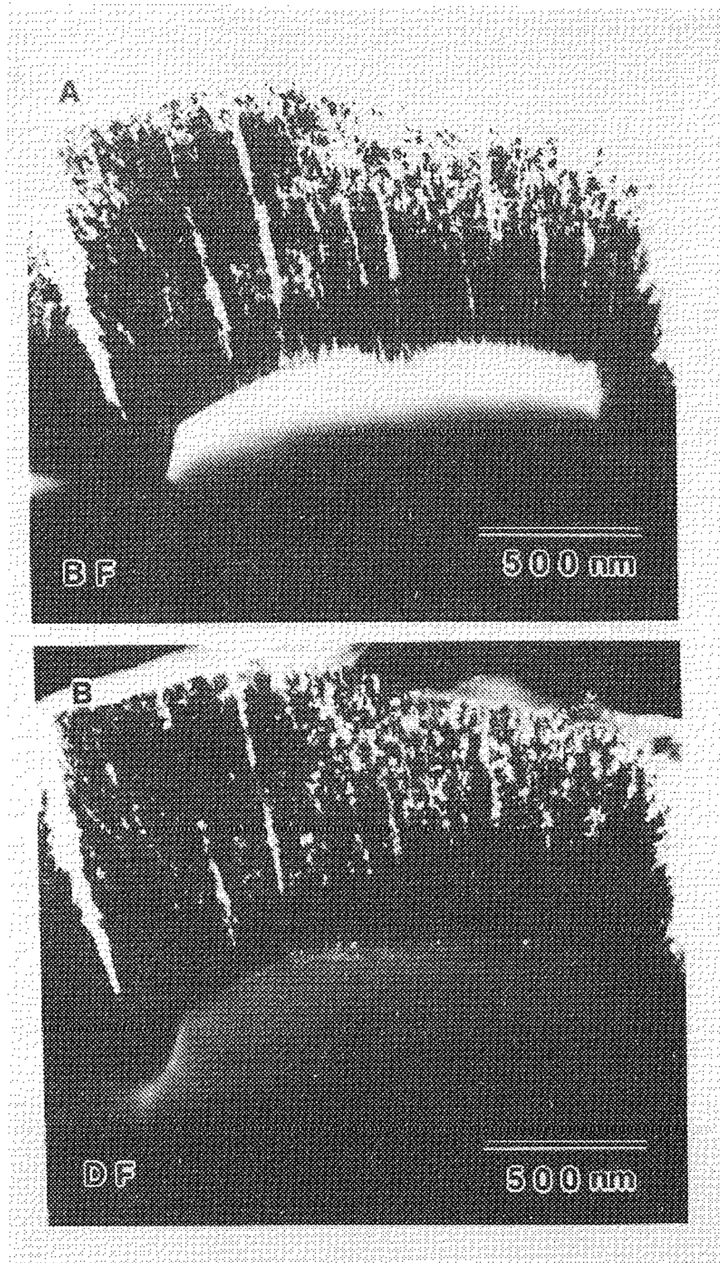

Figure 18: XTEM micrographs, Nickel/alumina, 0.0 kV, No sputter cleaning, As deposited
A) bright field
B) dark field

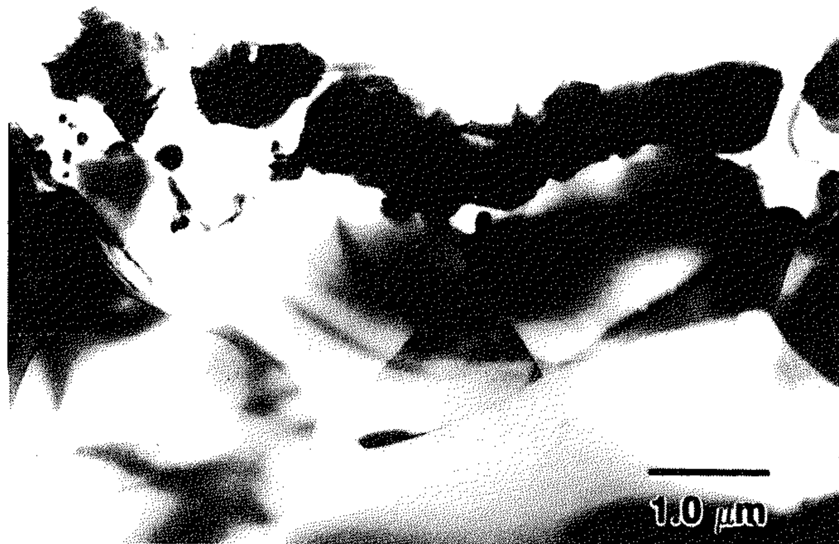

Figure 19: XTEM bright field micrograph, Nickel/alumina, 0.0 kV, No sputter cleaning, Annealed, 900 °C, 12 hrs.

RF Series		Sputter clean	Applied bias (RF)	Working gas	Deposition time (min)
I	A	No	No	None	30
	B	Yes	Yes	Argon	20
II	A	Yes	No	Argon	30
	B	Yes	Yes	Argon	30
	C	Yes	Yes	Oxygen/ Argon	30
III	A	Yes	Yes	Argon	10
	B	Yes	Yes	Argon	45

Table III: Specimen parameters, RF Nickel/sapphire

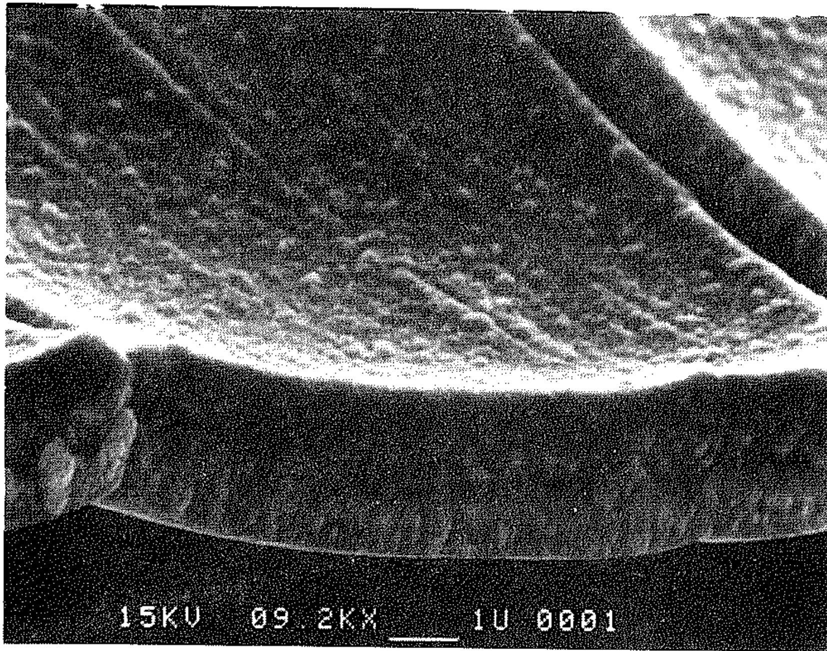

Figure 20: SEM fracture section, Nickel/sapphire, UHV deposition, RF series IA

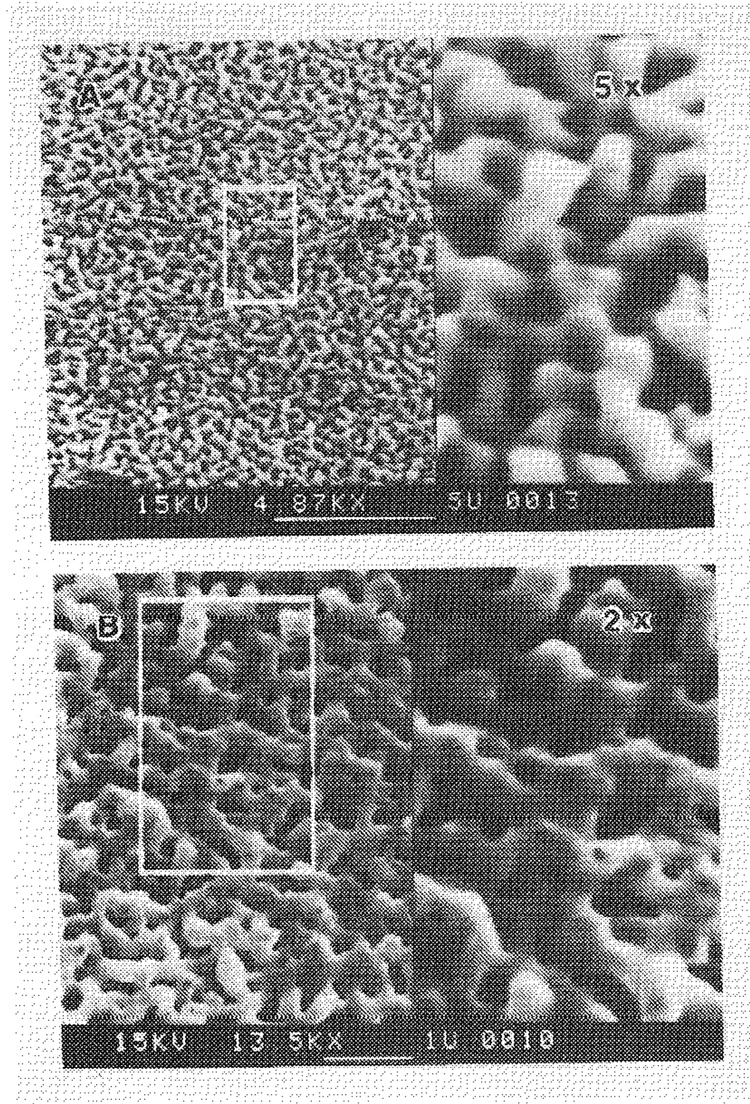

Figure 21: A) SEM micrograph, Nickel/sapphire, RF series IB
B) SEM micrograph, Nickel/sapphire, RF series IIIA

time revealed the progression in morphology; with island coalescence completed and the appearance of a second layer of grains, preferentially nucleated at polishing scratches (Fig. 22). The bi-layer morphology was again documented by a subsequent deposition series. The SEM investigation clearly demonstrated the growth of the original islands into a fully dense layer, with second layer particles forming on the new surface (Fig. 23). When oxygen was introduced into the RF glow discharge during deposition, the resultant nickel oxide film reverted back to a columnar morphology, as seen in the SEM micrograph (Fig. 24).

Mechanical properties of the nickel/sapphire composites were qualified by examining the resistance to film disbonding upon application of a load by a Vickers indenter. Figure (25) shows scanning electron micrographs of an indent, made with a 700 g load, in an evaporated nickel film. Cracks were evident in the composite, with a portion of the substrate being ejected, however, no film disbonding occurred. No disbonding was also observed in the plasma-assisted films, with cracks propagating subsurface (in the substrate) and the interface remaining intact (Fig. 26). The propagation of lateral cracks in the substrate and the lack of any film/substrate disbonding suggested the presence of a high toughness interface. This behavior was contrasted by that of the oxide films (Fig. 27). The indent induced cracks propagated along the film/substrate interface, as evidenced by the removal of portions of the film, leaving the original substrate surface exposed. No lateral cracking was seen in the substrate for the case of the oxide films.

The most revealing look at the composites was provided by XTEM. XTEM of the evaporated film confirmed the expected columnar morphology and demonstrated the random crystallographic orientation of the columns (Fig. 28). Some separation was observed between columns due to the lack of ion bombardment during deposition, while the inset SADP of figure (28) corresponded to that of a film consisting of multiple, randomly oriented grains. A limited damaged (structurally) zone, represented as a darker region below the interface and resulting from ion bombardment during the sputter cleaning cycle, was also identified.

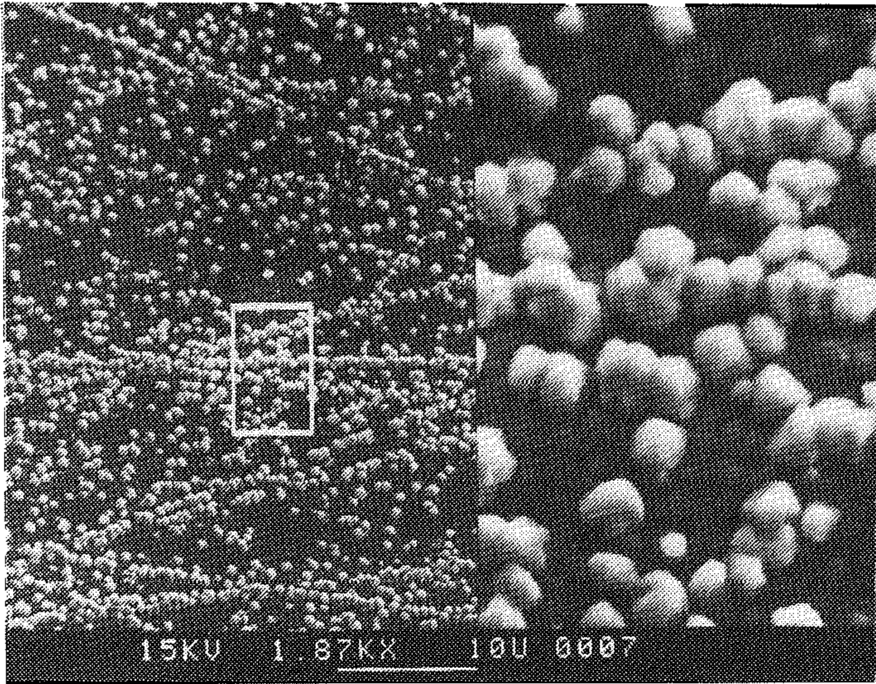

Figure 22: SEM micrograph, Nickel/sapphire, RF series IIB

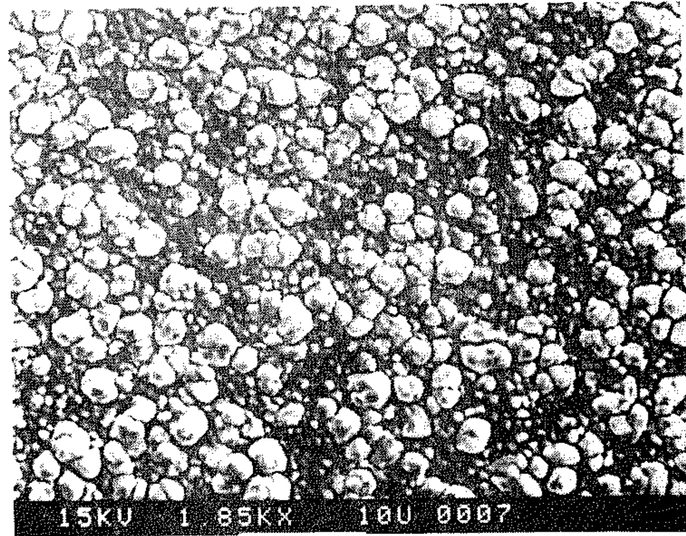

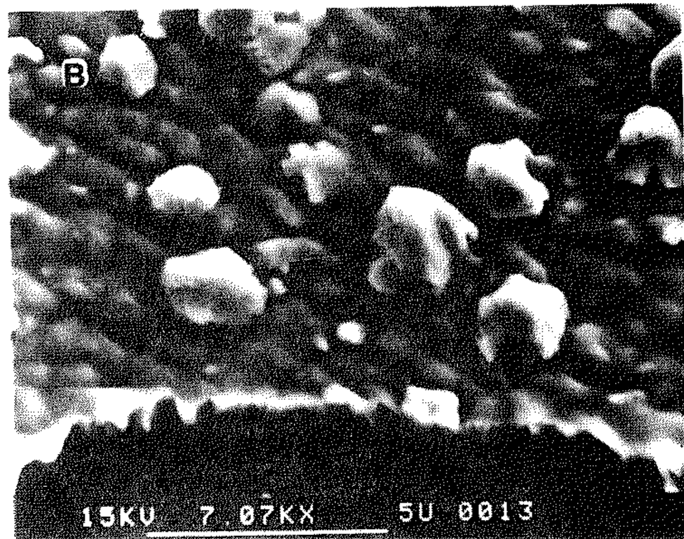

Figure 23: SEM micrographs, Nickel/sapphire, RF series IIIB
A) Surface view, Low magnification
B) Fracture section, Higher magnification

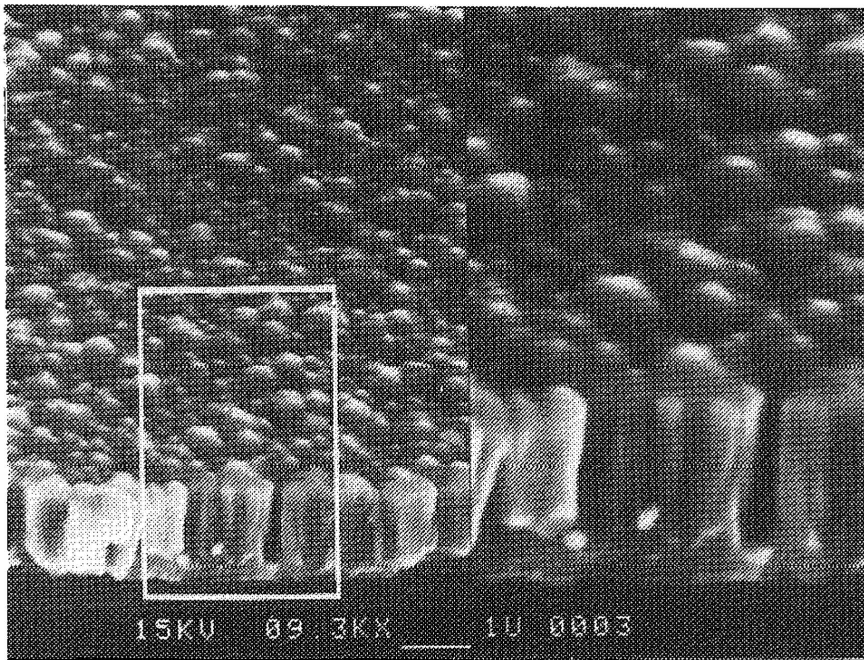

Figure 24: SEM fracture section, Nickel oxide/sapphire, RF series IIC

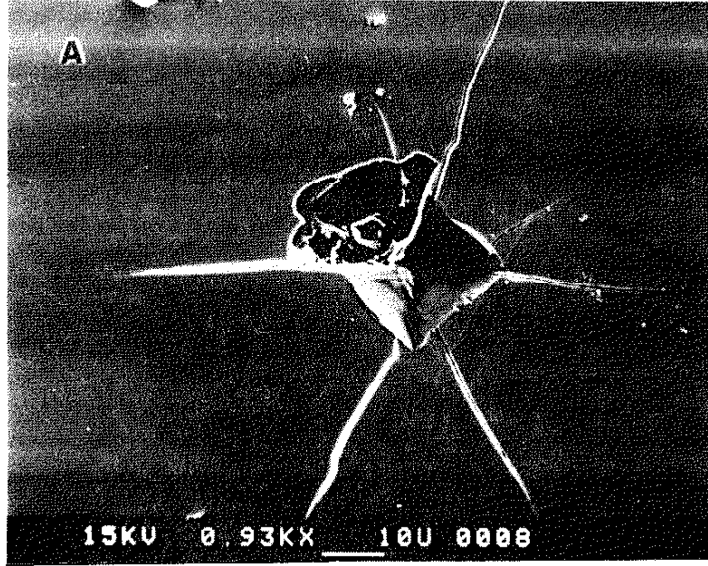

Figure 25: SEM micrographs of Vickers microhardness indents, Nickel/sapphire, RF series IIA, 700 g load
A) Low magnification
B) High magnification

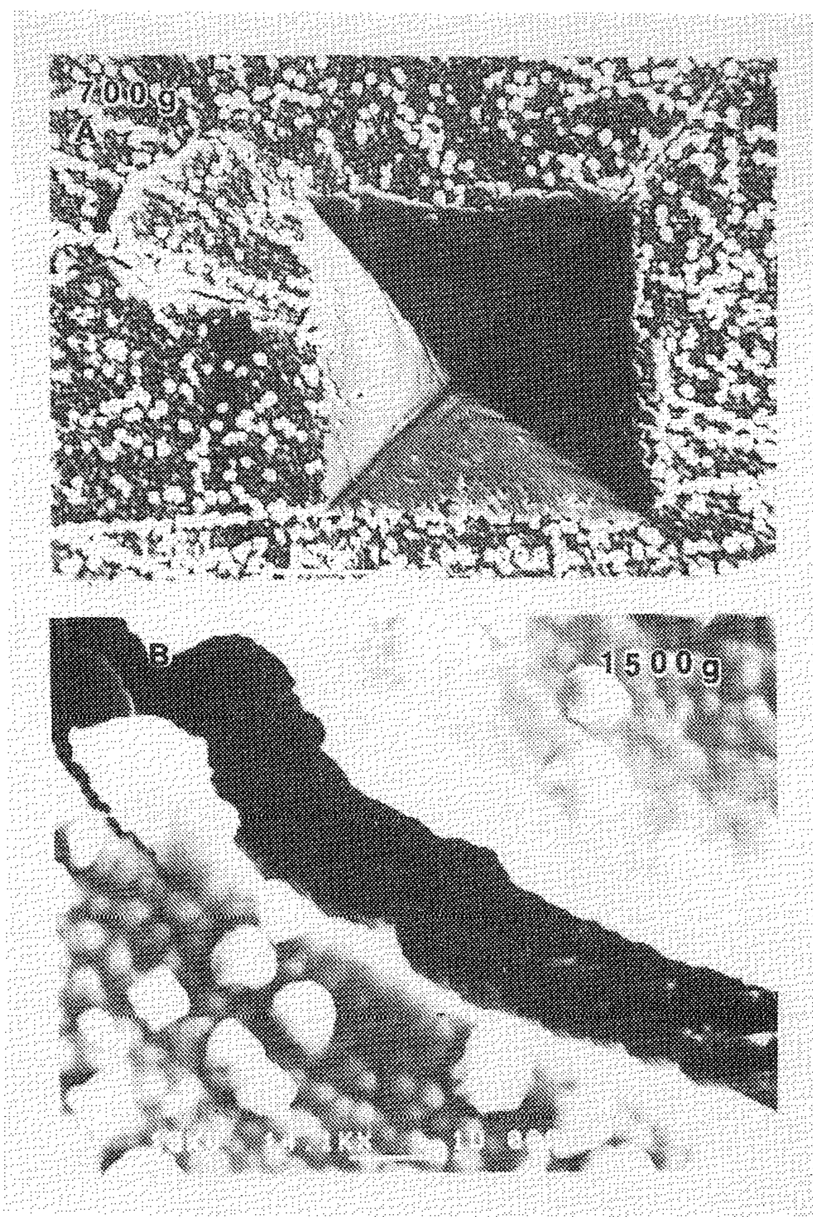

Figure 26: SEM micrographs of Vickers microhardness indents, Nickel/sapphire, RF series IIB
A) 700 g load
B) 1500 g load

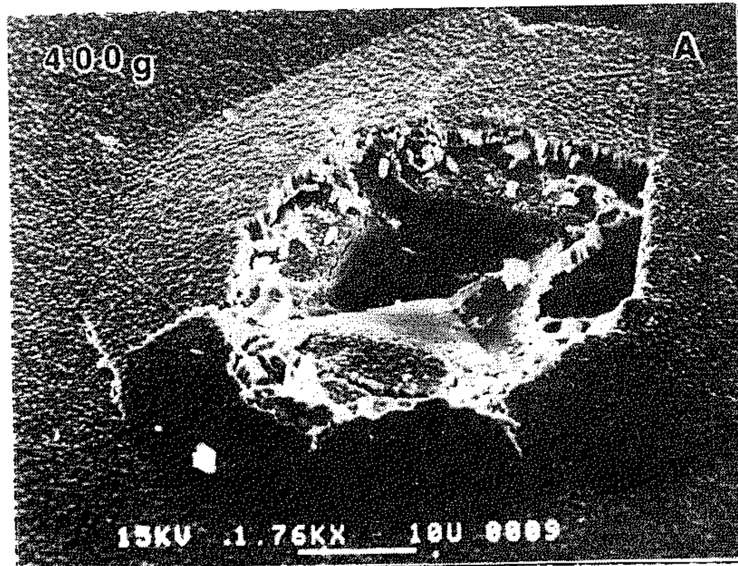

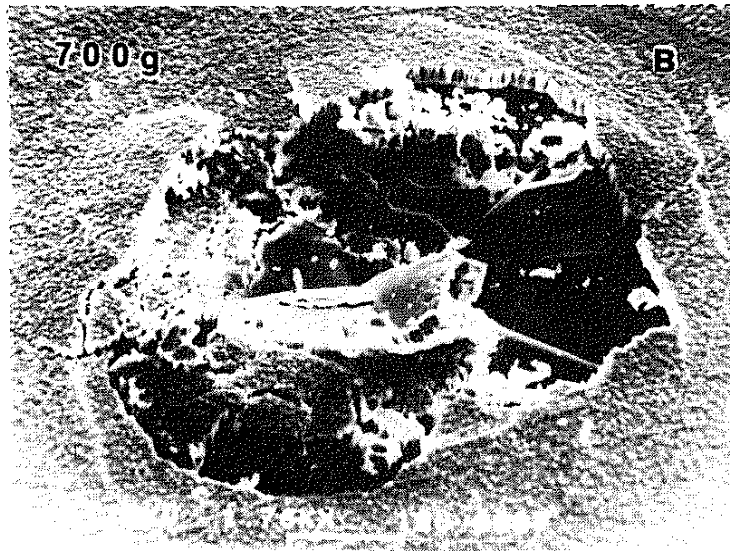

Figure 27: SEM micrographs of Vickers microhardness indents, Nickel oxide/sapphire, RF series IIC
A) 400 g load
B) 700 g load

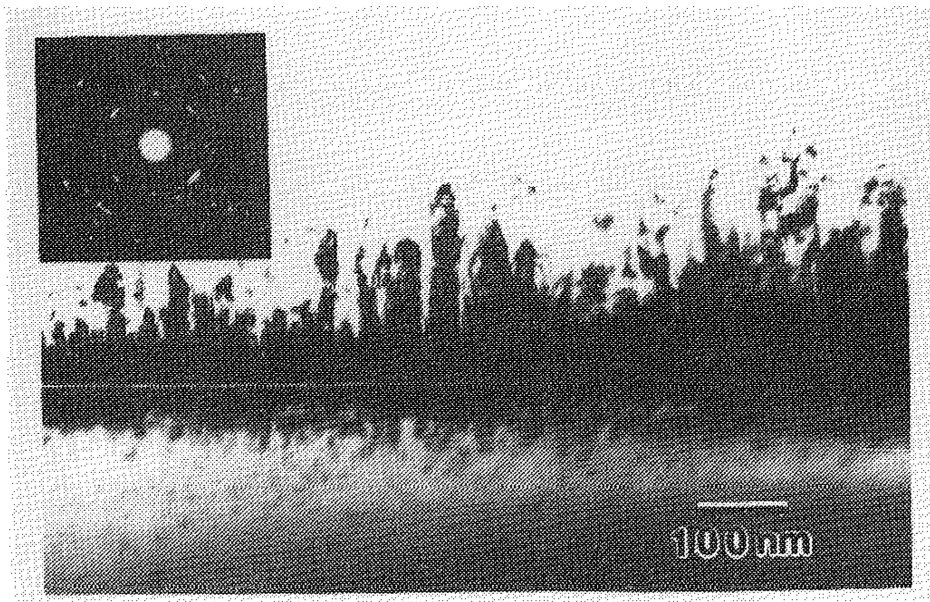

Figure 28: XTEM bright field micrograph with inset SADP, Nickel/sapphire, RF series IIA

Morphology and crystallography of the metallic RF deposited films are summarized by the next series of figures (29-35). An XTEM dark field image, formed using a film reflection, (Fig. 29) showed both layers of the film, as well as the damage profile in the substrate. Note the fracture at (or near) the film/substrate interface, most likely a result of specimen preparation. Crystallographically, the first layer (initial growth) has developed a distinct orientation relationship with the substrate, as evidenced by the superimposed zone axis patterns of figure (30B); while the ring pattern from the second layer grains indicated a random orientation (Fig. 30A). Note that the streaking visible in the film reflections of figure (30B) was due to slight variations in the orientation of the grains. The orientation relationships between the film and the substrate across the interface corresponding to figure (30B) were shown schematically in figure (31). The extent of the microstructural damage as a result of the ion-assisted deposition was further exemplified by the bright field XTEM image in figure (32), taken with the specimen oriented to enhance dislocation contrast. The dark field XTEM image of figure (33) showed the somewhat porous boundary between layers (initial growth layer and second layer as seen in the SEM, figure (23)) in the series III RF nickel/sapphire composite. The preferentially oriented vs random nature of the two layers shown in figure (33), analogous to that of the series II film (Fig. 30), was shown by the selected area diffraction patterns (SADPs) of figure (34), taken from each layer individually. Region 1 yielded a spot pattern, while the second layer pattern was representative of a polycrystalline material. The orientation relationship between the film and the substrate for this composite was depicted by the SADP of the interface shown in figure (35). Although the diffraction patterns of figures (30), (34) and (35) were obtained using different zone axes in the electron microscope, the orientation relationships between the film and substrate are crystallographically the same.

XTEM dark field analysis of the nickel oxide/sapphire composite confirmed the columnar morphology seen in the SEM, but revealed that each column is in this case a single grain; unlike a typical zone 1 morphology (Fig. 36). A large number of growth defects were present in

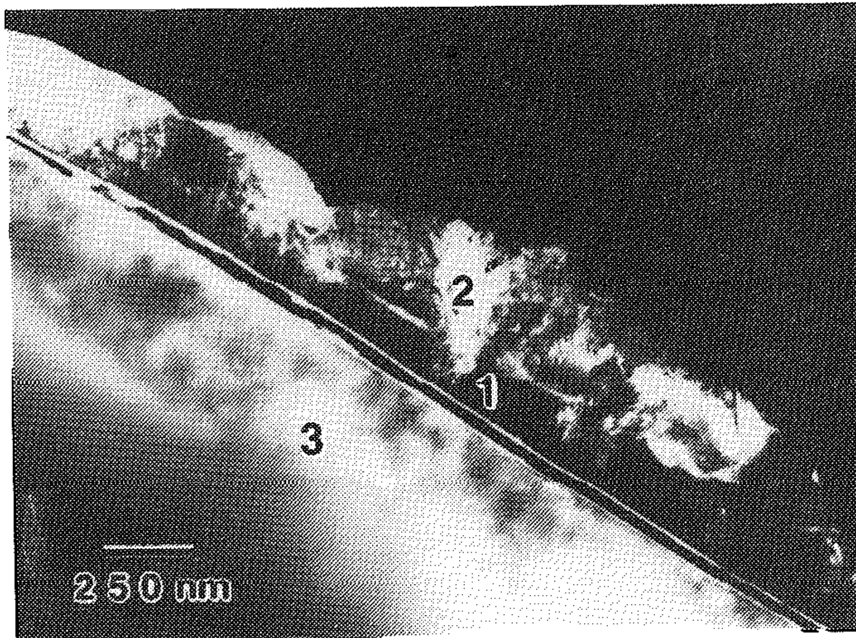

Figure 29: XTEM dark field micrograph, Nickel/sapphire, RF series IIB
1) First film layer
2) Second film layer
3) Damaged layer in substrate

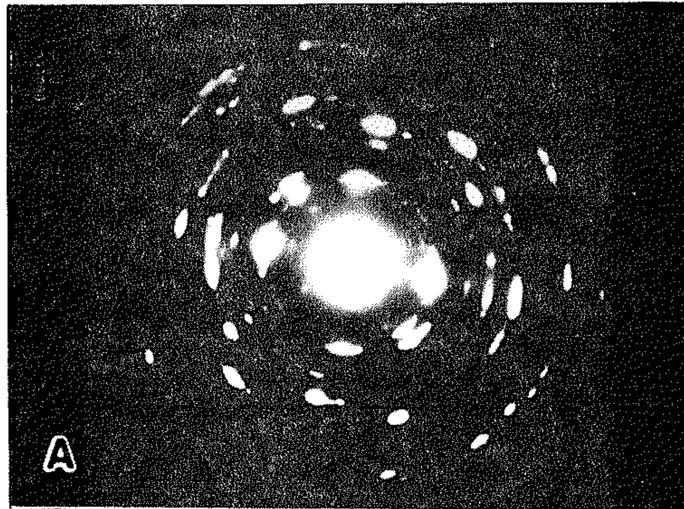

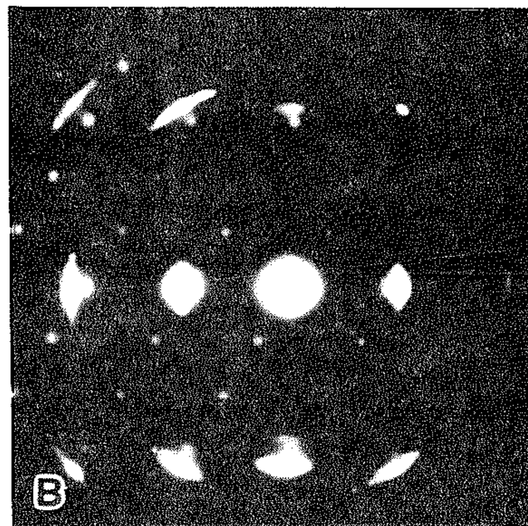

Figure 30: SADPs, Nickel/sapphire, RF series IIB
A) Second layer in film
B) Interface region

Ni/Sapphire RF Ion Plated

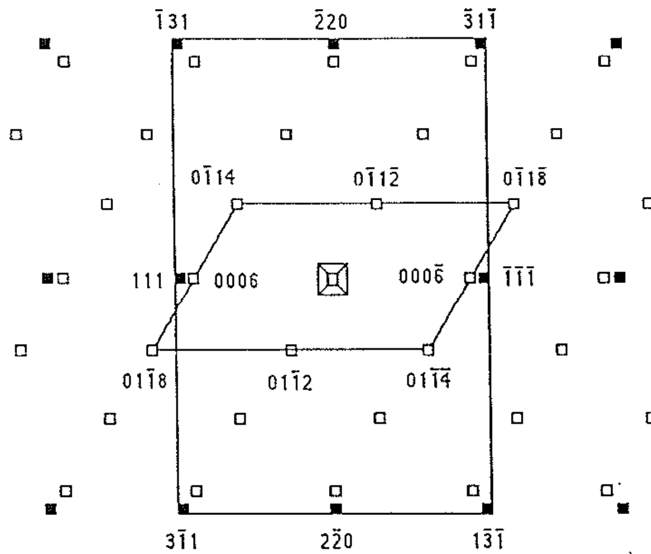

ZONE AXES: $2\bar{1}\bar{1}0$ // $\bar{1}\bar{1}2$ ▫ Alumina

PLANES: 0006 // 111 ▪ Nickel

Figure 31: Schematic SADP, Nickel/sapphire, RF series IIB, Interface region, (figure 30 B)

Figure 32: XTEM bright field micrograph, Nickel/sapphire, RF series IIB

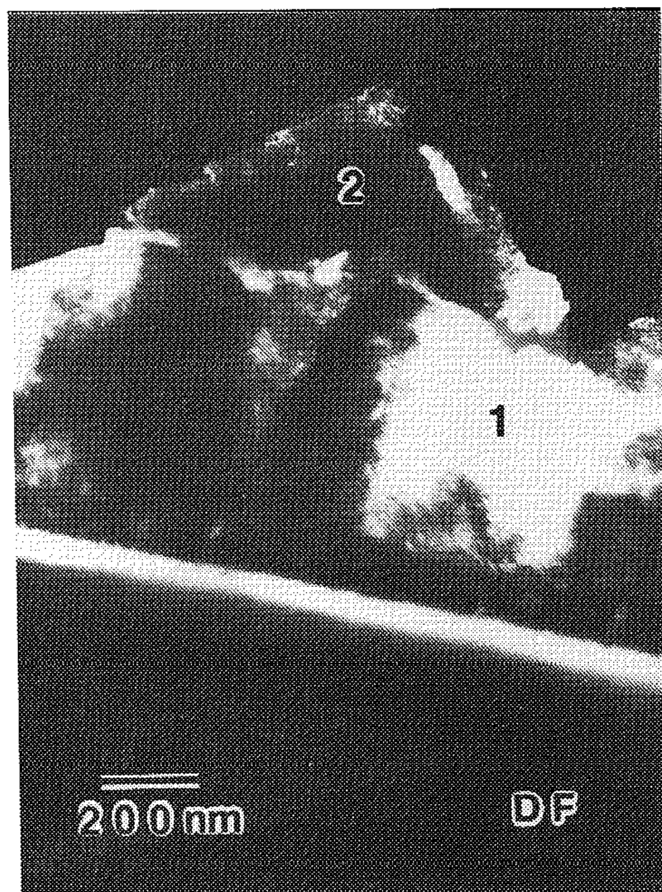

Figure 33: XTEM dark field micrograph, Nickel/sapphire, RF series IIIB
1) First layer in film
2) Second layer in film

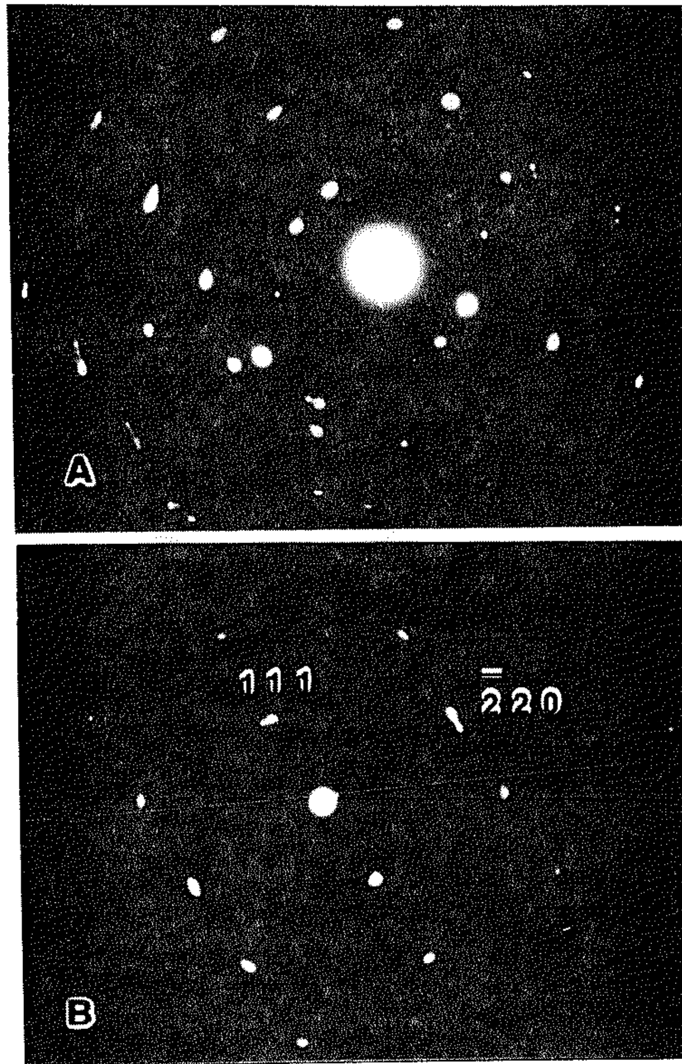

Figure 34: SADPs, Nickel/sapphire, RF series IIIB
A) Second layer in film, polycrystalline Ni
B) First layer in film, near interface, $\overline{11}2$ Ni

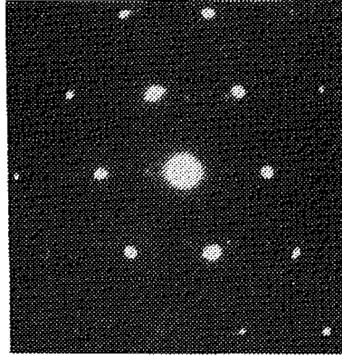

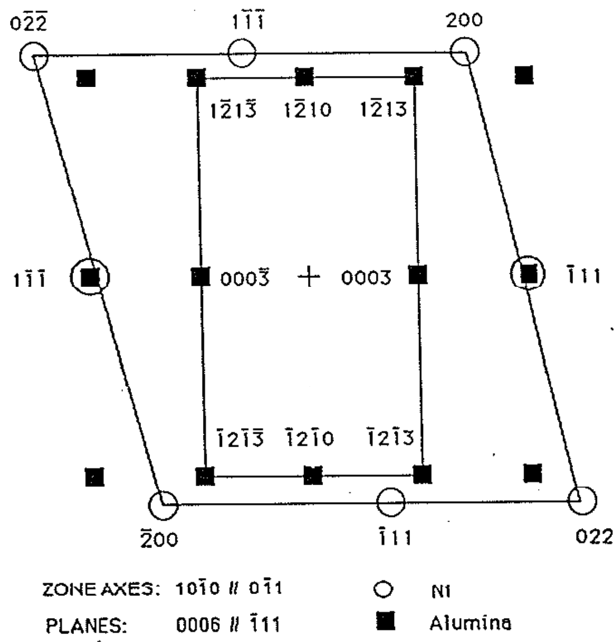

Figure 35: SADP, Nickel/sapphire, RF series IIIB, Interface region, 1010 Al_2O_3 // 110 Ni with 0006 Al_2O_3 // 111 Ni

Figure 36: XTEM dark field micrograph, Nickel oxide/sapphire, RF series IIC

the film, as was a dislocation density (structural damage) profile in the substrate which decreased with depth. The crystallography of the system consisted of two twin-related orientations with {111} planes growing parallel to the basal plane of the substrate (Fig. 37A). The microdiffraction pattern of figure (37B) was used to confirm that each column was a single grain, as well as to facilitate deconvolution of the overall diffraction pattern. The orientation relationships were summarized schematically in figure (38), with the two variants of {111} growth which satisfy the Bragg condition in the [110] zone being rotated 70.5 degrees (the angle between two [111] directions) with respect to each other about [110]. EDS analysis from regions in the film and substrate adjacent to the nickel oxide/alumina interface showed little mixing across the boundary, with the small amount of aluminum present in the film scan attributed to fluorescence of the substrate by the nickel (Fig. 39).

Further information concerning interface widths was derived from a series of Auger depth profiles of the three composites (Fig 40). The effect of ion bombardment during deposition on interface width was clearly demonstrated. The composition vs depth profiles for films deposited under concurrent ion bombardment (Fig. 40B, C) possessed a much more gradual slope, indicating a more diffuse interface, than that of the film grown without bombardment (Fig. 40A). Note that these differences were present even when considering instrumentally induced broadening of the profiles. Profile (40A) took the longest sputter time to reach the interface, suggesting the largest amount of artifactual broadening, yet had the sharpest interface.

C.2. Heat treated

In order to investigate potential reaction compound formation, the composites were heat treated under vacuum at 1000 °C for 2 hours. Specimens were initially heat treated in ceramic boats using a vacuum furnace (vacuum heat treated - VHT). Chemical analysis of these samples indicated magnesium contamination; however, some interesting observations could still be made. To correct this problem a second series of samples was encapsulated in evacuated quartz tubes and heat treated in

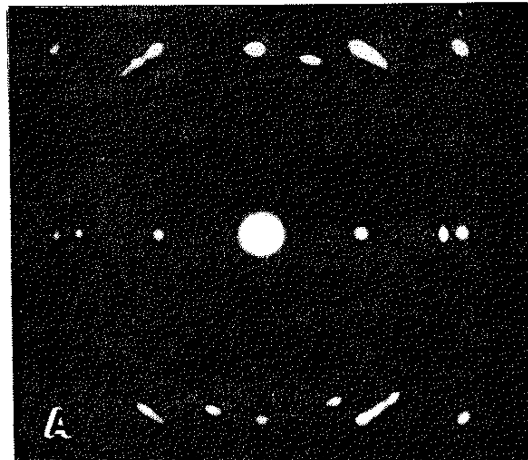

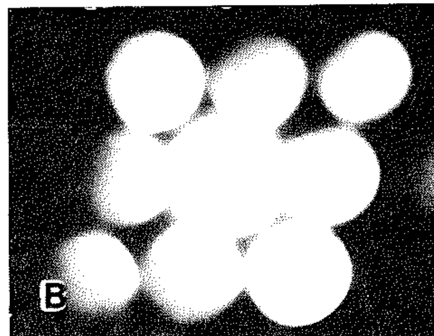

Figure 37: SADPs, Nickel oxide/sapphire, RF series IIC
A) Interface region
B) Microdiffraction from a single column of NiO

NiO / Sapphire RF Ion Plated

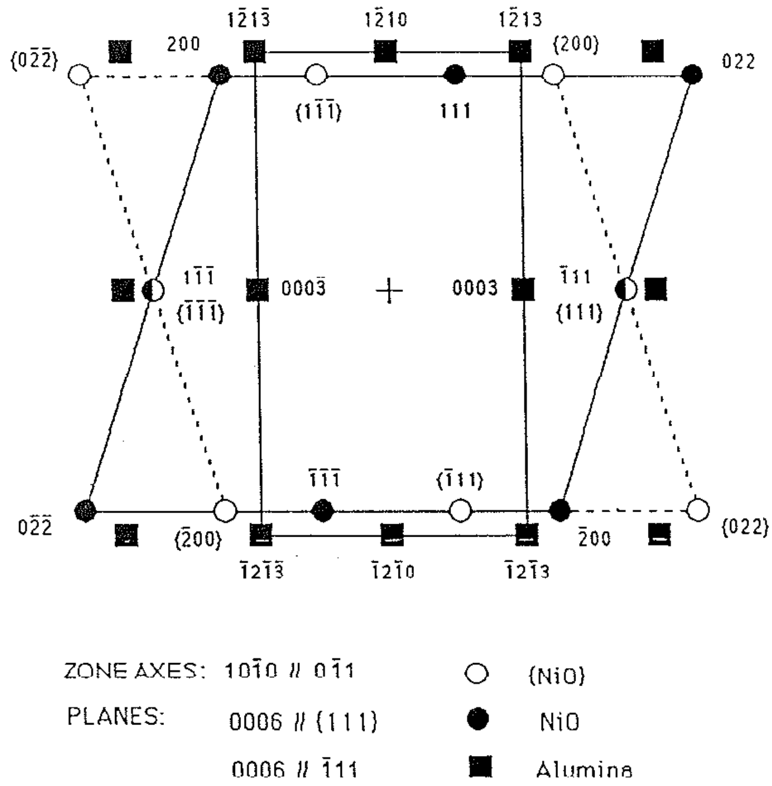

Figure 38: Schematic SADP, Nickel oxide/sapphire, RF series IIC, interface region, (figure 37 A)

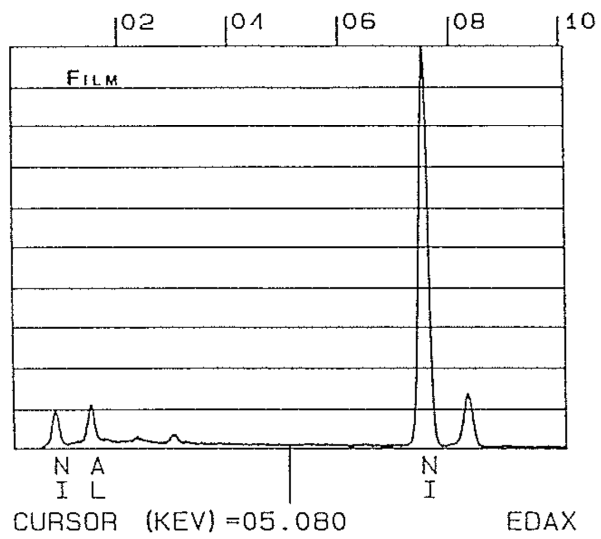

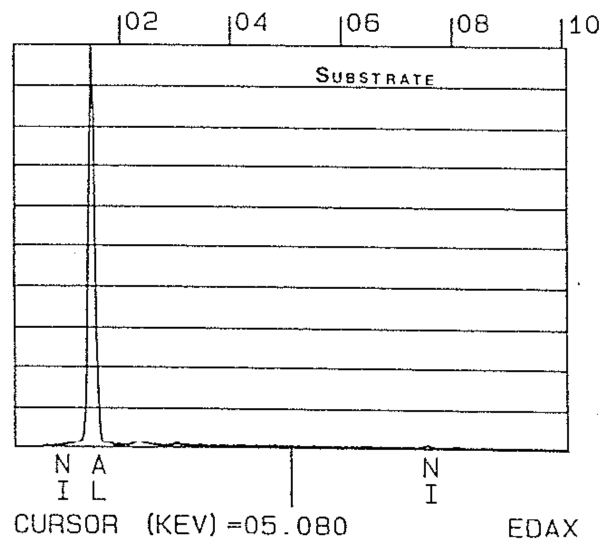

Figure 39: EDS Spectra, Nickel oxide/sapphire, RF series IIC

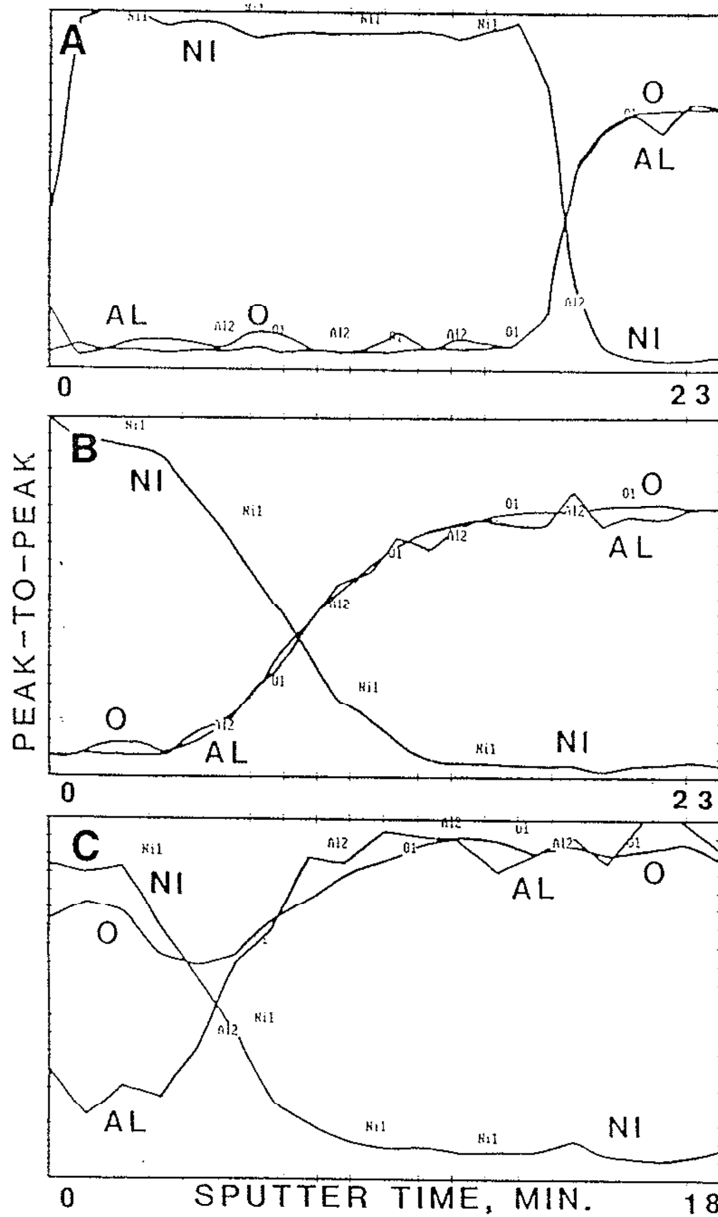

Figure 40: Auger depth profiles, RF series II, As-deposited
A) Nickel/sapphire, no bias
B) Nickel/sapphire, RF bias
C) Nickel oxide/sapphire, RF bias

a standard box furnace (encapsulated heat treated - EHT). The SEM micrograph of the vacuum heat treated 0.0 kV nickel film showed what appeared to be considerable recrystallization, with extensive regions exhibiting dewetting (Fig. 41). This was thought to be related to a balance between surface energy forces driving dewetting and adhesive forces at the interface trying to maintain a continuous film. Note the large scale of the features in figure (41), as compared to those in the upcoming figures. The morphology of the same film following encapsulated heat treatment consisted of smaller, circular dewet regions, with some surface topography present in the films (Fig. 42). Pieces of debris left behind in the unbonded regions may represent nucleation sites for dewetting at the interface. The RF deposited nickel film also recrystallized after VHT, with apparent separation at the film/substrate interface present in regions adjacent to the holes in the film (Fig. 43). In addition, very little structure or topography was visible in the film. After EHT, however, distinct grains with facetted surfaces were formed, with regions of exposed substrate in between, indicative of major recrystallization with the grains adopting equilibrium shapes (Fig. 44). It appeared as though, unlike the VHT case, that the recrystallized film remained fully adherent to the substrate. Note that the exposed surface was that of the original substrate, as evidenced by the polishing scratches visible in the micrograph. Heat treating of the oxide film in the vacuum furnace resulted in an incomplete recrystallization due to the higher melting point of the oxide, with the reaction initiating at the interface. This was demonstrated by the SEM micrograph (Fig. 45) in which the portion of the film adjacent to the substrate recrystallized, while the upper portion maintained a morphology similar to the columnar nature of the as-deposited film. Similar behavior was observed under encapsulated conditions, although the reaction seems to have proceeded much farther towards completion, with smaller regions of the original morphology (white areas) visible (Fig. 46).

Even though the morphological descriptions of the heat treated films derived from the SEM micrographs were useful in evaluating the films from an applications perspective, they did not provide any information concerning the nature of the interface. XTEM of VHT 0.0 kV nickel,

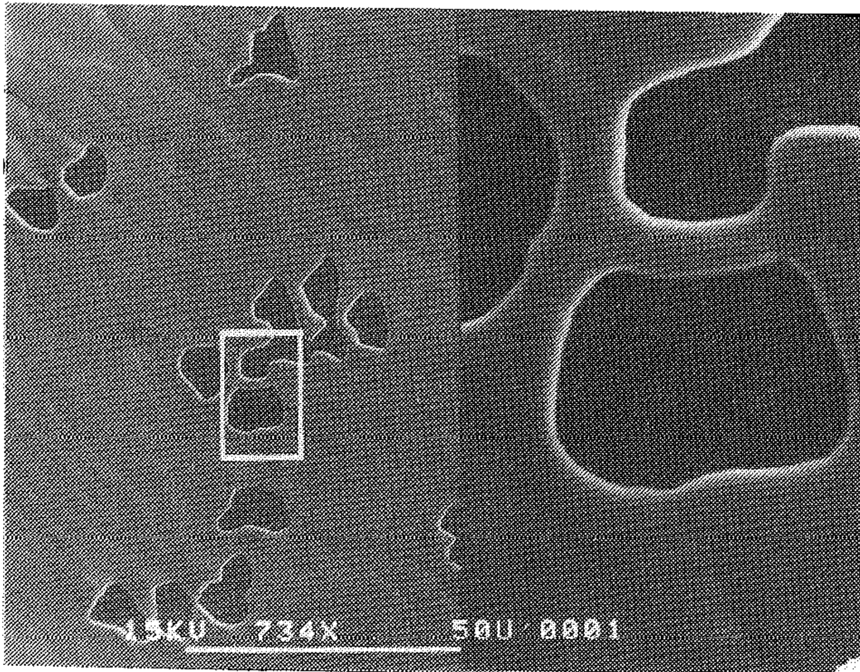

Figure 41: SEM micrograph, Nickel/sapphire, RF series IIA, Vacuum heat treated

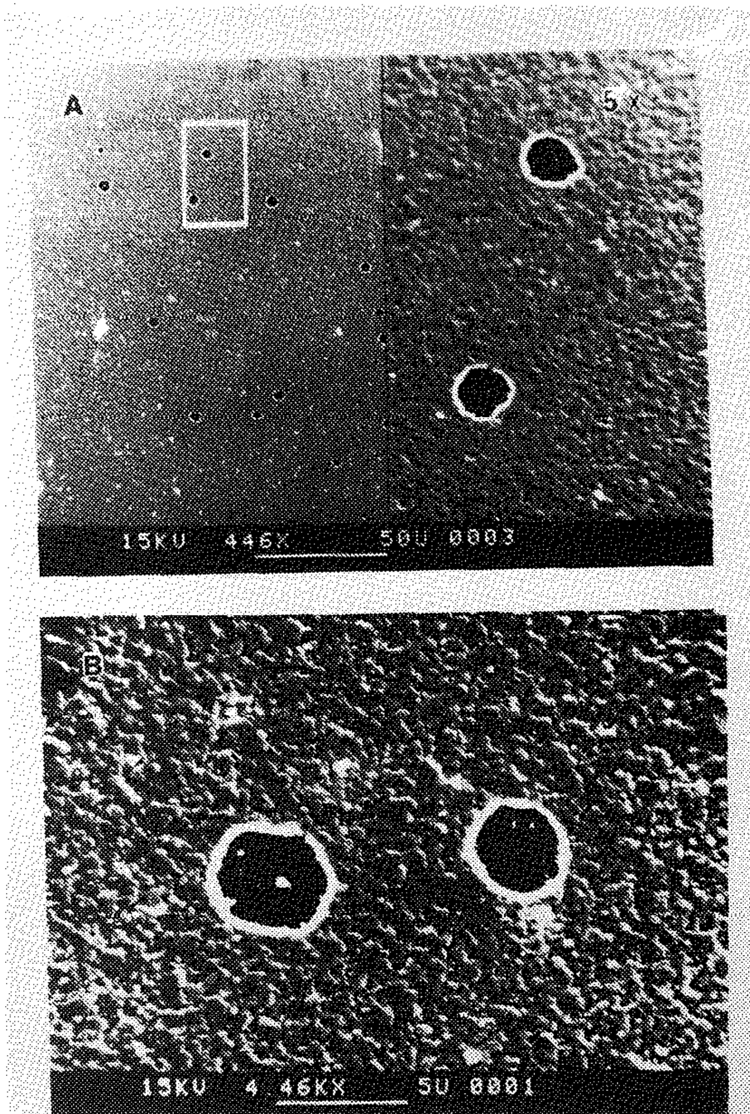

Figure 42: SEM micrograph, Nickel/sapphire, RF series IIA, Encapsulated heat treated

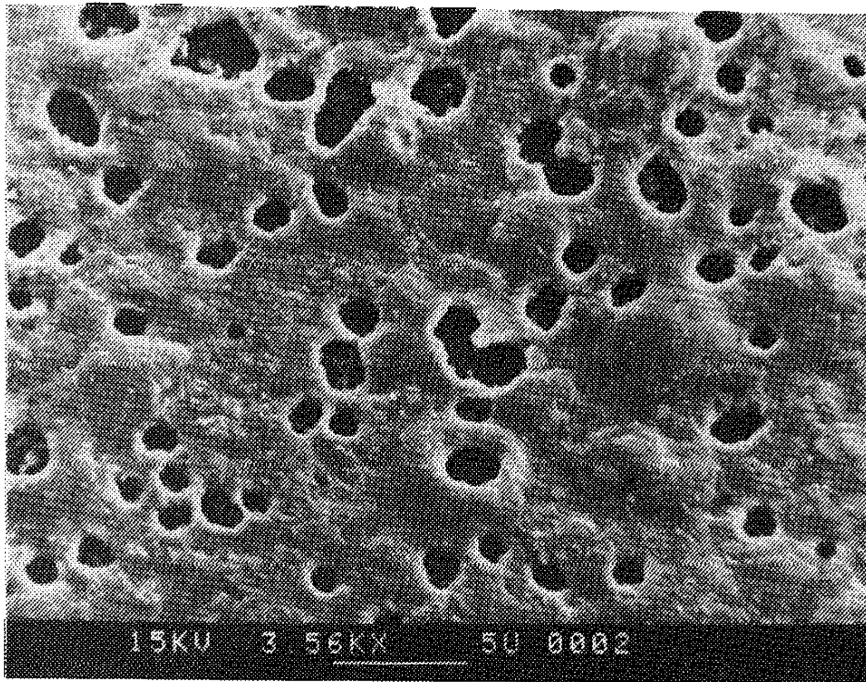

Figure 43: SEM micrograph, Nickel/sapphire, RF series IIB, Vacuum heat treated

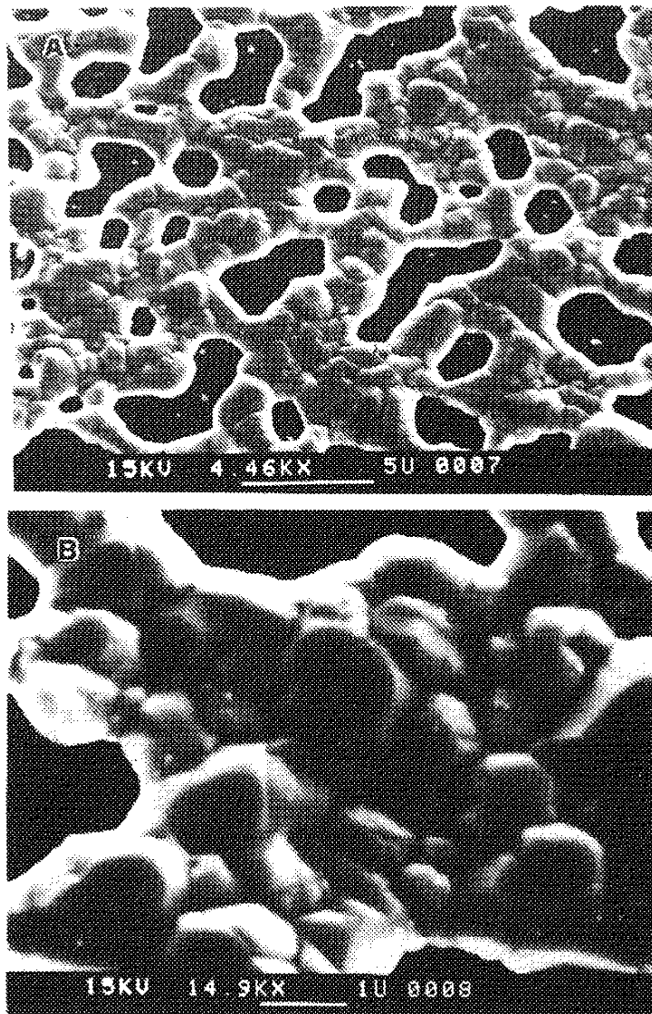

Figure 44: SEM micrograph, Nickel/sapphire, RF series IIB, Encapsulated heat treated

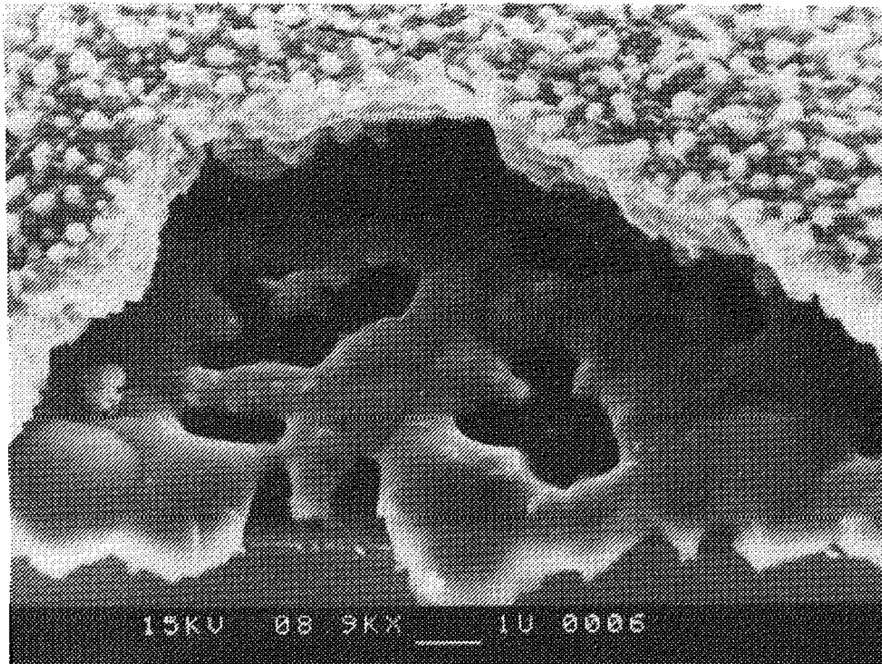

Figure 45: SEM micrograph, Nickel oxide/sapphire, RF series IIC, Vacuum heat treated

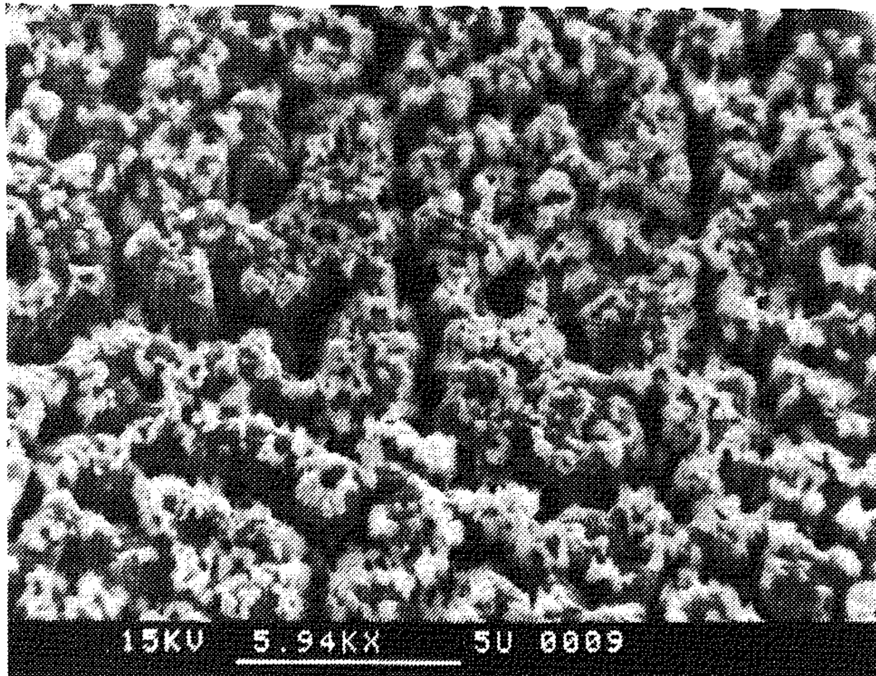

Figure 46: SEM micrograph, Nickel oxide/sapphire, RF series IIC, Encapsulated heat treated

however, revealed the presence of a 25 nm thick compound, with uniform thickness along the length of the interface (Fig. 47). Selected area diffraction analysis identified this phase as a spinel, presumably nickel aluminate: $NiAl_2O_4$. In the series of selected area diffraction patterns taken from the different regions of the composite, presented in figure (48), the development of distinct crystallographic orientation relationships between the film, interface phase and substrate, not present in the as-deposited case, was identified. The orientation was identical to that present in the case of the as-deposited films grown under ion-assisted conditions (e.g. Fig. 35), with the FCC spinel phase adopting the same orientation as the FCC nickel phase. Chemical analysis of the interface layer via STEM/EDS indicated that it consisted of a complex combination of cations due to contamination during heat treating (Fig. 49). Exact determination of the structure and composition of the layer was impossible since $NiAl_2O_4$ and $MgAl_2O_4$ possess identical crystal structures with nearly identical lattice parameters. It was also seen that the majority of the contaminants segregated to the interface layer since the spectrum from the film contained only nickel. A reaction layer 50 nm thick was similarly produced in the encapsulated specimen (Fig. 50) XTEM also depicted a large number of defects, primarily microtwins lying on {111} planes parallel to the plane of the substrate surface, in both the film and the interface layer. Crystallographically the composite was the same as in the VHT condition (having a preferred orientation), although the interface diffraction pattern was not as clearly defined (Fig. 51). In this case, however, the interface spinel phase was confirmed via EDS to be nickel aluminate - with no contaminant elements detected (Fig. 52). This result, along with Auger data, demonstrated the cleanliness of the encapsulated heat treated (EHT) composites.

The RF deposited nickel/sapphire composite formed an interfacial spinel (dark band in subsequent figures) upon heat treatment (EHT) as well. XTEM confirmed the SEM observations of film morphology, with large grains remaining in contact with the substrate (or interface layer) (Fig. 53). In addition, twins were detected in the film by imaging in dark field using matrix {200} and twin {111} reflections successively; with

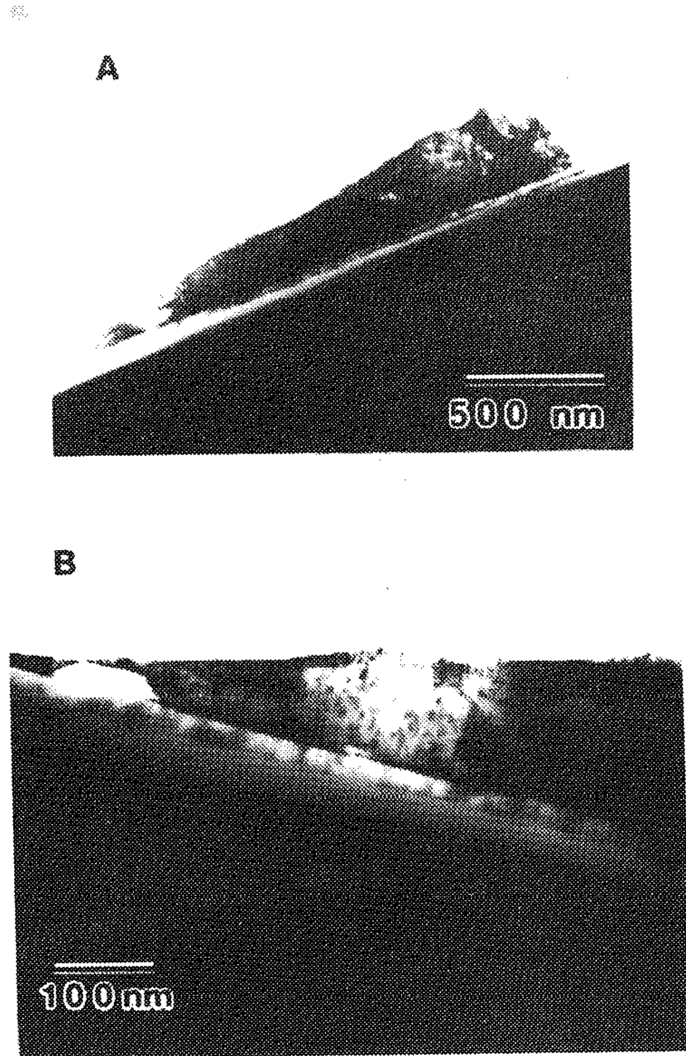

Figure 47: XTEM bright field micrographs, Nickel/sapphire, RF series IIA, Vacuum heat treated
A) Low magnification
B) Enlargement of interfacial region

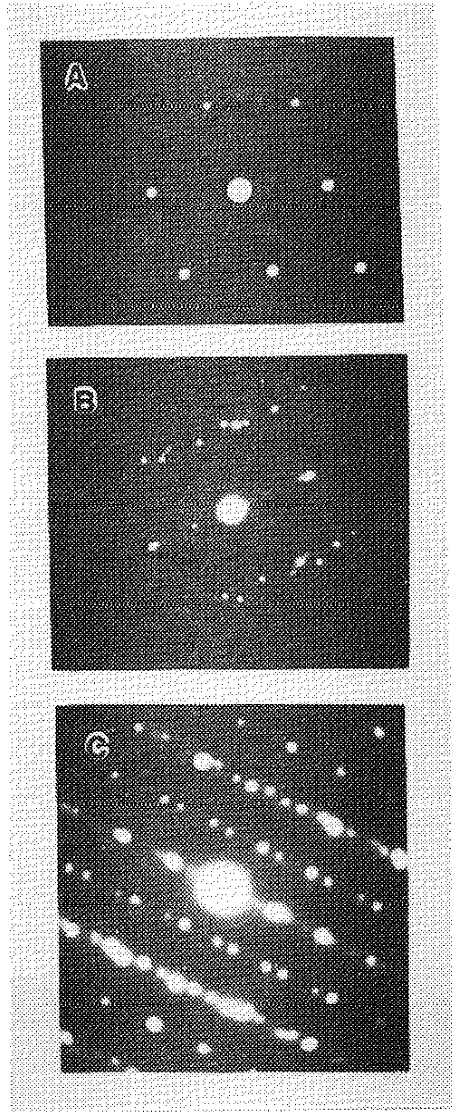

Figure 48: SADPs, Nickel/sapphire, RF series IIA, Vacuum heat treated, 110 Ni // 110 $MgAl_2O_4$ // $10\bar{1}0$ Al_2O_3

A) Film

B) Film, substrate, and interface region

C) Interface region and substrate

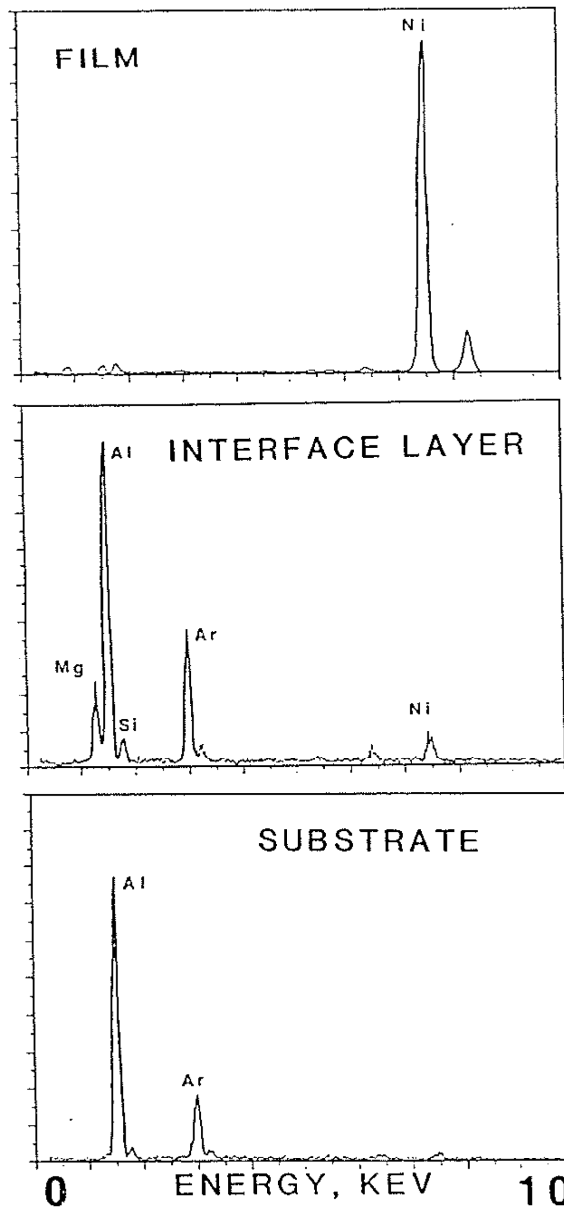

Figure 49: EDS spectra, Nickel/sapphire, RF series IIA, Vacuum heat treated

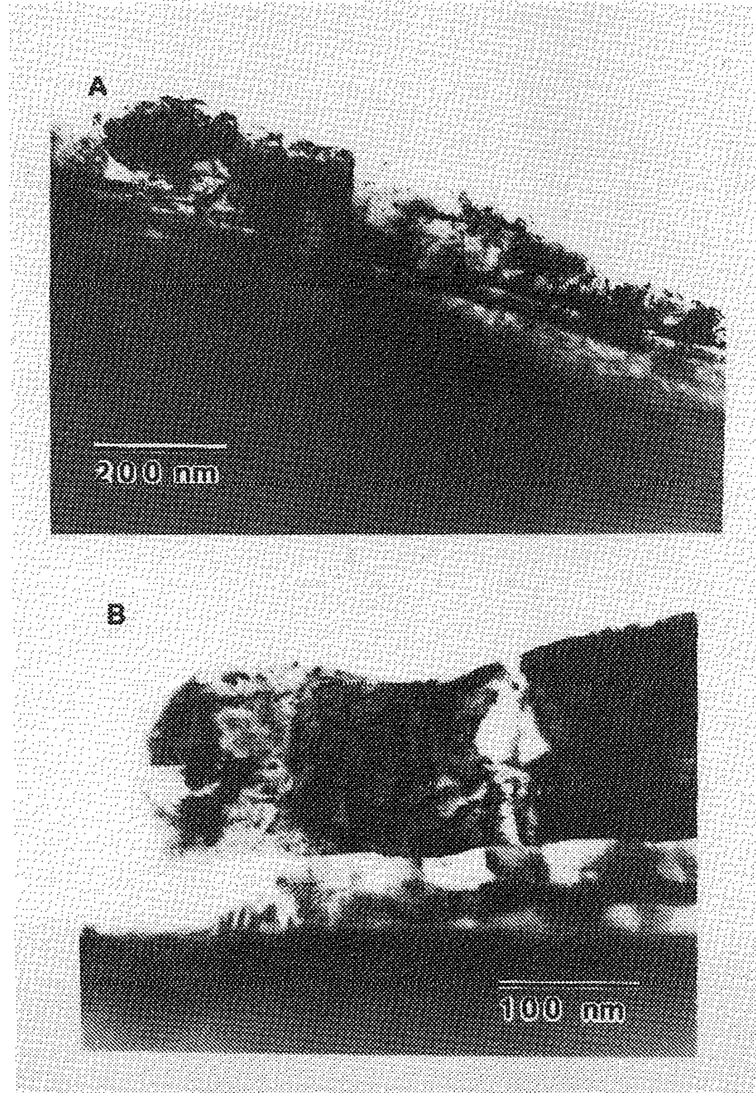

Figure 50: XTEM bright field micrographs, Nickel/sapphire, RF series IIA, Encapsulated heat treated
A) Low magnification
B) Enlargement of interfacial region

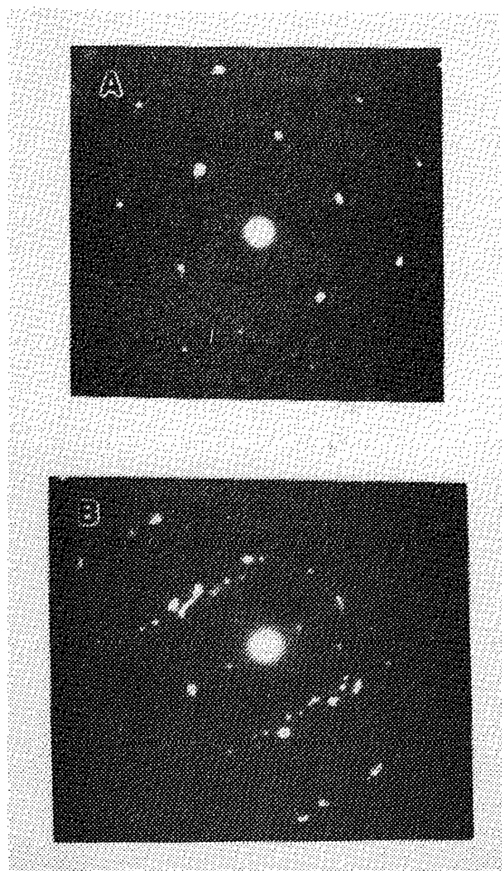

Figure 51: SADPs, Nickel/sapphire, RF series IIA, Encapsulated heat treated, 110 Ni // 110 $NiAl_2O_4$ // $10\bar{1}0$ Al_2O_3
A) Film
B) Film, substrate and interface region

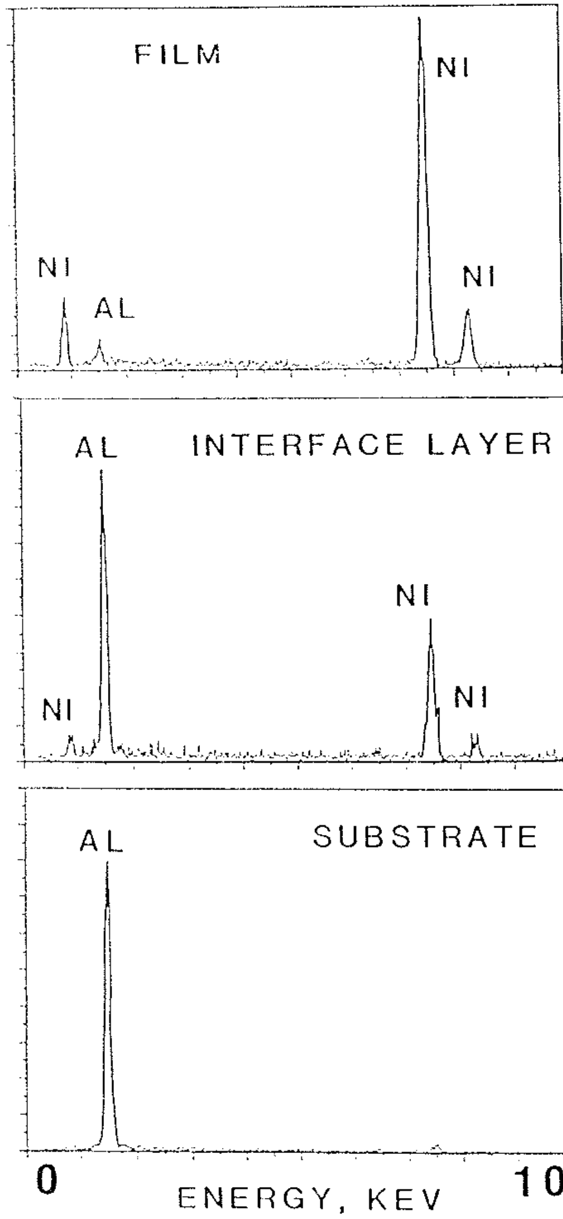

Figure 52: EDS spectra, Nickel/sapphire, RF series IIA, Encapsulated heat treated

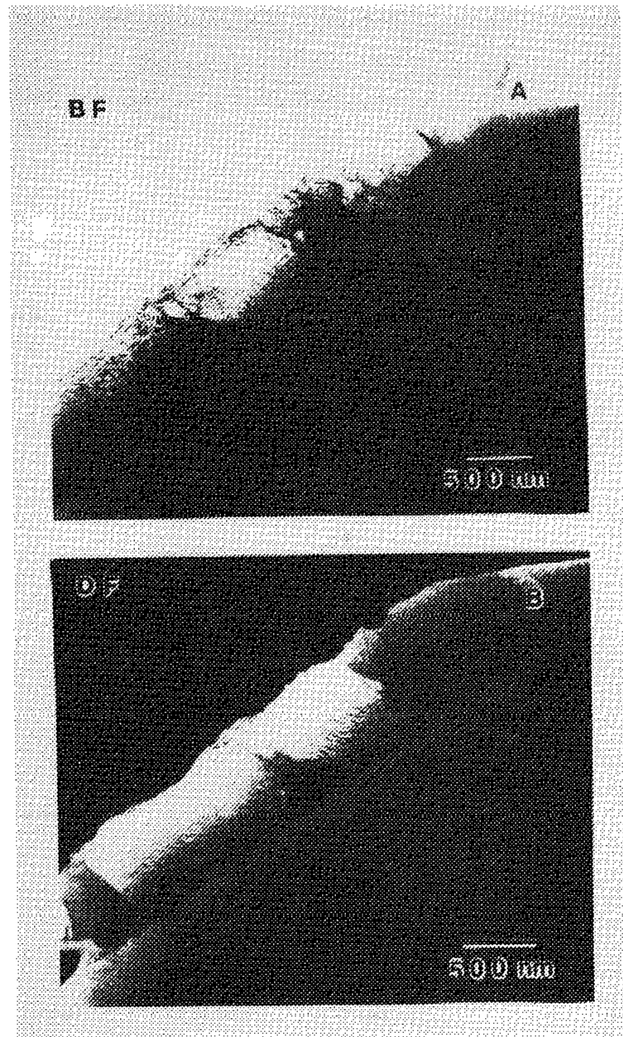

Figure 53: XTEM micrographs, Nickel/sapphire, RF series IIB, Encapsulated heat treated
A) Bright field
B) Dark field

twinning occurring on {111} planes, as expected for FCC materials (Fig. 54). A higher magnification XTEM bright field image of the composite (Fig. 55A) clearly revealed the interfacial spinel layer, with the crystallography being depicted in the accompanying SADPs (Fig. 55B,C). The faint reflections visible in figure (55B) corresponded to $NiAl_2O_4$, with both twin orientations of the FCC phase present (see Fig. 38). The film/substrate orientation for this composite (Fig. 55C) was also consistent with the previous specimens:

$$[110] \text{ Nickel } // \ [10\bar{1}0] \text{ Alumina,}$$
$$\text{with } (111) \text{ Nickel } // \ (0006) \text{ Alumina.}$$

The presence of oxygen in the nickel oxide/sapphire composites did not alter the behavior upon vacuum heat treatment, as compared to the metallic samples. A thick (100 nm) spinel layer was formed, and was shown to be crystallographically related to the film and substrate. The XTEM bright field image (Fig. 56A) contained regions where the spinel was exposed due to complete ion milling of the nickel oxide film, as well as other regions in which all three phases (film, interface and substrate) were intact. This allowed the individual phases to be analyzed, both structurally and chemically, in addition to facilitating determination of the orientation relationships present. These relationships were depicted in figures (56B,C,D), obtained from the different regions of the composite. This crystallography was summarized schematically in figure (57). Chemically, the spinel was shown to be nickel aluminate, via EDS analysis, with no accumulation of trace contaminants at the interface (Fig. 58). Encapsulation provided similar results. Figure (59) clearly demonstrated the presence of a spinel phase through the formation of a dark field XTEM image from a spinel reflection (Fig. 59B), along with a bright field image (A) and a dark field image formed using a combination of film and spinel reflections (C). Crystallographic orientation relationships and zone axis patterns seen in the SADP (Fig. 60) were identical to those in the vacuum heat treated case. Figure (61), a bright field XTEM micrograph of an encapsulated heat treated nickel oxide film showed that a semblance of the original columnar morphology was still present in the film.

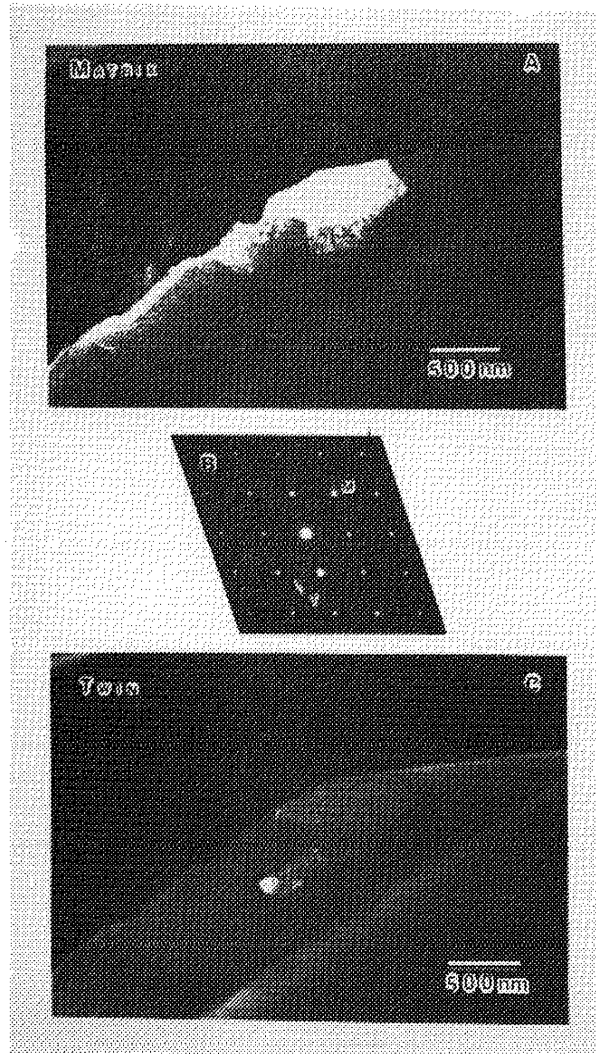

Figure 54: Nickel/sapphire, RF series IIB, Encapsulated heat treated
A) XTEM dark field micrograph, Matrix reflection (film)
B) SADP, 110 Ni
C) XTEM dark field micrograph, Twin reflection (film)

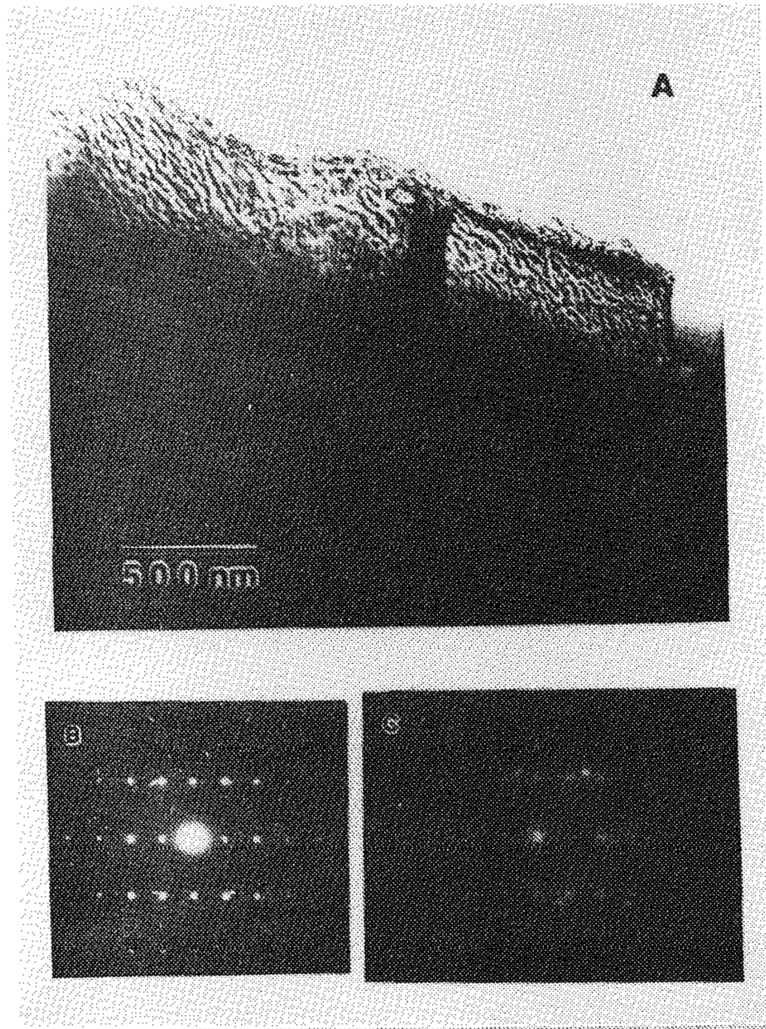

Figure 55: Nickel/sapphire, RF series IIB, Encapsulated heat treated
A) XTEM bright field micrograph
B) SADP, substrate and interface
C) SADP, film and substrate

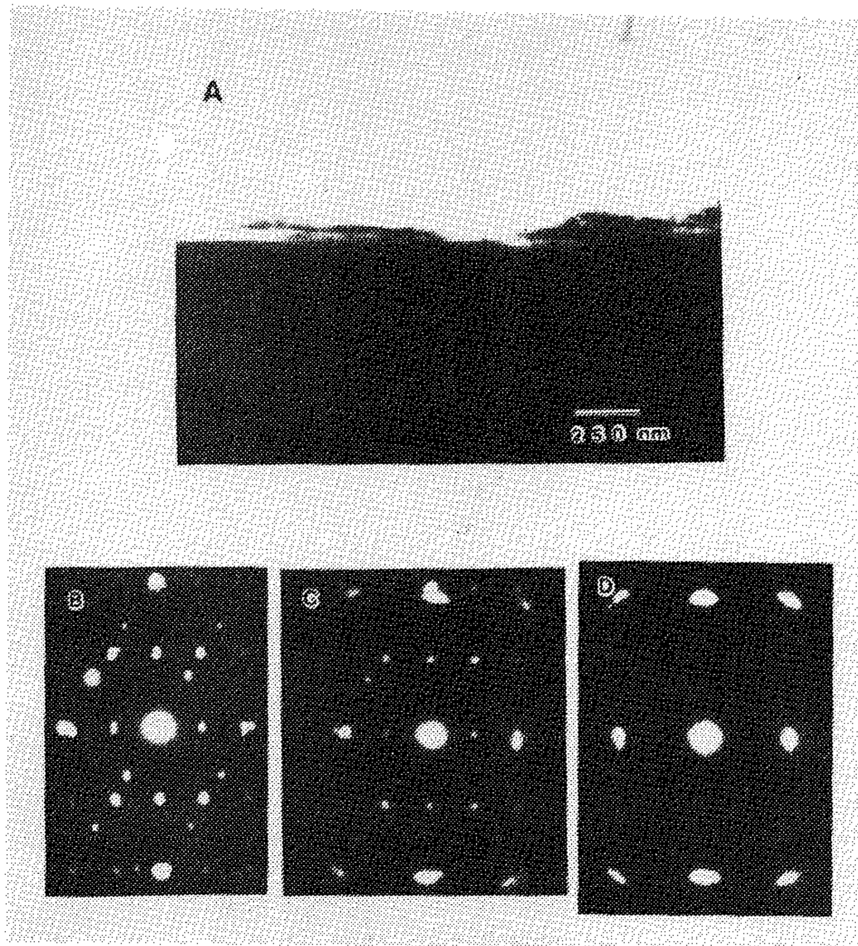

Figure 56: Nickel oxide/sapphire, RF series IIC, Vacuum heat treated
A) XTEM bright field micrograph
B) SADP, Substrate and interface region
C) SADP, Film, substrate and interface region
D) SADP, Film and interface region

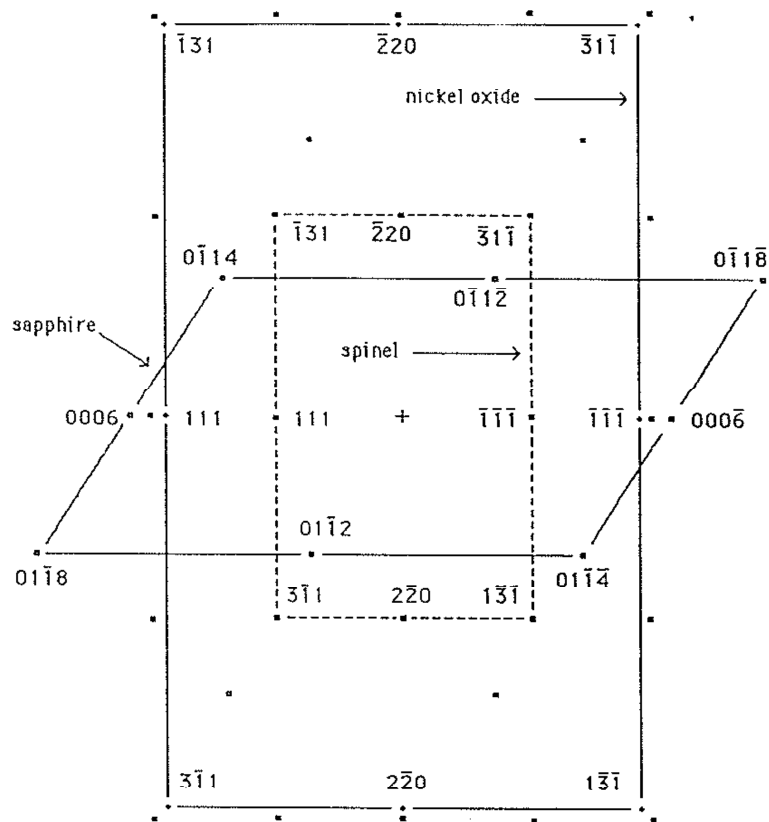

NiO	$\bar{1}\bar{1}2$	·
$NiAl_2O_4$	$\bar{1}\bar{1}2$	--- ▪
Al_2O_3	$2\bar{1}\bar{1}0$	— ▪

NiO/Al_2O_3
RF Ion Plated
Heat Treated
1000 C   2 hrs

Figure 57: Schematic SADP, Nickel oxide/sapphire, RF series IIC, Vacuum heat treated (figure 56 C)

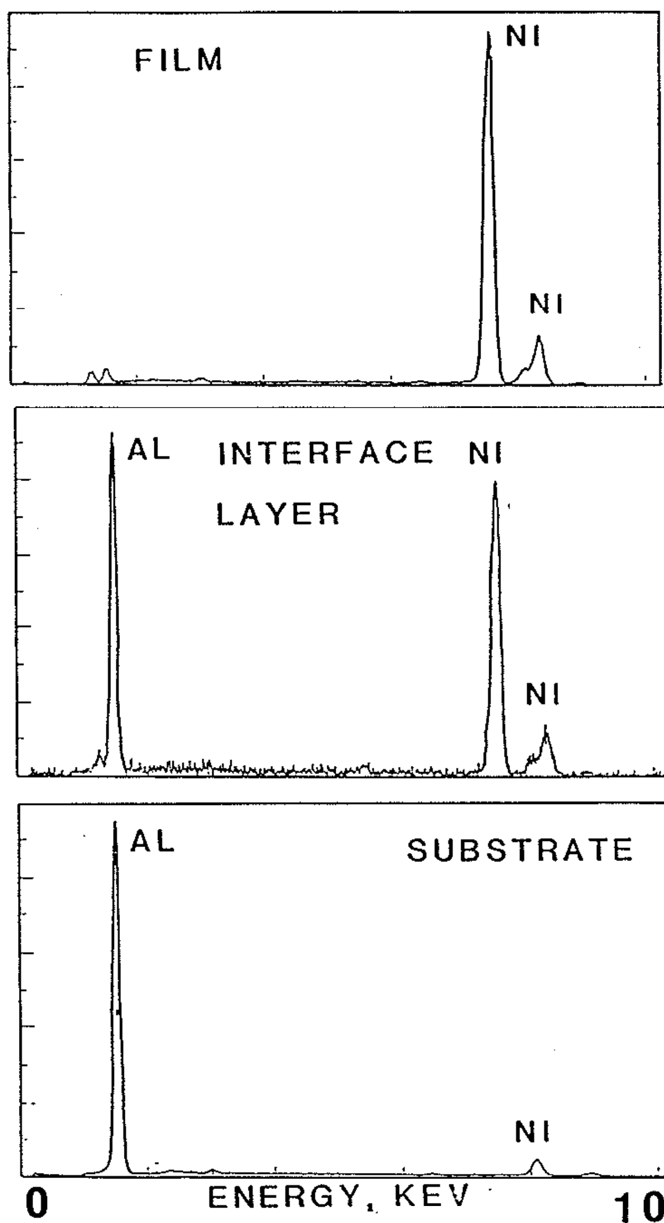

Figure 58: EDS spectra, Nickel oxide/sapphire, RF series IIC, Vacuum heat treated

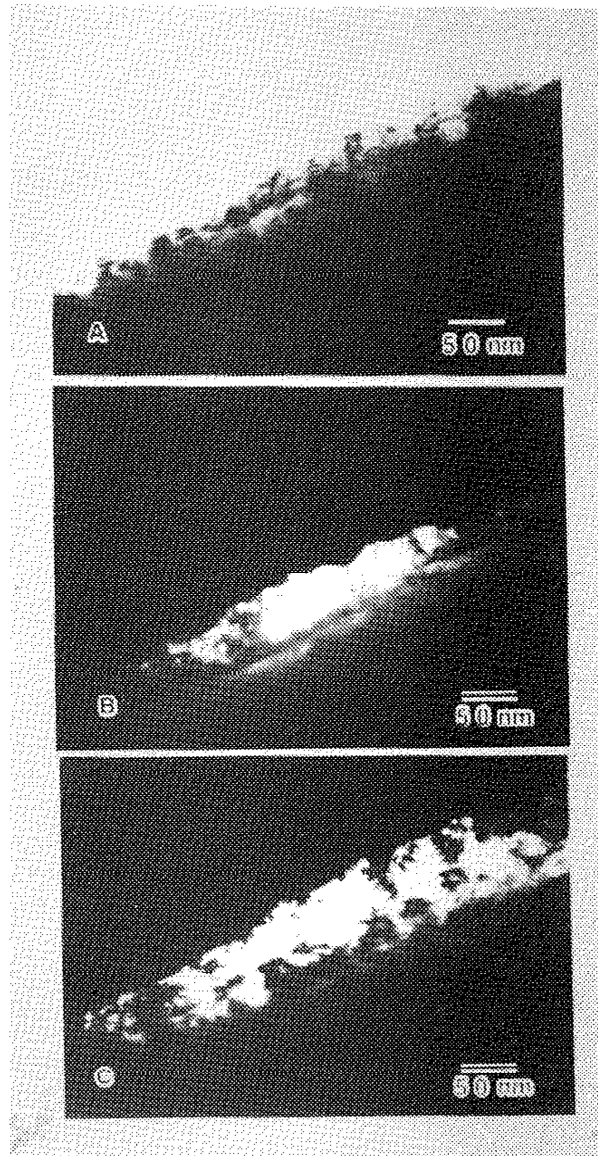

Figure 59: Nickel oxide/sapphire, RF series IIC, Encapsulated heat treated
A) XTEM bright field micrograph
B) XTEM dark field micrograph, $NiAl_2O_4$ reflection
C) XTEM dark field micrograph, $NiAl_2O_4$ and NiO reflections

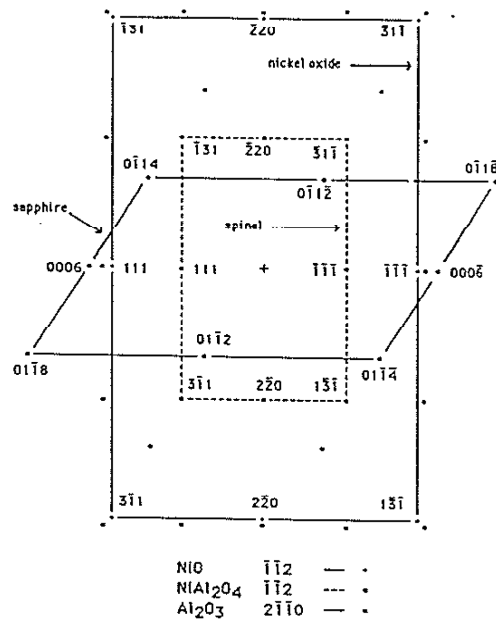

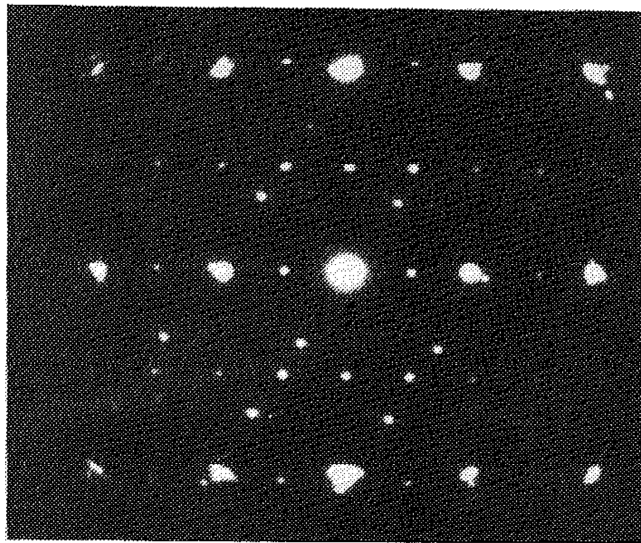

Figure 60: SADP, Nickel oxide/sapphire, RF series IIC, Encapsulated heat treated, $\overline{1}\overline{1}2$ NiO // $\overline{1}\overline{1}2$ $NiAl_2O_4$ // $2\overline{1}\overline{1}0$ Al_2O_3

Figure 61: XTEM bright field micrograph, Nickel oxide/sapphire, RF series IIC, Encapsulated heat treated

Auger electron spectroscopy depth profiles were unable to detect any reaction phases in the heat treated composites, but did show an apparent increase in interfacial width (chemical) as compared to the as-deposited case. Both the evaporated and ion-assisted metallic films, which had markedly different interface widths in the as deposited condition (Fig. 40), were found to have identical composition v.s. depth profiles after heat treatment (Fig. 62). The profiles were all smooth, however, and did not possess any step function characteristics, as expected for composites with distinct interfacial phases. This indicated that the resolution of the depth profiling technique was limited due to the fact that the instrumentally induced broadening was on the order of the thickness of the interfacial phases.

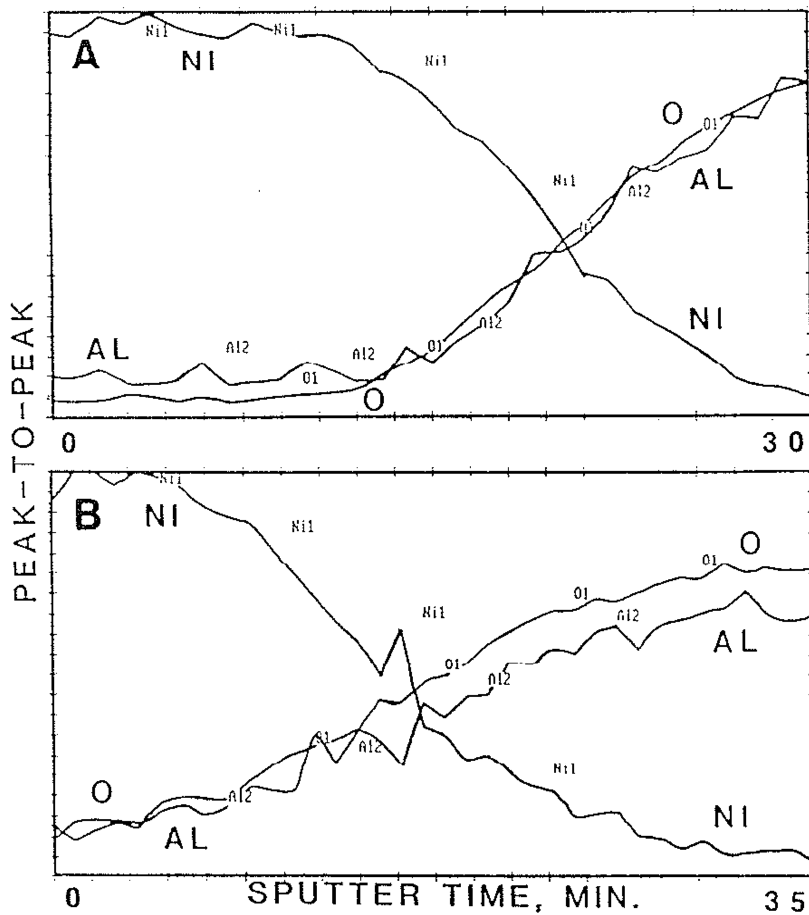

Figure 62: Auger depth profiles, Nickel/sapphire, Encapsulated heat treated
A) RF series IIA
B) RF series IIB

V. DISCUSSION

A. Adhesion

A.1. Tensile test

Adhesion of nickel films deposited onto cordierite substrates by ion plating demonstrated a significant (factor of 10) improvement over conventionally evaporated films. An increase in the DC bias applied to the substrate, which corresponds to an increase in the average energy of the depositing ions and neutrals, resulted in enhanced adhesion for the case of substrates which were not sputter cleaned. This result was as expected from the literature. When the substrates were sputter cleaned prior to deposition, however, maximum adhesion was achieved with the absence of a glow discharge during growth. Films grown under these conditions were also the most thermally stable, from the viewpoint of adhesion, in both inert and reducing atmospheres. Addition of an applied bias caused a decrease in adhesive strength on the sputter cleaned substrates. This result was contrary to what was found for the non sputter cleaned case, as well as for a prior examination of Cu/Cordierite [70], and was not yet fully understood. Possible explanations included the doping of the surface by contaminant atoms from adjacent fixtures during sputter cleaning, thus creating an active surface for growth; and/or a change in the film stress state with bias for the sputter cleaned case. Note that the only other report of adhesion data was that of Baglin and Clark [71] who found that adhesion increased with the dose of implanted ions for Cu/Alumina. No data for nickel adhesion was found.

A.2. Indentation test

The tensile adhesion test employed in the cordierite portion of the research program proved unsuitable for analysis of films grown on both polycrystalline and single crystal aluminum oxide substrates. Polycrystalline substrates possessed an excessive amount of surface topography, precluding growth of a continuous, planar film. The consequence was an uncertainty in the load-bearing area during testing, as

well as the possibility that the quantity being measured was the adhesion of the alumina surface layer rather than that of the film. Single crystal sapphire substrates, due to their brittle nature and small thickness, fractured prior to any film disbonding; regardless of the growth conditions for the composite being tested.

Use of the mechanical properties microprobe in the analysis of nickel/sapphire thin-film composites also proved unsuitable. When examining the films in plan-view, the load cell of the instrument was insufficient to drive the tip completely through the film; not allowing the interface region to be sampled. Morphological features such as columns inhibited the data analysis as well. Sliding of one column past another via failure of the column boundary, along with deformation of the columns themselves, contributed to the indentation resistance. In cross-section, the size of the film and interfacial region necessitated the indents being placed in close proximity to each other. Accuracy of the instrument at the shallow depths required to avoid overlap at the small separations involved was questionable, as was the certainty in the position of the indents. The results of this study indicated that the mechanical property microprobe was better suited for analysis of thin, uniform films in plan-view, or thick films with large interface regions in cross-section.

Load cell limitations were overcome by using a standard Vickers microhardness tester to produce indents through the films. Although no quantitative data was obtained, a qualitative indication of adhesive behavior was achieved. The propagation of lateral cracks emanating from the indents was taken as a measure of adhesion. For metallic nickel films, both with and without an applied bias during deposition, cracks were shown to propagate through the film and in the substrate (Fig. 25, 26). No lateral spreading of the cracks along the interface was detected, with the film remaining adherent to the substrate. In contrast, nickel oxide films exhibited gross disbonding following indentation (Fig. 27). No cracking was visible in the substrate, indicating a clean interfacial failure. Adopting the model of Chiang et. al. [61], the nickel oxide/sapphire interface was shown to have a low fracture toughness, a measure of adherence, as compared to the nickel/sapphire interface whose toughness was greater than that of the

sapphire. This failure of the oxide/oxide bond was somewhat contradictory to the notion of creating an oxide bonding phase between a metal and a ceramic in order to enhance adhesion. It was also interesting to note the pronounced failures at column boundaries in the nickel oxide film, demonstrating the importance of morphological features in a thin-film mechanics analysis.

B. Morphology

B.1. Zone models

Film morphology for the nickel/cordierite system, with films produced via DC ion plating, was as predicted by the various zone models [28-33]. Note that although all films were deposited at approximately room temperature (T/T_m = 0.17 for nickel), elevated temperature conditions were expected to be simulated through the use of a glow discharge. Without the use of a bias, a classic zone 1 morphology was produced, having polycrystalline columns with open boundaries between them (Fig. 16). Introduction of the glow discharge during deposition, imparting energy to the species arriving at the substrate, eliminated the porosity between columns and resulted in a fully dense film with slightly larger grains (Fig. 15). This observation substantiated the claims that a higher temperature morphology can be achieved, while maintaining the substrate at room temperature, through the application of a substrate bias. This was attributed to enhanced adatom mobility, as well as sputtering and redeposition in the growing film [72]. The DC glow discharge was not sufficient, however, to produce single grain columns or preferentially oriented films on polycrystalline substrates.

Changing to a single crystal substrate did not alter film morphology for non-biased deposition; with an open columnar structure present in the nickel/sapphire UHV and evaporated composites (Fig. 20, 28). This was as expected since the mobility of the incoming atoms was not sufficient to allow migration to preferred growth sites on the sapphire. Nickel/sapphire morphology under RF glow discharge growth conditions, however, was radically different and thus discussed in a separate section. RF deposited

nickel oxide on sapphire, based on SEM results (Fig. 24), appeared to have a zone 1 columnar morphology. It may be concluded that since nickel oxide has a higher melting point, the zone 1 boundary was shifted towards a higher temperature as compared to the metallic nickel; with the result being a columnar morphology even under conditions of concurrent ion bombardment during growth. This analysis was proven incorrect, however, upon evaluation of the XTEM data (Fig. 36-38). Although the film was columnar, the columns were found to consist of single grains - corresponding to an elevated temperature zone 2 morphology in the Thornton SZM [29]. This again confirmed the development of ion bombardment induced high temperature morphologies, as well as the need for transmission electron microscopy and crystallographic analyses.

B.2. RF metallic nickel

Deposition of metallic nickel on sapphire in the presence of an RF glow discharge resulted in a rather unusual bi-layer morphology not observed under any other growth conditions (Fig. 21-23). Initially, growth proceeded through the nucleation of islands, which grow and coalesce with time. Although unlike other ion plated films, this island growth correlated well with films grown by Sparks et. al. [51]. Sparks reported island growth for nickel films evaporated on sapphire substrates at high substrate temperatures (~900 °C) and low deposition rates (~0.2 nm/sec). The RF ion plated films were deposited at approximately the same deposition rate, with the glow discharge able to provide the energy and subsequent adatom mobility to simulate the elevated temperature behavior. For the case of the ion plated films, when island coalescence was complete, a second nickel layer nucleated and grew.

Reasons for the transition to the growth of the second layer are as yet unconfirmed, although some explanations have been proposed. Sputter cleaning prior to deposition provides numerous heterogeneous nucleation sites, resulting in a high density of islands. A balance between surface, interface and strain energies then dictates the relationship between lateral and upward growth rates, defining the point in thickness/time at which coalescence is completed. This completed first layer then serves as a

multi-grain substrate for subsequent nickel growth, which again proceeds by island formation. Either a decrease in nucleation site density or an increase in adatom mobility as compared to initial growth results in an increase in second layer island spacing. It is not known how the growth continues from this stage onwards.

B.3. Heat treated morphology

Heat treatment of the nickel/sapphire composites at 1000 °C for 2 hours caused extensive recrystallization, with complete loss of any original as-deposited film morphology (Fig. 41-46). Similar behavior was observed in the nickel/alumina system as well. With dewet regions being present in all the heat treated composites, they were no longer useful from an applications perspective, but did provide information concerning metal/ceramic bonding. Most of the information was obtained via XTEM, as discussed in a following subsection, yet SEM morphological examinations did yield some insight into heat treated composite behavior. Evaporated nickel/sapphire contaminated with magnesium during vacuum heat treating exhibited the largest amount of dewetting, indicating the least stable bond. Exposed regions in between the recrystallized grains in the EHT RF nickel/sapphire couple were determined to be the original substrate surface, suggesting that recrystallization and dewetting occurred prior to interface compound formation. It was unlikely that a reaction phase would form and subsequently break away from the substrate. If this phase did form prior to dewetting, the dewetting would more likely occur at the nickel/reaction phase interface, leaving the reaction phase behind on the substrate. This condition was not observed. The nickel oxide film, having a higher melting point than the metallic nickel, did not recrystallize fully. The reaction proceeded from the interface towards the film surface, indicating the driving force to be related to an interface energy.

C. Interface characteristics

C.1. Orientation relationships

In addition to altering the morphology of the growing films, another major effect of ion bombardment from the glow discharge was the initiation of distinct crystallographic orientation relationships across the film/substrate interface when single crystal substrates were employed. For room temperature deposition, adatom mobility was expected to be insufficient to result in epitaxial or preferred orientation growth at practical deposition rates. Note that as the deposition rate decreases; the mobility (and thus temperature) required for epitaxy decreases, however, contamination from adsorbed species in the chamber becomes more significant. For the nickel/sapphire composites produced without a bias, selected area diffraction patterns indicated a random crystallographic orientation (Fig. 28). When the RF glow discharge was maintained during deposition, ion bombardment induced mobility was sufficient to trigger preferential orientation of the film (Fig. 30, 34, 35). The initial growth layer of the bi-layer RF nickel morphology was shown to have the relationship:

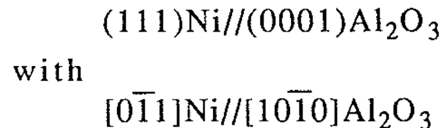

$$(111)Ni//(0001)Al_2O_3$$

with

$$[0\bar{1}1]Ni//[10\bar{1}0]Al_2O_3$$

This orientation was further confirmed by examination along another zone axis, showing:

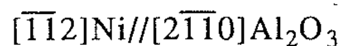

$$[\bar{1}\bar{1}2]Ni//[2\bar{1}\bar{1}0]Al_2O_3$$

Both the close packed planes as well as directions were parallel, with the close packed direction in the film being normal to the plane of growth. An identical orientation relationship was observed for nickel oxide (Fig. 37), as expected since it has the same FCC crystal structure as metallic nickel. The observed relationships were consistent with those reported by Sparks [51]

for evaporated nickel/sapphire at elevated temperatures and those of Carter [48-50] for nickel oxide/alumina, although multiple variations of orientation as reported by Carter were not found. Having close packed planes and directions parallel across the interface was also consistent with the observations by Ruhle [43,44] in the Nb/Al_2O_3 system. Since preferentially oriented interfaces generally result from elevated temperature deposition or processing, this transition from random to oriented growth with applied bias was clear evidence of the ability of ion bombardment to produce high temperature effects while maintaining a low bulk substrate temperature.

Although ion-assisted deposition resulted in preferential orientation, the films were not truly epitaxial, as demonstrated by the morphological boundaries visible in the SEM and XTEM images. These boundaries could be attributed to a number of factors which would still be consistent with single crystal selected area diffraction patterns. The first case was that of low density boundaries separating grains with slight misorientations, rotated about the growth axis, which would not be detected in an SADP. Boundaries may also result from intersections of twin-related columns (grains), as seen in the nickel oxide/sapphire composite (Fig. 36). Two twin-related variants of {111} growth are possible, with either [111] or [$\bar{1}$11] normal to the substrate surface. When viewed along the [0$\bar{1}$1] zone axis both twin orientations satisfied the Laue condition, resulting in two superimposed single crystal patterns. Note that when viewed along [$\bar{1}\bar{1}$2] (the other axis used in this investigation), the two orientations were indistinguishable. This type of twin-related growth was also reported by Sparks [51] for nickel/sapphire, although the x-ray diffraction techniques utilized were not able to identify the orientation of individual islands.

C.2. Phase analysis

XTEM structural and crystallographic analyses of the composite interfaces revealed the absence of any reaction phases in the as-deposited condition. This result was consistent with the investigation by Sparks [51], which did not detect any reaction compounds via x-ray diffraction for the case of nickel deposited on sapphire at up to 1400 °C. Carter [50] reported

the minimum temperature for any nickel oxide/alumina reaction to be 1100 °C. The presence of oxygen was also reported to be critical to nickel aluminate spinel formation [47], perhaps explaining the absence of spinel in the high temperature experiments of Sparks. Although ion-assisted deposition was shown to produce elevated temperature morphologies and preferred orientation, it was not sufficient to create an interfacial spinel phase, even in the case of oxide growth. This could be due to the fact that even though the film atoms gain sufficient energy from the glow discharge, the substrate remains at a lower temperature and is unable to react.

Heat treatment of the films on sapphire substrates at 1000 °C did, however, produce interfacial spinels in all cases (Fig. 47-61). No spinel was found for nickel/polycrystalline alumina (Fig. 19), although a detailed interfacial analysis was impeded by the surface topography. The additional driving force required to precipitate the reaction at a temperature below the reported minimum was provided by the high defect density at the interface resulting from the sputter cleaning prior to deposition. The oxygen requirement was most likely satisfied by residual oxygen introduced into the films during growth or by residual oxygen in the vacuum during heat treatment. In the case of metallic nickel films with magnesium contamination, all of the magnesium segregated to the interface and formed $MgAl_2O_4$, with no $NiAl_2O_4$ detected (Fig. 47-49). Such segregation was not observed in the nickel oxide films. All of the nickel aluminate spinels formed were crystallographically oriented with both the substrate and the film, even in the case of the evaporated film which was randomly oriented in the as-deposited condition. The original nickel or nickel oxide to sapphire relations were maintained, with the spinel adopting the same orientation as the films. The initially random film recrystallized to the same orientation as the ion-assisted films upon heat treatment. Thus, all composites developed the same crystallography after annealing, having close packed planes and directions aligned:

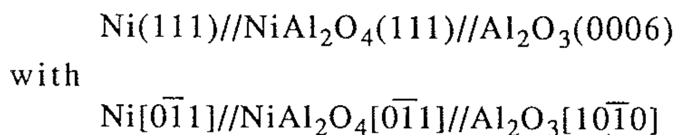

$$Ni(111)//NiAl_2O_4(111)//Al_2O_3(0006)$$

with

$$Ni[0\bar{1}1]//NiAl_2O_4[0\bar{1}1]//Al_2O_3[10\bar{1}0]$$

or equivalently

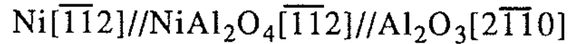

$$Ni[\overline{1}\overline{1}2]//NiAl_2O_4[\overline{1}\overline{1}2]//Al_2O_3[2\overline{1}\overline{1}0]$$

These orientation relationships were again consistent with those in the literature [46,49,50].

C.3. Microstructure

Ion bombardment, both prior to and during deposition, was shown to alter substrate microstructure at the interface. An "altered layer" was produced in the cordierite substrates as a result of the DC glow discharge (Fig. 15, 16). No detailed description of this region could be formulated due to the inhomogeneity and instability of the cordierite. Exposure to a condensed beam in the electron microscope induced a crystalline to amorphous transformation, masking any effect of processing history. Such difficulties were avoided in the nickel/sapphire system, where damaged zones may be clearly imaged. Selected area diffraction did not detect any amorphization in these regions, although a fairly high defect density is present. The damage density was seen to gradually decrease with depth, consistent with an ion bombardment related phenomenon. The creation of the damaged zones was further correlated with ion bombardment by examining damage extent as a function of processing conditions. Specimens which were only sputter cleaned but did not have a bias during growth exhibited the least amount of damage (Fig. 28), while ion-assisted deposition resulted in a greater damage depth (Fig. 32, 36). The extent of these damaged regions (100 - 200 nm) was much larger than the projected range of the incoming ions, which is on the order of 20 nm for high energy (100 keV) ions [73]. This may be attributed to the extremely high doses involved, up to 5×10^{18} ions/cm^2 during the sputter cleaning cycle.

C.4. Chemistry

In addition to creating structural damage in the cordierite substrates, ion bombardment resulted in chemical mixing across the nickel/cordierite interface. Nickel was found to be present in the altered substrate layers via STEM/EDS (Fig. 17); however, even semi-quantitative analyses were

precluded by the substrate inhomogeneity. In contrast, the damaged zones in the nickel/sapphire system did not contain detectable amounts of nickel, indicating little, if any, chemical mixing. Changes in interfacial width (chemical) as a function of processing were detected by the Auger depth profiles (Fig. 40). Although instrumentally induced broadening was likely present in all the profiles, interfacial width clearly increased as a result of ion bombardment during deposition. Interfacial width also increased upon heat treatment; however, any variation with deposition condition was no longer present (Fig. 62). This type of analysis was not successful in the nickel/cordierite system due to the roughness of the original substrate surface overshadowing any dependence on processing, as suggested by XTEM.

VI. CONCLUSIONS

Based on the investigations conducted in this research program, a number of conclusions may be formulated. Ion plating was demonstrated as a viable technique for the production of highly adherent nickel films on cordierite substrates. Within the processing window defined in this study, film adhesion was stable with temperature (up to 400 °C) in both inert and reducing environments. Energetic particle bombardment resulting from the glow discharge, characteristic of the ion plating process, was shown to produce damaged zones in the substrates, as well as alter the film morphology. Elevated temperature morphologies could be achieved, while maintaining a low bulk substrate temperature, through the use of ion bombardment. In addition, an RF glow discharge could impart sufficient energy, with the associated adatom mobility, to make the transition from random to preferred orientation growth on single crystal substrates. In all cases observed, close packed planes and directions of the film and substrate were aligned. Ion-assisted deposition was not sufficient, however, to generate an interfacial reaction phase in the as-deposited condition. Nickel aluminate spinel layers, crystallographically oriented with the film and substrate, were precipitated at the interface upon heat treatment (1000 °C) in vacuum. Residual oxygen in the films or vacuum was sufficient to allow spinel formation. Qualitatively, metallic films produced via ion-assisted deposition exhibited better resistance to disbonding than oxide films, contradictory to the concept of intermediary oxide bonding layers. Finally, despite the difficulties encountered in specimen preparation (most of which were eliminated during the course of this investigation), cross sectional transmission electron microscopy was determined to be the optimal technique for evaluation of the microstructure, crystallography, and chemistry of thin-film composites.

REFERENCES

1. Thin Films, Papers Presented at a Seminar of the American Society for Metals, October 1963, American Society for Metals, (1984)

2. L. I. Maissel and R. Glang, Handbook of Thin Film Technology, McGraw-Hill, (1970)

3. R. F. Bunshah et. al., Deposition Technologies for Films and Coatings, Noyes Publications, Park Ridge, NJ, (1982)

4. de Lodyguine, U. S. Patent 575002, (1893)

5. D. R. Gaskell, Introduction to Metallurgical Thermodynamics, McGraw-Hill, (1981)

6. J. A. Thornton, Semiconductor Materials and Process Technologies, ed. by G. E. McGuire, Noyes Publications, Park Ridge, NJ, (1984)

7. R. Nahrwold, Weid Ann, **34**, 469, (1888)

8. R. Z. Bachrach, "MBE Evaporative Growth", Crystal Growth, ed. by B. R. Pamplin, Pergamon, NY, p. 221, (1980)

9. P. Sigmund, Phys. Rev., **184**, 383, (1969)

10. W. D. Grove, Phil. Trans., **B142**, 87, (1852)

11. J. A. Thornton, Metal Finishing, **77**, 45, (1979)

12. D. M. Mattox, Electrochem. Tech., **2**, 295, (1964)

13. D. G. Teer, Proceedings of the Conference on Ion Plating and Allied Techniques, C.E.P. Consultants, Ltd., Edinburgh, p. 13, (1977)

14. D. M. Mattox, Proceedings of the Conference on Ion Plating and Allied Techniques, C.E.P. Consultants, Ltd., Edinburgh, p. 1, (1979)

15. P. A. Walley, Proceedings of the Conference on Ion Plating and Allied Techniques, C.E.P. Consultants, Ltd., Edinburgh, p. 1, (1977)

16. N. A. G. Ahmed, Ion Plating Technology, John Wiley & Sons, New York, NY, (1987)

17. D. L. Chambers and D. C. Carmichael, Research/Development Mag., **22**, 323, (1971)

18. B. Chapman, Glow Discharge Processes, John Wiley & Sons, New York, NY, (1980)

19. A. Matthews and D. G. Teer, Thin Solid Films, **80**, 41, (1981)

20. P. Saulnier, A. Debhi, and J. Machet, Vacuum, **34**, 765, (1984)

21. T. Spalvins, Journal of Vacuum Science and Technology, **17**, 315, (1980)

22. W. D. Davis and T. A. Vanderslice, Phys. Rev., **131**, 219, (1963)

23. D. G. Teer, J. Adhesion, **8**, 289, (1977)

24. D. G. Armour et. al., Vacuum, **34**, 295, (1984)

25. R. Buhl, H. K. Pulker and E. Moll, Thin Solid Films, **80**, 265, (1981)

26. J. H. Givens et. al., to be published in Proceedings of the Symposium on Ceramic Thin and Thick Films, Indianapolis, IN, (1989)

27. Y. W. Lee et. al., Proceedings of the Conference on Ion Plating and Allied Techniques, C.E.P. Consultants, Ltd., Edinburgh, p. 249, (1987)

28. B. A. Movchan and A. V. Demchishin, Fiz. Metal. Metalloved., **28**, 83, (1969)

29. J. A. Thornton, Journal of Vacuum Science and Technology, **A4**, 3059, (1986)

30. C. R. M. Grovenor, H. T. G. Hentzell and D. A. Smith, Acta. Metall., **32**, 773, (1984)

31. R. Messier, A. P. Giri and R. A. Roy, Journal of Vacuum Science and Technology, **A2**, 500, (1984)

32. R. Messier, Journal of Vacuum Science and Technology, **A4**, 490, (1986)

33. D. Srolovitz, A. Mazor and B. G. Bukiet, Journal of Vacuum Science and Technology, **A6**, 2371, (1988)

34. K. L. Mittal, Adhesion Measurements of Thin Films, Thick Films and Bulk Coatings, ASTM STP 640, ed. by K. L. Mittal, American Society for Testing and Materials, p. 5, (1978)

35. J. E. E. Baglin, Ion Beam Modification of Insulators, ed. by P. Mazzoldi and G. W. Arnold, Elsevier, p. 585, (1987)

36. B. A. Chapman et. al., Technology of Glass, Ceramic or Glass-Ceramic to Metal Sealing, ed. by W. E. Moddeman, C. W. Merten and D. P. Kramer, American Society of Mechanical Engineers, New York, p. 77, (1987)

37. Nano-indenter, Microscience, Inc., 182 Forbes Road, Braintree, MA 02184

38. W. C. Oliver et. al., Materials Research Society Symposium Proceedings, **60**, 515, (1986)

39. A. J. Blodgett, Jr. and D. R. Barbour, IBM J. Research and Development, **26**, 30, (1982)

40. K. M. Prewo, Interim Technical Report R77-912245-3, United Technologies Research Center, E. Hartford, CT, (1977)

41. S. D. Crudele, M.S. Thesis, University of Illinois at Urbana-Champaign, (1989)

42. H. Hindam and D. P. Whittle, Oxidation of Metals, **18**, 245, (1982)

43. M. Ruhle and A. G. Evans, Materials Science and Engineering, **A107**, 187, (1989)

44. W. Mader and M. Ruhle, Acta Metall., **37**, 853, (1989)

45. K. P. Trumble and M. Ruhle, Paper No. 101-B-88 presented at the 90th Annual Meeting and Exposition of the American Ceramic Society, Inc., Cincinnati, OH, (1988)

46. J. A. Wasynczuk and M. Ruhle, Ceramic Microstructures '86, ed. by J. A. Pask and A. G. Evans, Plenum Press, p. 341, (1987)

47. K. P. Trumble, Proceedings of the 47th Annual Meeting of the Electron Microscopy Society of America, ed. by G. W. Bailey, San Francisco Press, Inc., p. 554, (1989)

48. Y. K. Simpson and C. B. Carter, Phil. Mag. A, **53**, L1, (1986)

49. Y. K. Simpson and C. B. Carter, Materials Research Society Proceedings, **60**, 265, (1986)

50. D. W. Susnitzky, S. R. Summerfelt and C. B. Carter, Scripta Metallurgica, **22**, 1149, (1988)

51. C. J. Sparks et. al., Materials Research Society Proceedings, **77**, 495, (1987)

52. J. E. E. Baglin et. al., Nuclear Instruments and Methods in Physics Research, **B19/20**, 782, (1987)

53. S. H. Risbud, G. D. Allen and J. E. Poetzinger, Ceramic Microstructures '86, ed. by J. A. Pask and A. G. Evans, Plenum Press, p. 359, (1987)

54. W. M. Kriven and S. H. Risbud, Materials Research Society Proceedings, **77**, 323, (1985)

55. A. G. Evans, M. Ruhle and M. Turwitt, Journal De Physique, **46**, C4-613, (1985)

56. A. G. Evans et. al., Acta Metall., **34**, 1643, (1986)

57. G. Elssner, T. Suga and M. Turwitt, Journal De Physique, **46**, C4-597, (1985)

58. B. J. Dalgleish, M. C. Lu and A. G. Evans, Acta Metall., **36**, 2029, (1988)

59. H. C. Cao, M. D. Thouless and A. G. Evans, Acta Metall., **36**, 2037, (1988)

60. T.S. Oh et. al., Acta Metall., **36**, 2083, (1988)

61. S. S. Chiang, D. B. Marshall and A. G. Evans, Surfaces and Interfaces in Ceramic and Ceramic-Metal Systems, ed. by J. A. Pask and A. G. Evans, Plenum Press, p. 603, (1981)

62. M. S. Hu and A. G. Evans, Acta Metall., **37**, 917, (1989)

63. M. S. Hu, M. D. Thouless and A. G. Evans, Acta Metall., **36**, 1301, (1988)

64. M. D. Drory, M. D. Thouless and A. G. Evans, Acta Metall., **36**, 2019, (1988)

65. A. S. Argon et. al., Materials Science and Engineering, **A107**, 41, (1989)

66. Adolph Meller Co., P.O. Box 6001, Providence, RI, 02904

67. J. C. Bravman and R. Sinclair, Journal of Electron Microscopy Techniques, **1**, 53, (1984)

68. Walmark Corp., Adhesive Division, 100 West Route 120, P.O. Box R, Roundlake Park, IL 60073

69. Quad Group, 2030 Alameda Padre Serra, Santa Barbara, CA 93103

70. M. M. Shah, P. A. Scott and J. M. Rigsbee, Proceedings of the Conference on Ion Plating and Allied Techniques, C.E.P. Consultants, Ltd., Edinburgh, p. 397, (1987)

71. J. E. E. Baglin and G. J. Clark, Nuclear Instruments and Methods in Physics Research, **B7/8**, 881, (1985)

72. J. A. Thornton, Thin Solid Films, **40**, 335, (1977)

73. A. P. Mouritz, et. al., Nuclear Instruments and Methods in Physics Research, **B19/20**, 805, (1987)

VITA

Mihir Mahendra Shah was born in Manchester, England on December 26, 1963. He was raised in Elmira, New York, where he received his primary and secondary education. Mr. Shah obtained his Bachelor of Science degree, cum laude, in Materials Engineering from Rensselaer Polytechnic Institute in May, 1984. While at Rensselaer, he was awarded the Matthew A. Hunter prize in Materials Engineering. During the summers of 1983 and 1984, he was employed as a pre-professional with the IBM Corporation in East Fishkill, NY. Since August of 1984, Mr. Shah has been a graduate research assistant working under the direction of Professor J. M. Rigsbee, in the Department of Materials Science and Engineering (formerly Metallurgical Engineering) of the University of Illinois at Urbana-Champaign. He was also appointed as an ARCO Fellow in Metallurgy by the department. He received his Master of Science degree in Metallurgical Engineering from the University of Illinois in January of 1987, with his thesis being entitled Structure/Chemistry/Properties of Ion Plated Nickel Films on Glass-Ceramic Substrates. Mr. Shah is a member of Tau Beta Pi, the American Ceramic Society, the American Society for Metals and the Metallurgical Society of AIME.